A Novel Combination Therapy of Cisplatin with a Molecular Promoter for Cancer Treatment

by

Qinrong Zhang

A thesis

presented to the University of Waterloo

in fulfillment of the

thesis requirement for the degree of

Doctor of Philosophy

in

Physics

Waterloo, Ontario, Canada, 2017

AUTHOR'S DECLARATION

I hereby declare that I am the sole author of this thesis. This is a true copy of the thesis, including any required final revisions, as accepted by my examiners.

I understand that my thesis may be made electronically available to the public.

Abstract

Cisplatin is the first and most widely used platinum-based chemotherapy drug and is the cornerstone agent in treating a broad spectrum of cancers, including ovarian cancer, testicular cancer, cervical cancer, bladder cancer, lung cancer, head and neck cancer, lymphoma, and brain tumors. It is one of the few curative anti-cancer agents; however, its clinical application is often limited by severe toxic side effects and resistance possessed by some cancers.

Our group has recently, through the femtomedicine approach, unraveled a new molecular mechanism of Cisplatin. It has been found that Cisplatin is extremely effective for the dissociative electron transfer (DET) reaction with weakly-bound electrons to produce reactive radicals that cause DNA strand breaks, apoptosis, and final clonogenic cell kill.

Based on this DET mechanism, it is proposed that Cisplatin may be administered in combination with a biological electron donor to enhance its chemotherapeutic efficacy. We have tried a few combinations of Cisplatin and electron-donating compounds. In this thesis, we show results of the combination: Cisplatin and Rhodamine-B, the one with the greatest potential as demonstrated in both *in vitro* assays and *in vivo* xenograft mouse cancer models. This thesis begins with an introduction to cancer and cancer therapies in Chapter 1, where the theory, objective, and scope of this thesis are introduced. Chapter 2 focuses on some new understandings of Cisplatin-induced DNA damage. *In vitro* and *in vivo* experiment results on the effectiveness of the combination of Cisplatin and Rhodamine-B are presented in Chapter 3 and Chapter 4, respectively. In Chapter 5, time-resolved femtosecond laser spectroscopic studies on the reaction between Cisplatin and Rhodamine-B are shown. Chapter 6 as the last Chapter summarizes results obtained in this project and proposes some possible future research.

In vitro experiments confirm the potential of this proposed combination of Cisplatin and Rhodamine-B to treat cancer. From cell survival tests, by applying MTT assays and clonogenic assays, it has been shown that our proposed combination significantly enhances the cell-killing efficacy in cancer cells; but surprisingly, not in normal cells. Besides, plasmid DNA gel electrophoresis and γ-H2AX staining in treated cells indicate that more double-strand breaks can be induced using our combination, compared to Cisplatin only. In addition, measurements on Caspase 3/7 activation and Annexin V-FITC labeling flow cytometry experiments clearly show a significant enhancement in the population of apoptotic cells using our combination. To further verify the effectiveness of the combination of Cisplatin and Rhodamine-B, *in vivo* xenograft mouse models have been developed. Our combination greatly enhances the tumor growth inhibition and even tumor shrinkage in three different mouse models. Acute toxicity analysis and body weight measurements do not show additional side effects induced by the addition of Rhodamine-B. Lastly, spectroscopic measurements have confirmed that Cisplatin and Rhodamine-B can react, and the reaction is an electron transfer reaction.

Acknowledgements

First and foremost, I would like to give my sincere appreciation to my PhD supervisor Dr. Qing-Bin Lu, for giving me the opportunity to study and work in his lab. Thank you, Professor Lu, for your continuous support, trust, and encouragement in my study, research, and life. Your help over these years have been greatly appreciated. I am very fortunate to have a supervisor like Dr. Lu.

My gratitude also goes to my committee members, Dr. Kesen Ma, Dr. Hartwig Peemoeller, Dr. Russell Thompson, and Dr. Anton Burkov for serving as my committee members and for their helpful comments and encouragement during my PhD studies. Special thanks go to Dr. Francis Lin for being my external examiner.

I would like to thank everyone whom I have worked with in the group. I would like to thank Chunrong Wang, Ting Luo, and Zheng Li for training me when I came to this group. I would like to thank Jenny Warrington for her help on animal (mouse) experiments. I would also like to thank Ning Ou, Wei Hong, Yang Hu, Yurui Wu, Zhi Li, Yaowen Mei, Hanwen Liu, and all other group members for their valuable discussion, help, and friendship.

I also thank some other professors and administrative staff in the Department of Physics and Astronomy: thank you Dr. Zoya Leonenko for the care and trust you have given me while I was your teaching assistant. Thank you, Rohan Jayasundera and Tan Dinh for your kindness, help, and smile since I was an undergrad student. Thank you, Mr. Zhenwen Wang. Your knowledge and skills greatly helped me with my experiments. Many thanks go to Judy McDonnell, Linda Stadig, Anja Drygala for helping me to arrange committee meetings and thesis defence, to schedule my comprehensive exam, and to place orders. Nancy Gibson, Jean Flanagan, and Angela Wagler from the Central Animal Facility (CAF) are appreciated for the help and patience they have given me during my animal experiments.

Dedication

To My Parents:

Beloved Mrs. Zhang and Mr. Zhang

And My Grandmother Mrs. Wei

Table of Contents

List of Figures

xviii

List of Tables

List of Abbreviations

e^-_{pre}	Pre-hydrated electron
5-FU	5-Fluorouracil
6-MP	6-Mercaptopurine
a.u.	Arbitrary unit
AKI	Acute kidney injury
ALL	Acute lymphocytic leukemia
ALP	Alkaline phosphatase
ALT	Alanine aminotransferase
APC	Adenomatous polyposis coli
ATCC	American type culture collection
BCS	Body condition score
CAC	Cancer-associated cachexia
CAF	Central animal facility
CDDP	Cisplatin, Cis-Diammineplatinum(II) dichloride
CR	Complete response
CRC	Convert colorectal cancer
CT	Computed tomography
Ctr1	Copper transporter 1
DBSs	Double strand breaks
DET	Dissociative electron transfer
DMSO	Dimethyl sulfoxide
DNA	Deoxyribonucleic acid
E. Coli.	*Escherichia Coli*
EGF	Epidermal growth factor

EGFR	Epidermal growth factor receptor
ER	Estrogen-receptor
EtBr	Ethidium bromide
EV	Extracellular vesicles
Ex/Em	Excitation/Emission
F12K	Nutrient mixture F12 Ham Kaighn's modification
FBS	Fetal bovine serum
FDA	Food and drug administration
FITC	Fluorochrome fluorescein isothiocyanate
fs	Femtosecond
GFR	Glomerular filtration rate
GPC	Glypican
GSH	γ-glutamyl-cysteinyl-glycine
HMG	High-mobility group
HPV	Human papillomavirus
IC_{50}	Drug concentration causing 50% inhibition
IP	Intraperitoneal
JCOG	Japanese cooperative oncology group
LD_{50}	Lethal dose$_{50}$, dose required to kill 50% of test sample
mAbs	Monoclonal antibodies
MEM	Minimum essential medium eagle
mM	Millimolar
MTD	Maximum tolerated dose
MTT	3-(4,5-dimethylthiazol-2-yl)-2,5-diphenyltetrazolium bromide
NER	Nucleotide excision repair

NIH	National cancer institute
NSCLC	Non-small-cell-lung cancer
OCT	Organic cation transporters
OPA	Optical parametric amplifier
OS	Overall survival
Pap	Papanicolaou
PBS	Phosphate buffered saline
PCR	Polymerase chain reaction
PDAC	Pancreatic ductal adenocarcinoma
PDT	Photodynamic therapy
PF	Paraformaldehyde
PF (combination)	Cisplatin + 5-Fluorouracil
PI	Cisplatin + Irinotecan
PI (fluorophore)	Propidium iodide
PIE	Cisplatin + Irinotecan + Etoposide
PR	Progesterone-receptor
PS (cell culture)	Penicillin-streptomycin antibodies
PS (cell membrane)	Phospholipid phosphatidylserine
RBC	Red blood cell
RDM-B/RB/RDMB	Rhodamine-B
RNA	Ribonucleic acid
rpm	Revolutions per minute
s.e.m.	Standard error of the mean
SC	Supercoiled
SCCHN	Squamous cell carcinoma of the head and neck (cancer)

SCID	Severe combined immunodeficient disease
SDS	Sodium dodecyl sulfate
SSBs	Single strand breaks
TBL	Total bilirubin
TILs	Tumor-infiltrating lymphocytes
TOC	Total organic content
TPF	Cisplatin + 5-Fluorouracil + Docetaxel
TUNEL	Terminal deoxynucleotidyl transferase (TdT)-mediated dUTP nick end labeling
UV	Ultra-violet
VIA	Visual inspection with acetic acid
WHO	World health organization
μM	Micromolar

Chapter 1

Introduction

1.1 Cancer

In Canada and the United States cancer is becoming the leading cause of death. About 40% of Canadians will develop cancer in their lifetime, and about 25% of Canadians will die of cancer. It has been estimated that 202,400 Canadians will develop cancer in 2016 and 78,800 of them will die of cancer[1]; the corresponding estimated numbers are 1,685,210 and 595,690 in the United of Sates in 2016[2]. Cancer has become a major worldwide public health issue. According to the National Cancer Institute (NIH), within the next two decades, 22 million people in the world will develop cancer. Cancer research is getting more and more important and pressing.

1.1.1 Understanding of Cancer

The fundamental cellular division and DNA replication mechanisms sometimes fail, compromising the genome integrity, and result in cancer formation[3]. Cancer is identified as genetic: it is a group of diseases that are extremely complex. Six hallmark biological capabilities of cancer, which describe the organization and complexity of neoplastic diseases, were proposed in 2000 by Hanahan and Weinberg[4] (Figure 1-1). These are: sustaining proliferative signaling, evading growth suppressors, resisting cell death, enabling replicative immortality, inducing angiogenesis, and activating invasion and metastasis. Two other hallmarks were added to the list a decade later: reprogramming of energy metabolism and evading immune destruction[5]. Additionally, the concept of "tumor micro-environment" is introduced, and is exhibited by the specific tumor structure[5].
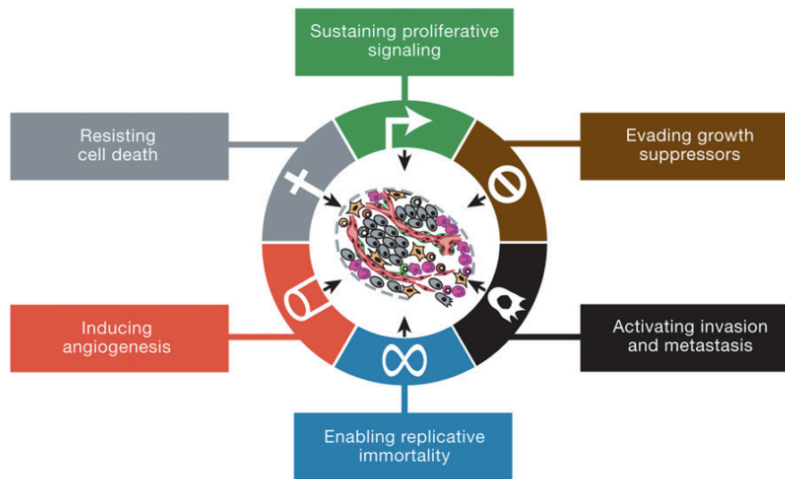
Figure 1-1: Cancer hallmarks[4].

Technologies have advanced our understandings of cancer. It has been known that for a specific cancer, cancer cells are not identical because of various genetic alterations and tumor micro-environment[6,7]. Cancer cells have subpopulations like the cancer stem cells that have been identified[8]. Cancer cells are heterogeneous. This nature makes the treatment of cancer even more challenging[9]. Besides, cancer cells can evolve via the communication between cells. Cells have been shown to exchange biomolecules such as proteins, lipids, and nucleic acids, by the release and uptake of extracellular vesicles (EVs)[10]. Recently, extracellular exchange of signals has been demonstrated among tumor cells in living mice[11]. Using the high-resolution intravital imaging and a Cre recombinase-based method, the study provided the first direct evidence *in vivo* of the exchange of active biomolecules between cancer cells. The researchers directly visualized the EVs released from more malignant MDA-MB-231 cells to less malignant cells. It was observed that by taking up these EVs, less malignant cells became more migratory and metastatic.

Understanding metabolism is also crucial. Cancer is life threatening. It has been shown that approximately 30% of late-stage patients die not only from the tumor itself, but also from cancer-associated cachexia (CAC)[12,13]. Recently, two studies have been conducted in fruit flies showing that a

protein secreted by tumor cells blocks insulin signaling, which results in organ wasting that accounts for ~20% of cancer deaths[14,15].

The study of cancer is expanding from the cellular level to the tumor microenvironment, and to the whole system.

1.1.2 Causes of Cancer

Cancer can be caused by both intrinsic factors like inherited mutations, hormones, immune conditions and mutations from metabolism, and external factors like tobacco, infectious organisms, chemicals and radiation[16]. To date, factors that are correlated with the occurrence of three types of cancer have been identified: skin cancer, lung cancer, and cervical cancer.

From the 1930s to the 1970s, after researchers discovered that tobacco-smoking can cause cancer, the lung cancer incidence rate decreased dramatically due to public awareness[17] of this link. Quitting smoking can effectively prevent lung cancer. Radon exposure has also drawn much attention as the second leading cause of lung cancer[18]. It has been estimated that approximately 650 lung cancer deaths per year are prevented in the United States due to radon mitigation and prevention measures. In the area of skin cancer research, it has been found that UV radiation can damage skin[19,20] and it has been estimated by the Cancer Council NSW that ~95% of melanomas and ~99% of non-melanoma skin cancers are caused by UV exposure. Although the numbers might vary by institutes, the causality is certain. Skin cancers are almost completely preventable by minimizing UV exposure through various measures such as using sunscreen.

Recently, the correlation between virus infection and cancer has drawn much attention and some new messages have been delivered. Human papillomavirus (HPV), a ubiquitous pathogen that will affect almost everyone at some point in their lives, is responsible for 99% of cervical cancers, and a small proportion of genital cancers. Since this discovery, three HPV vaccines have been developed and

manufactured, and they are now commonly given to teenage girls, and even boys. The story does not end here: in 2005, Gillison analyzed the samples she had collected for seven years from 300 participants: she found that head and neck cancer patients were 15 times more likely to be infected with HPV in their mouths or throats than healthy people[21]. Earlier Gillison also demonstrated that HPV could integrate its DNA into the nuclei of throat cells and produce potent oncoproteins[22]. Her later studies also showed that HPV-positive and HPV-negative oropharyngeal cancers had different risk profiles; as a result, they should be considered as two different diseases[23] and therefore be treated differently[24]. A further question was asked: "if HPV can get into the mucous membranes of the mouth and throat, where does it stop?"[25] Studies were conducted to investigate if HPV is correlated with lung cancer incidence. Current data do not affirmatively support this correlation: some studies have shown the existence of HPV DNA is more likely in lung tumors compared to healthy samples[26,27] and concluded "HPV is the second most important cause of lung cancer after cigarette-smoking", while some did not[28]. If the correlation between HPV infection and more other forms of cancers is confirmed, to save more lives, HPV vaccines should be given to a larger population and not restricted to young girls.

The public is also concerned if low-dose radiation from sources such as cellphones or medical exams is a carcinogenic factor. It has been shown that the amount of radiation is indeed increasing, but the correlation is very difficult to confirm[29].

1.1.3 The Best We Can Do: Early Cancer Diagnosis and Prevention

Early diagnosis is crucial because cancers in their early stages are more likely to be curable. Taking lung cancer as an example, an early diagnosis (before any symptoms) gives patients an 88% chance of living for another decade[30]; and it has been shown that low-dose computed tomography (CT) screening reduces lung cancer death by 20%[31]. Other cancers like ovarian cancer[32] and pancreatic cancer[33] have extremely high mortality that is largely attributed to the failure and/or difficulty of early diagnosis. More than 70%

of ovarian cancer patients are diagnosed with advanced disease[32]; the 5-year survival of which is only 20-30%, compared to a 70%-90% *cure* rate of early stage patients (confined to the ovary)[34]. More than 80% of pancreatic cancer patients are diagnosed with distant metastasis[35], at this late stage primary tumors have been unresectable. In the clinic, exocrine pancreatic cancer has the lowest survival rate among all cancers: 74% of patients die within the first year after diagnosis and 94% of patients die within five years[33]. However, if patients could be diagnosed at stage I, the four-year survival rate is dramatically increased to higher than 75%[36].

Researchers are working on developing diagnostic methods that are applicable, sensitive, accurate, and non-invasive. A recent study of secreted exsomes[37] shows the possibility of early detection of some cancer types, including pancreatic cancer and breast cancer. Exsomes, lipid-bilayer-enclosed extracellular vesicles[38] often contain important bio-information in the form of proteins and nucleic acids[39]. That study identified glypican-1 (GPC1), a cell surface proteoglycan as enriched in exsomes from cancer cells. GPC1 can be detected in patients' serum and its level is associated with tumor burden and survival. Additionally, serum sample test is simple and non-invasive. In recent efforts, massive population screening is advocated for breast cancer by regular mammography. Besides, women who carry a deleterious mutation in the BRCA gene will have a higher risk of developing breast cancer and ovarian cancer[40]. Biological kits are now commercially available to detect this mutation by simply sending companies a small bottle of saliva sample. Early cervical cancer detection is possible by routine Papanicolaou (Pap) test, named after Dr. Georgios Papanikolaou. This cytology-screening test has so far been the most successful cancer-screening test in history. However, the Pap test is unaffordable in some developing countries and an alternative is using acetic acid to perform visual inspection of the cervix (VIA: visual inspection with acetic acid) to reduce costs[41]. Also, biomarkers are targets to be detected for cancer diagnosis. By the nature of cancer formation, gene alterations should have taken place before a normal cell becomes cancerous. Taking colon cancer as an example, accumulated gene changes have been confirmed in the cancer forming

process[42–44]. This process provides an opportunity to detect cancer at an early stage or even before it occurs. Individuals with adenomatous polyposis coli (APC) gene mutations will get colon cancer in the future at a risk of almost 100%, and 60% of colorectal carcinoma patients carry this mutation[45,46]. Polymerase chain reaction (PCR) makes the mutation possible to be detected. Mutations in oncogenes such as K-*ras* (an early appearance)[47,48] and tumor suppressor genes such as *p53* (a later event)[49,50] are also targets for the detection of colon cancer[46]. Advanced pancreatic cancer is extremely lethal; therefore, developing clinically possible early detection methods is of great importance. MicroRNAs, non-coding short RNAs (17- to 25-nucleotide-long) that regulate ~30% of human genes[51], have been recently found to play crucial roles in cancer formation and metastasis[52,53]. Similar to a coding gene, a microRNA may act as a tumor suppressor *as well as* an oncogene if its function is lost/altered, and as a result a normal cell may be transformed to a malignant one[52,54]. Recently a study was conducted to identify if microRNAs in the whole blood can be used to detect pancreatic cancer[55]. It compared the expression of microRNAs in the whole blood of pancreatic cancer patients and healthy people. It was found that 38 microRNAs were possible biomarkers which can differentiate pancreatic cancer patients from healthy participants, and it also suggested two diagnosing panels, using a combination of multiple microRNAs to diagnose pancreatic cancer. The application of microRNAs' expression detection is beneficial not only for early and accurate detection of cancer but also for therapeutic strategies and prognosis[54].

According to the World Health Organization (WHO), at least one third of cancers can be prevented by quitting smoking, regular physical activity, healthy diet, prevention of infection, etc[56]. Finding ways to prevent cancer largely depends how well we understand cancer causes. The cervical cancer vaccine is a perfect example.

1.2 Cancer Therapies

1.2.1 Surgery

Cancer surgery is an operation to remove the tumor with some surrounding tissues including lymph nodes. Surgery can be preventive, reconstructive, palliative, and curative; it can also be a process to diagnose, stage, and de-bulk[57].

  Surgery is the oldest cancer treatment and it remains the major treatment for many types of cancer. Surgery can be curative when the tumor is localized and it is often combined with chemotherapy and/or radiation therapy. Now minimally invasive surgery is preferred, such as laparoscopic surgery, laser surgery, cryosurgery, microscopically controlled surgery, and endoscopy[57]. Robotic surgery is the newest technique in cancer surgery and it is achieving success in treating solid tumors such as lung cancer[58–60]. The da Vinci Si robotic system allows the surgery to be more visual and more precise; in addition, it provides quicker patient recovery.

1.2.2 Radiation Therapy

Radiation cancer therapy is the therapy utilizing ionizing radiation to kill cancer cells and/or to shrink tumors. The development of radiation medicine has four eras[61], as shown in Figure 1-2. From the discovery to the successful application of x-ray in treating cancer, from knowing little about its biological activity to a precise management of radiation dosage and schedule, it has taken more than 100 years, and is still ongoing.

7
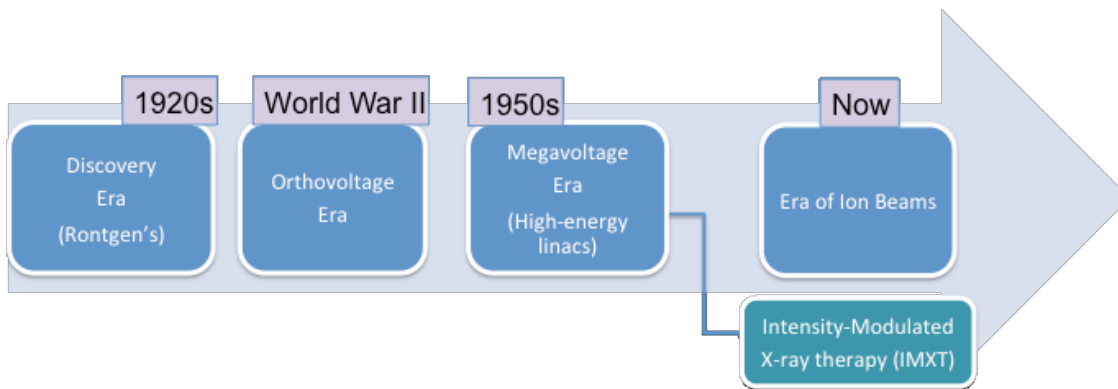
Figure 1-2: Revolution of radiation therapy.

The major target of radiotherapy is DNA, and the anti-cancer effect of ionizing radiation is generally thought to be a consequence of chemical modification of DNA[62–64]. Both of the two forms of ionizing radiation, electromagnetic and particle radiation are used in cancer treatment.

1.2.3 Targeted Therapy

Targeted therapy, as its name indicates, is a therapy that targets the difference in cell growth between cancer cells and normal cells; in this way, targeted drugs can selectively kill cancer cells without inducing severe side effects as traditional chemotherapies usually do. The most essential difference between cancer cells and normal cells is the difference in DNA; as a result, their produced proteins are different. Conventional targeted therapy focuses on unique/over-expressed proteins that are involved in cancer cell growth.

Currently, targeted therapy medicines include enzyme inhibitors, apoptosis-inducing drugs, angiogenesis inhibitors, etc[65]. Gefitinib is a drug that targets the epidermal growth factor receptors (EGFR), which are over-expressed in some cancers[66]. Gefitinib can block the signal from binding to EGFR and therefore to slow/stop cancer cell growth. Non-small-cell lung cancer has sensitive alterations

in EGFR and it has been shown very responsive to Gefitinib (a much better response compared to the standard carboplatin-paclitaxel chemotherapy group)[67].

Though these "*conventional*" targeted therapies have achieved some clinical success, some *new* concepts have emerged in recent years. Conventional targeted cancer therapy targets the characteristics that *exclusively* exist or are overexpressed in cancer cells. However, little research has been done in the *opposite* direction: targeting characteristics that cancer cells lack/lose. Alterations in the *p53*-encoding gene *TP53* are the most common genetic alterations that have been confirmed in 12 of the most common cancer types[68], either mutated or deleted. Molecules with similar functions have not been found. Several other attempts have shown promise for a new strategy in targeted therapy.

MDM2 and MDMX proteins inhibit the tumor suppressor gene *p53* by blocking its transcriptional activity[69], and the expression of these proteins is found amplified in many tumors[70–72]. These findings led to the identification of MDM2 and MDMX proteins as targets for cancer treatment. Nutlin-3a is a small molecule that can block the binding between *p53* and MDM2, through which *p53* is stabilized[73]. Nutlin-3a has been found to suppress tumor cell proliferation and promote apoptosis[74,75]. In addition, it has been shown that nutlin-3 can radio-sensitize laryngeal carcinoma cells[76]. Human trials on derivatives of nutlin-3a began recently.

When a tumor suppressor gene is mutated/deleted, its neighboring genes are often altered at the same time. These "passenger" genes are also targets of interest. A recent study was conducted to propose *ENO1* as a new target in treating glioblastomas and possibly other cancers[77]. As a part of the lp36 locus, where several tumor suppressor genes locate[78,79], the passenger gene *ENO1* is often homozygously deleted in glioblastomas. While *ENO1* still expresses in normal cells, *ENO2*, the back-up gene of *ENO1* makes the cancer cells tolerable. It was hypothesized that if *ENO2* is blocked then *ENO2* inhibitors can exclusively kill the cancer cells[77]. Furthermore, it has been estimated that among all protein-coding genes in the

human genome, 11% are deleted in cancers[80]. This *ENO1-ENO2* model can potentially be applied to other cancer types.

These "passenger events" are attracting much attention. Other alterations such as the loss of POLR2A in colorectal cancer[81] and the deletion of PSMC2 in ovarian cancer[82], are giving us a better idea in this new area of targeted therapy.

1.2.4 Immunotherapy

Cancer is a result of gene mutations; however, as a part of human body, cancer cells are still, to some extent, under the control of the body's own immune system. That is to say, cancer cells are not completely autonomous in their growth. Based on this fact, it is proposed that by stimulating the body's immune system, cancer cells can be more effectively recognized and killed.

Back in the 1990s, the role of Interferon γ (IFN-γ), a pleiotropic cytokine, in promoting host resistance to infectious organisms was unequivocally confirmed[83,84]. In 1998 it was first demonstrated that IFN-γ played a critical role in cancer *immunesurveillance*[85]. In that study the authors found mice lacking IFN-γ sensitivity were more frequently and rapidly to develop tumors when they were exposed to methylcholanthrene, a chemical carcinogen. Then in 2001 Shankaran and coworkers further revealed that by collaborating with lymphocytes, IFN-γ could restrain the development of sarcomas (carcinogen-induced) and epithelial carcinomas (spontaneous), as well as reduce *immunogenicity*[86]. However, this process would also result in the immune-selection of tumor cells that were more adaptable in the immune-competent environment. Now we understand that the action taken on cancer cells by the immune system is a duality: the immune system can suppress tumor growth on one hand, and can promote tumor growth on the other hand. This duality is called *immunoediting*[3]. It has been shown that patients who have

undergone organ transplantation have a higher risk of developing cancer due to the long-term uptake of immune-suppression medication to prevent transplant rejection[87].

Recall the hallmarks of tumor formation: one of the capabilities is evading immune destruction; without this step a tumor cannot be formed[5]. In an immune-competent host, cancer cells survive and grow, either by producing signals that can escape detection/destruction by the immune system or by making changes to make them more difficult to be detected. The idea of immunotherapy is to restore and/or to enhance the immune system to fight against cancer, either by stimulating activities of specific components of the immune system, or by counteracting those "cheating signals" produced by cancer cells.

Current immunotherapies can be classified into five main categories: tumor antigen-targeted monoclonal antibodies, immunological checkpoint modulators, cell therapy, vaccines, and immune-modifying agents[88]. Following is a brief introduction to mAbs infusion and cell therapy.

Tumor-specific monoclonal antibodies (mAbs) infusion is a passive immunization. Tumor-specific monoclonal mAbs can directly or indirectly activate immune response and result in cell death via different mechanisms[89]. About 25% of breast cancers have been found to overexpress Her2[90], the human epithelial growth factor (EGF) receptor 2. The binding of EGF and the EGF receptor controls a key cellular growth regulatory pathway. On the basis of this knowledge, blocking the binding of EGF and EGF receptor and /or inhibiting the EGF receptor kinase would possibly inhibit tumor growth.

Cell therapy is an active immunization. "Active" means that this therapy uses the natural killers in the body, T cells, to fight against cancer cells. It has been shown that *intratumoral* T cells are crucial in the overall survival of various cancers[91–93]. For example, by measuring the tumor-infiltrating T cells in tumor specimens from advanced ovarian carcinoma patients, it was found that the median overall survival (OS) of patients with intratumoral T cells is 50.3 months, which is significantly longer than that of patients without intratumoral T cells, which is 18.0 months. Moreover, the 5-year OS had a dramatic increase from 4.5% to 38%[91]. With this understanding, it was proposed that if immune cell concentration can be

11

increased locally then cancer cells can be killed more effectively. This immunotherapy is called *adoptive cell transfer* (ACT). One form of ACT is called tumor-infiltrating lymphocytes (TILs), in which cytotoxic T cells that have invaded a patient's tumor are harvested outside the human body, and then a large amount of these cells are infused back into the patient to kill cancer cells[94].

1.2.5 Hormonal Therapy

Hormonal therapy is also known as endocrine therapy, it is a therapy that targets the signaling pathway of the production of hormones, estrogen, for example. Estrogen production starts from the hypothalamus. After the signal arrives the pituitary gland, the adrenal glands, estrogen is produced and goes to the breasts. Estrogen can control the growth of breast cancer cells[95,96].

Among all breast cancer patients, 70% to 80% are estrogen-receptor (ER) and/or progesterone-receptor (PR) positive[97]; that is to say, these cancer cells can receive signals from estrogen or progesterone and therefore their growth can be promoted. These breast cancer patients are considered hormone responsive. Moreover, it has been found that estrogen and progesterone are possibly involved in tumor metastasis[98].

There are multiple ways to prevent the growth promotion caused by estrogen binding with receptors. Drugs are used to decrease the concentration of estrogen in the body. GnRH antagonists such as Leuprolide act as agonists at pituitary GnRH receptors, which interfere with the normal pulsatile stimulation and finally desensitize GnRH receptors[99]. Aromatase inhibitors such as Anastrozole interfere with the production of estrogen by blocking aromatase that is involved in transferring antigen to estrogen[100]. These two types of inhibitors can effectively reduce the estrogen level in the body, and therefore the disease can be controlled[101]. Another alternative is to directly block the binding of estrogen to its receptor on cancer cells. An example is Tamoxifen and it has achieved great success[102,103]. Dr. Daniel Rayson, a medical oncologist, said, "Any degree of estrogen receptor (ER) or progesterone receptor (PR) positivity (≥1%) indicates potential hormonally-responsive disease and identifies women

12

who are candidates for Tamoxifen". Hormonal therapy is also promising in treating other hormone-sensitive cancers like prostate cancer[104].

1.2.6 Other New Cancer Treatments

Up to now, cancer therapies are applying the "cell-killing" method to treat cancers. Researchers are also working on other strategies. A recent study by Dow and coworkers shows that it is possible to convert colorectal cancer (CRC) cells to functional normal cells[105]. It has been shown that the predominant (80%-90%) CRC-associated event is the disruption of adenomatous polyposis coli (APC), which is a tumor suppressor[106]. Dow's work shows APC loss plays an important role in the maintenance of CRC. It has been found that APC has the capability to re-establish control over crypt homeostasis in mice with aggressive polyps/cancer. APC disruption causes polyp development (ON Dox); and by restoring APC, the adenoma regresses (OFF Dox) along with the recovery of normal intestinal function.

1.3 Chemotherapy

The term "chemotherapy" was first used in the early 1990s by the German chemist Paul Ehrlich, meaning using chemicals to treat diseases. The history of cancer chemotherapy is summarized in the timetable shown in Figure 1-3[107]. Successful systematic cancer chemotherapy was marked by the use of nitrogen mustard to treat lymphoma[108]. At that moment, the time for modern cancer chemotherapy began.
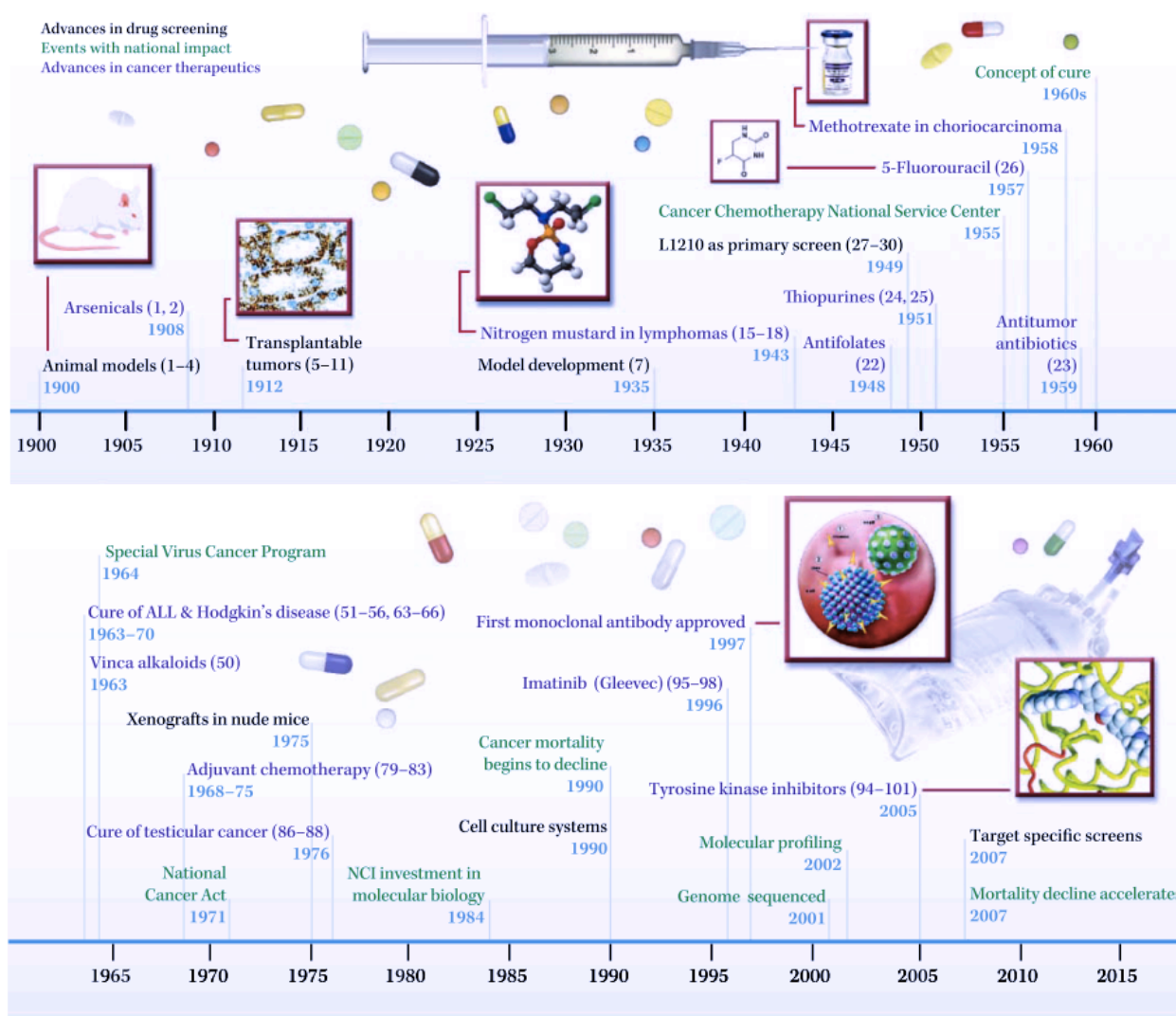
Figure 1-3: History of chemotherapy[107].

14

Chemotherapy is aimed to kill cancer cells by cytotoxic agents. Several cellular targets have been identified: DNA, DNA regulatory proteins, microtubules, and antimetabolites. Chemotherapeutic drugs targeting these cellular parts are introduced as follows.

1.3.1 Targeting DNA: DNA Cross-linking Agents

Deoxyribonucleic acid, DNA, which carries the most of the genetic information, is the target for a big family of anti-cancer agents. These agents, intended to kill cancer cells, are DNA cross-linking agents. DNA cross-linking agents are classified as alkylating agents and platinum complexes (sometimes termed semi-alkylating agents).

Alkylating agents' cytotoxicity arises from their capability of forming covalent linkage to nucleophilic sites (e.g. DNA bases) by their electrophilic/substituted alkyl groups[109]. As a result, DNA replication and transcription could be disrupted. The "cross-linking" takes place through the replacement of a hydrogen atom in a DNA molecule (or other molecules) by an alkyl radical in the alkylating agent[110].

An example of alkylating agent is mechlorethamine, which was the first alkylating agent used to treat cancer. A simplified schematic graph showing the mechanism of its action is shown in Figure 1-4:
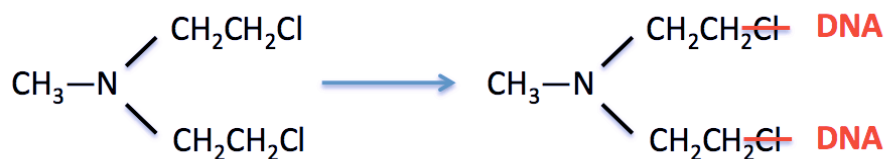
Figure 1-4: Mechanism of mechlorethamine alkylating DNA.

As can be seen, these agents possess two reactive groups and therefore they are able to form cross-links between molecules. Structurally, alkylating agents can be classified into: nitrogen mustards (aka

bischloroethylamines), nitrosoureas, and others. Alkylating agents are generally considered to have poor selectivity due to the fact that they can also alkylate nucleophilic groups on proteins[111].

Platinum complexes, especially Cisplatin, will be introduced in detail in later sections.

1.3.2 Targeting DNA Regulatory Proteins: Topoisomerase Inhibitors

Several classes of enzymes regulate the action of DNA: DNA polymerases, DNA ligase, RNA primer, DNA primase, helicases, single strand binding proteins, topoisomerases, etc. DNA topoisomerases are a crucial group of nuclear enzymes involved in a number of DNA metabolic events (replication, transcription, recombination, chromosome condensation, and segregation)[112] through the alteration of the conformation and topology of the DNA during these cellular processes, specifically by causing transient DNA breaks on one (type I) or both DNA strands (type II)[113–116]. Based on these findings, it is expected that when the enzyme-mediated DNA breaks fail to reseal, cell death could be induced, and that is how topoisomerase inhibitors/poisons execute their anticancer activities[117,118].

1.3.3 Targeting Metabolic Processes: Antimetabolites

Antimetabolites are defined as drugs that interfere with normal cellular metabolic processes[119], and they belong to an important family of cytotoxic chemotherapeutic drugs. Antimetabolites have similar structures as natural cellular molecules used in DNA and RNA synthesis, and they execute their anti-tumor activity by incorporating themselves into RNA or DNA molecules or blocking the pathways that allow a cell to make DNA/RNA and divide[120,121]. Three categories of antimetabolites are used in cancer treatment: pyrimidine antagonists, purine antagonists, and folate antagonists. Attention has been drawn to the anti-cancer activity of antimetabolites from Farber's discovery that aminopterin could cause remission of leukemia[122].

1.3.4 Targeting Microtubules: Microtubule Poisons

Precisely regulated cell cycle events guarantee the proliferation of eukaryotic cells, and it has been noticed that the cell cycle and its check points potentially make valid anti-cancer targets[123–125]. Functions of microtubules maintain cell shape and help cellular movements[126]. Moreover, the involvement of microtubules in chromosomal separation during mitosis suggests the disruption of microtubules would induce mitotic arrest and eventually cell death. Tubulins are building blocks of microtubules; microtubule poisons are classified into two main groups, based on their binding sites on tubulins and their mechanisms of action; they are: taxanes and vinca alkaloids. Taxanes block the disassembly of microtubules and thereby induce a G_2-M arrest followed by apoptosis, whereas vinca alkaloids block the assembly of microtubules. Taxanes such as paclitaxel, docetaxel, albumin-bound paclitaxel, vinca alkaloids such as vincristine, vinblastine, and vinorelbine, have all been applied in clinical cancer therapy.

1.4 Cisplatin

Platinum compounds are important cytotoxic drugs in treating cancer, and Cisplatin is the most commonly used chemotherapy drug in North America. As mentioned previously, Cisplatin, a platinum complex, is a DNA cross-linking agent that possesses anti-cancer activity. In this section, its discovery, success, and clinical limitations will be discussed. The chemical structure of Cisplatin is shown in Figure 1-5:
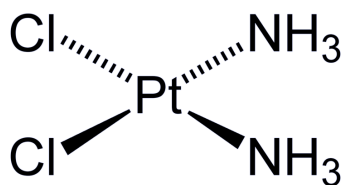
Figure 1-5: Chemical structure of Cisplatin

1.4.1 The Discovery of Cisplatin and Its Clinical Success

The discovery of Cisplatin was serendipitous and legendary. It was first synthesized in the year of 1844 by M. Peyrone[127], and the structure of which was deduced by Alfred Werner in 1893[128]. For his work of proposing the octahedral configuration of transition metal complexes Alfred Werner won the Nobel Prize in Chemistry in 1913. In the 1960s, a biophysicist Barnett Rosenberg and his coworkers put platinum electrodes into a solution. When they turned on the power, bacteria in the solution stopped dividing. At that time, platinum was considered to have no biological activity; therefore, they thought they had discovered a new way to inhibit cell division by electrical current. After two years' research in this direction they found that rather than electrical current it was a compound released from the electrode that inhibited the growth of bacteria. Rosenberg's group spent another two years to identify this compound[129,130], which is the now well-known Cisplatin.
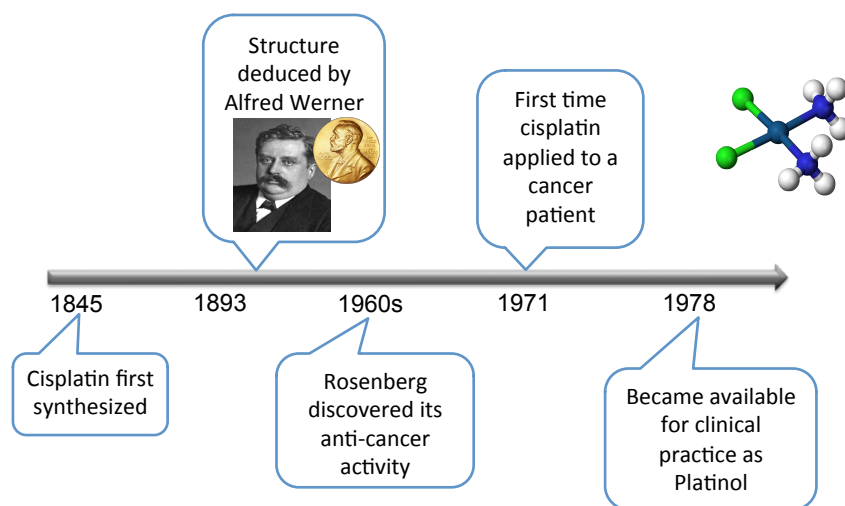
Figure 1-6: History of Cisplatin being an anti-cancer drug.

Following their previous discoveries, Rosenberg's team did further research to test if Cisplatin can inhibit cancer cell divisions and obtained positive results in mice with sarcoma[131]. In the year 1971 Cisplatin was first used to treat a cancer patient; the Food and Drug Administration (FDA) approved its clinical use in 1978.

Since being clinically used in treating cancer patients, Cisplatin has achieved great success with a broad spectrum of cancers. Across this spectrum, Cisplatin treatment of testicular cancer is phenomenal. The treatment of testicular cancer has demarcated the "pre-Cisplatin chemotherapy era" to "the era of Cisplatin"[132]. In the 1950s, the 1-year survival of metastatic testicular cancer patients was as low as 10%; now, with the help of Cisplatin, the overall 10-year survival of testicular cancer is 95%[133] and the *cure* rate of its *metastatic* disease is higher than 80%[132]. Testicular cancer is now the most curable solid tumor.

Now, Cisplatin-based treatments are considered as standard treatments for ovarian cancer[134], cervical cancer[135], lung cancer[136], head and neck cancer[137], bladder cancer[138], and lymphoma[139]. Although new therapies are emerging, platinum-based drugs are still being prescribed to 10~20% of all cancer patients, according to the NIH (National Cancer Institute).

19

1.4.2 Limitations of Cisplatin

Although Cisplatin is such a potent anti-cancer drug, its severe toxicity and the development of resistance to Cisplatin often limit its clinical application. In this section different forms of Cisplatin-related toxicities and intrinsic/acquired resistance of Cisplatin will be introduced in detail.

1.4.2.1 Cisplatin Related Toxicity

Cisplatin-related toxicities are dose-dependent, and they occur mostly on organs, including the kidneys, the nervous system, and the organ of Corti[140]. In this section, several forms of Cisplatin-induced toxicities, especially nephrotoxicity and neurotoxicity, and clinical measures to ameliorate these toxicities will be introduced.

1.4.2.1.1 Nephrotoxicity

It has been known for years that heavy metals cause human nephrotoxicity, such as renal failure with tubular injury and chronic dysfunctions[141]. Nephrotoxicity is the most common and the most clinically significant side effect associated with the administration of Cisplatin[142], and it has been the major dose-limiting toxicity[143,144]; high-dose Cisplatin treatment induces severe renal dysfunction in ~20% of patients[145].

Nephrotoxicity induced by Cisplatin presents in various forms, and these renal manifestations have been summarized by Ronald Miller[146], which are shown in table 1-1:

Cisplatin Treatment Induced Renal Manifestations	
Acute Kidney Injury (20-30%)	Hypomagnesemia (40-100%)
Fanconi-like Syndrome	Distal Renal Tubular Acidosis
Hypocalcemia	Renal Salt Wasting
Renal Concentrating Defect	Hyperuricemia
Transient Proteinuria	Erythropoietin Deficiency
Thrombotic Microangiopathy	Chronic Renal Failure

Table 1-1: Cisplatin-induced renal manifestations.

Among these types of nephrotoxicity, acute kidney injury (AKI) is the most serious as well as a very common form.

Several factors account for Cisplatin-induced nephrotoxicity. First, from the perspective of pharmacology, the kidneys are the major organs for the excretion of Cisplatin. Studies in rats suggest that after 24 hours of Cisplatin injection, 50% of Cisplatin is excreted through urine; most platinum shows up in the first hour after treatment. It has been estimated that the concentration of Cisplatin in proximal tubular epithelial cells is about 5 times higher than that in the plasma[147]. Second, it has been demonstrated that Cisplatin molecules undergo metabolic activation to become more toxic in the kidney[148,149]. Unfortunately but inevitably, other reasons for nephrotoxicity (renal cell death) are related to the cytotoxicity of Cisplatin (which will be discussed in later sections). Pathways involved in nephrotoxicity also contribute to Cisplatin's anti-tumor activity. That is to say, methods that are used to reduce Cisplatin-induced kidney dysfunction may also reduce its anti-cancer effectiveness.

Supportive measures have been developed to ameliorate nephrotoxicity caused by Cisplatin. NaCl hydration prevents Cisplatin ligand exchange and subsequent platinum-protein damage[150]; at the same time, it shortens the time that Cisplatin molecules are in contact with renal tubules[151]. The current standard method is to combine adequate hydration before, during, and after Cisplatin administration with osmotic

diuretics such as mannitol or furosemide; this method has been proved effective in mitigating the side effects of platinum compounds[152–154]. It has also been found that the prolongation of Cisplatin infusion (> 6 hrs) can reduce Cisplatin-induced renal insufficiency[155]. Besides, how drugs are given also matters; dose fractionation[156,157] and chronomodulated schedule[158] have also been proposed to lower the incidence of kidney damage and organ toxicity. In addition, different kinds of agents have been found to have the potential to ameliorate nephrotoxicity. These include antioxidant/antilipid peroxidation agents[159–162] and nitric oxide modulators & adenosine[159,163].

1.4.2.1.2 Neurotoxicity

According to the "Overview of neurologic complications of platinum-based chemotherapy" from 2016 UpToDate®, Cisplatin-induced peripheral neuropathy is summarized in Table 1-2:

Cisplatin Treatment Induced Peripheral Neuropathy				
Sensory	Motor	Reflexes	Autonomic	Recovery
Distal, symmetric loss of sensation to all modalities, stocking glove distribution; painful paresthesias or numbness	Normal	In proportion to sensory loss	Rare	Partial; may progress for several months after drug is discontinued

Table 1-2: Cisplatin-induced peripheral neuropathy.

The incidence of peripheral neuropathy is largely related to the cumulative dose of Cisplatin. Neuropathy starts to develop when the cumulative dose reaches 300 mg/m^2; and almost all patients will experience neuropathy when the cumulative dose exceeds 500 mg/m^2 [164,165]. More treatments may aggravate neuropathy and result in "generalized loss of deep tendon reflexes and more proximal vibratory sensory impairment"[164]. Moreover, time-course studies have suggested that only 11% of patients

experience neurotoxicity right after the completion of Cisplatin treatment, while the proportion goes up to 65% after an additional 3 months of treatment[140].

Generally speaking, platinum-based drugs affect the axons, myelin sheath, neuronal cell body, and the glial structures of the neurons[166]. At the cellular level, these drugs damage DNA by interfering with DNA replication and metabolism in the neurons[167], just as they do to the cancer cells. From the perspective of the whole system, platinum compounds cannot readily penetrate the blood-brain barrier. However, they can easily enter the dorsal root ganglia and peripheral nerves; that explains the finding that the dorsal root is the primary site of neurotoxicity[168]. Besides, oxidative stress and mitochondrial dysfunction have also been proposed as the reasons for neuronal apoptosis[169–171].

Some measures used to reduce platinum nephrotoxicity have been effective, such as dose fractionation and the prolongation of infusion[172]. In addition, neuro-protectants agents have been tested[156,164].

1.4.2.1.3 Ototoxicity

Ototoxicity, presented as tinnitus and bilateral high-frequency hearing loss, occurs in 75-100% of patients treated with Cisplatin, it is cumulative and possibly irreversible[173]. The formation of highly reactive oxygen radicals and the depletion of glutathione have been suggested to be responsible for Cisplatin-induced damage to the outer hairy cells of the cochlea[174]. Amifostine that has been used to reduce neurotoxicity is applied as a tissue protectant, and it has been also proved effective in reducing Cisplatin-induced ototoxicity[175].

1.4.2.1.4 Other forms of Cisplatin-related toxicities

Other forms of Cisplatin-induced side effects are also observed. Nausea and vomiting are common in patients receiving Cisplatin treatment, which can be ameliorated by adjusting the time of drug administration and the application of antiemetic agents like aprepitant[140]. Cardiovascular toxicity has also been observed short after Cisplatin infusion[140].

Overall, the most severe toxicity of Cisplatin is mainly due to the binding of the heavy-metal platinum (Pt) to proteins in kidneys[176,177]. The problem is so severe that it even prompted the call to discontinue the clinical use of Pt-based anticancer drugs[178].

1.4.2.2 Intrinsic and Acquired Resistance of Cisplatin

In Cisplatin-based cancer therapy, drug resistance is another problem. Resistance is the most important limitation for the effectiveness of cancer chemotherapy, and it accounts for more than 90% of treatment failure in patients with metastatic diseases[179]. Two forms of chemotherapy resistance are: intrinsic and acquired. In this section, both forms of resistance to Cisplatin will be discussed.

Intrinsic resistance means that before receiving the treatment, there are "resistance-mediating factors pre-exist in the bulk of tumor cells that make the therapy ineffective"[180]. Non-small-cell lung cancer, which accounts for 80-85% of lung cancer cases[181], is an example of cancer that is intrinsically resistant to Cisplatin treatment. The response rate is normally lower than 20%[182].

Acquired resistance develops during treatment which is effective initially. Compared to intrinsic resistance, acquired resistance is more complex. Causes can be mutations, cellular adaptive responses, and the activation of alternative compensatory signaling pathways[179]. One example of acquired resistance to Cisplatin is ovarian cancer. Patients generally have a good initial response rate of ~70% while the 5-year

survival rate is only 15-20%; of which the primary reason is drug resistance[183]. Another example is the small-cell lung cancer, with a reported relapse rate of ~95%[184].

Chemotherapy resistance is a self-protective strategy for tumor cells. Studies on cellular/molecular mechanisms for Cisplatin resistance are of great clinical importance. From the exposure to Cisplatin to the final cell death (apoptosis), each step provides a chance for a cell to fight and survive and hence to develop drug resistance. Chemotherapy resistance, not limited to that against Cisplatin, takes place at different levels which are summarized in Figure 1-7[179]:
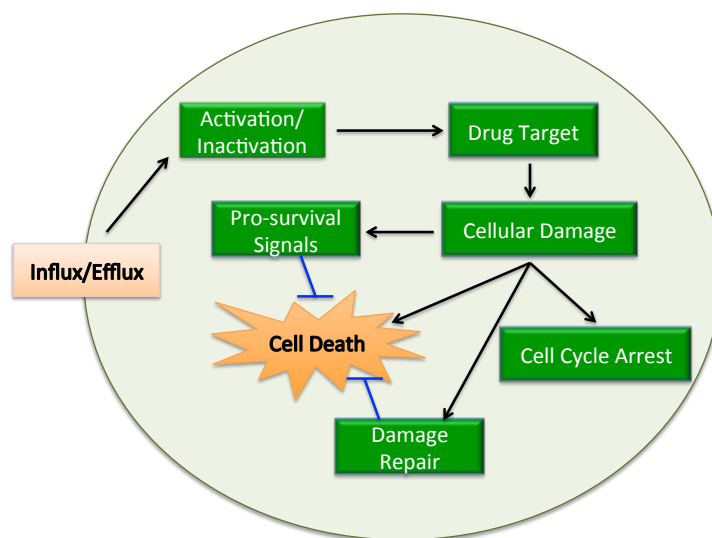
Figure 1-7: Big picture of chemotherapy resistance mechanisms.

It has been suggested by Dr. Lorenzo Galluzzi and coworkers that mechanisms accounting for Cisplatin resistance are studied based on when they occur: pre-target, on-target, post-target, and off-target[185]. (1) Pre-target resistance involves two major mechanisms: reduced intra-cellular accumulation of Cisplatin, and increased consumption of Cisplatin by scavengers like Glutathione (GSH, γ-glutamyl-cysteinyl-glycine), metallothioneins, or other nucleophilic species in the cell. Non-small-cell lung cancer, which is intrinsically resistant to Cisplatin, has a significantly higher level of GSH than that in normal lung

tissues[186]. (2) On-target resistance involves the recognition of Cisplatin-induced DNA adducts as well as the final apoptotic signal, and the DNA repair process. It has been found that in cancer cells that are resistant to Cisplatin, cellular damage recognition is often poor. The NER (nucleotide excision repair) system is responsible for the repair of DNA adducts, the major lesions caused by Cisplatin[187]. An important group of proteins participate in NER is ERCC1; it has been found that ERCC1 expression is inversely correlated with the effectiveness of Cisplatin-based treatment in several cancers, including non-small-cell lung[188], colorectal[189], and ovarian cancers[190]. (3) Post-target resistance presents as the interference with apoptosis pathways, and it can be achieved by genetic/epigenetic alterations. In approximately half of cancers, *TP53* is inactivated[191]. As we have discussed in the previous section, testicular cancer is very sensitive to Cisplatin-based treatment. It has been shown that in testicular germ tumor cells, *TP53* is almost *never* inactivated[192]. In addition, ovarian cancer patients with *TP53* mutations have a lower chance of taking advantage from Cisplatin-based treatment, compared to those do not have *TP53* mutations[193]. (4) Off-target resistance caused by signaling pathway changes that are not directly related to the exposure of Cisplatin. These changes may interfere with apoptosis signals induced by Cisplatin. HER-2 over-expression[194,195], autophagy[196,197], and the heat-shock response[198,199] have been shown to contribute to Cisplatin resistance.

Understanding the mechanisms of chemotherapy resistance to Cisplatin and other anti-cancer drugs helps to design more effective treatment.

1.5 Chemotherapy and Combination Chemotherapy

1.5.1 Why Combination Chemotherapy

The history of using drugs to treat cancers goes back at least 500 years. However, successful systematic cancer chemotherapy was actually developed in the 1940's, marked by the first clinical trial of nitrogen mustard in patients with lymphosarcoma, conducted by Gilman, Goodman, Lindskog, and Dougherty in 1942[108]. The first cured cancer by chemotherapy was reported in 1961 when women with gestational choriocarcinoma were cured by one of the antimetabolites, methotrexate[200]. Since then, various classes of anti-cancer agents have been developed, including alkylating agents targeting the DNA, antimetabolites targeting the DNA synthetic pathways, topoisomerase inhibitors targeting DNA regulatory proteins, and mitotic spindle poisons targeting microtubules[201], as discussed in the previous section.

There are two issues when single anti-cancer agents are used to treat cancer. First, currently there is no anti-cancer drug with a "perfect" selectivity. The use of these cytotoxic agents would induce toxicity more or less to normal tissues. Taking Cisplatin as an example, to get satisfactory/curing effect, the required dose is often high enough to induce severe nephrotoxicity, neurotoxicity, ototoxicity, etc[140,156,173]. Second, though many anti-cancer drugs have been shown effective, "even the most successful targeted therapies lose potency with time"[202]. Both intrinsic[203] and acquired[204] drug resistance are limiting the long-term efficacy of a single drug. Because of these two issues, clinical response from a single agent is limited.

Combination therapy was proposed to overcome these two limitations. By using two or more drugs together to treat cancer, the individual dose of each drug can be reduced and therefore the individual toxicity from each drug is expected to be limited (when they have different forms of toxicity). Meanwhile if multiple drugs are combined, the probability of selecting tumor cells that are resistant to *all* of these drugs will be lower, given they have different biochemical mechanisms of resistance[205]. Overcoming the drug resistance was "the most important factor that prompted studies of the effects of drug combination in

cancer treatment"[206]. Additionally, by combining multiple drugs that target different components of a cell and/or different cell cycles, the cell-killing efficacy may be enhanced. A classic example of the value of combination chemotherapy is the treatment of acute lymphocytic leukemia (ALL) in childhood. Before the development of the drug 6-Mercaptopurine (6-MP), the average survival for children with ALL was 3~4 months. With 6-MP's single-agent chemotherapy, remissions were induced[207]; however, subsequent courses of this mono-therapy became progressively less effective, yielding a median survival of 6 months. By using the regimen combining vinblastine, prednisone, and methotrexate with 6-MP, a > 95% of complete response (CR) was achieved and 10% of patients were *cured*; and other combinations of more drugs (7 or 10 drugs) gave > 95% of CR and 75-80% of *cure* rate[208,209].

As we can see, combination chemotherapy does give a hope to cure cancer, and different combinations give different responses.

1.5.2 Synergy Evaluation

Currently, almost all anti-cancer drugs are given in combinations; the clinical use of a combination for a specific type of cancer needs the approval from the FDA. There is a long way from bench to bedside; therefore, in order to give a better prediction on the clinical success of a combination, it is important to build accurate and robust evaluation systems for preclinical trials.

1.5.2.1 Building Good Models

To test the anti-cancer efficacy of drugs, preclinical trials include *in vitro* assays on cell cultures and *in vivo* animal experiments. When multiple drugs are used in combination, three possible interactions between/among drugs are: synergistic ("working together"), antagonistic ("working against each other"), or simply "additive" (or "expected"). Preclinical trials give us survival curves of cultures, dosages of

drugs, effective sequencings of drug administration, etc. In order to predict the clinical value from these data, a model has to be built to assess the interaction. The model should be simple but robust, and should take each drug's pharmacokinetic profiles into account[210].

Dr. Patrick Reyholds suggested five principles for *in vitro* digital image microscopy-based cytotoxicity assay (DIMSCAN) to test drug combinations; these can also be transferred to other *in vitro* tests[211]:

(a) Cell survival should cover a wide range, and the "two-log" rule should be followed[212].

(b) More than one cell line should be tested (both drug-sensitive and drug-resistant cell lines).

(c) The mechanism of each drug's resistance should be identified.

(d) The dosage and schedule should be achievable in the clinic.

(e) Effects under hypoxic conditions should be investigated.

In addition, other aspects like the growth conditions (human plasma) should be also taken into account.

After building good models and obtaining concentration-effect curves, whether or not synergy exists between two/multiple drugs is ready to be assessed. When researchers get the raw data, the most important task is to extract biological significance from the statistical significance, which remains challenging, although a number of sophisticated methods have been developed[213]. Different evaluation methods will be introduced in this next section.

1.5.2.2 Synergy Evaluation Methods

1.5.2.2.1 Fractional effect analysis

The first synergism analysis method, which was proposed by Webb in 1963, is known as the fractional effect analysis, and remains the simplest and the most straightforward method[214]. Based on this method, when the observed effect is greater than the product of the effects of each individual agent, the combination will be considered synergistic. Survival from the calculated product of the effects of each

agent is called the "additive" or "expected" survival. By comparing the observed and the expected curves, synergy can be concluded when the observed survival is lower than that of the expected.

The fractional effect method is the most straightforward. Based on this analysis the "additive" effect of two drugs is assumed be the product of the fractional activities:

$$(f_u)_{1,2} = (f_u)_1 \times (f_u)_2$$

In the above formula, $(f_u)_{1,2}$ represents the *expected* fraction of the system unaffected by the combination treatment of drug 1 and 2. $(f_u)_1$ and $(f_u)_2$ represent the fractions of the system unaffected by the treatment of drug 1, and drug 2, respectively.

This expression agrees with the nonexclusive first-order behavior. It means the fractional product method cannot be used for cases where drugs are mutually exclusive. As a result, if two drugs with similar mechanisms of action are used in combination, their interaction cannot be analyzed using this method. In addition, by using this method it is assumed that the concentration-effect relationship is hyperbolic. However, different drugs exhibit different survivals (sigmoidal or flat sigmoidal curves), so this method does not apply to all cases. Moreover, only a mathematical expression is considered in this model, no biology is taken into account. Furthermore, only when the dose-effect relationships of the two drugs follow Michaelis-Menten-type hyperbola (m=1) can the fractional product method be used.

Though the application of the fractional effect method is highly restricted, it is still frequently used due to its simplicity[215]. This fractional effect analysis will be used in this thesis for the evaluation of synergy.

1.5.2.2.2 Other synergy evaluation methods

Another synergism analysis method is to plot isobolograms of the effects from using single/combined drugs, which has been taken as the gold standard in the assessment of synergism[216,217]. From *in vitro* cell survival experiments of single agents A and B, a straight line connecting their equally effective (e.g. 50%

of the untreated, IC_{50}) doses gives the additive isobole for that specified effect (killing 50%). Through survival experiments testing the combination of A and B, "pairs" of concentrations that give the same cell-killing/survival (IC_{50}) can be determined. These "pairs" are used to plot the "iso-effect" curve. If the plotted curve is lower than the additive isobole, the tested combination is considered as synergistic; if the curve is higher than the isobole, the combination is considered as antagonistic.

Based on the isobologram method, Berenbaum introduced the "interaction index" in 1989[217] to numerically indicate if a combination is synergistic or antagonistic. This index can be used for not only two-drug combinations, but also multiple-drug systems. The "additive curves" are defined by:

$$\sum_{i=1}^{n} \frac{d_i}{D_i} = 1 \ (i = 1, 2, \dots, n)$$

When the sum of observed effects of a given combination is smaller than 1, the combination is considered as synergistic; when the observed value is greater than 1, the combination is considered as antagonistic. The response surface approach was introduced based on the isobologram method[218]. However, it is not frequently used due to its mathematical complexity.

Chou and Talalay developed the median-drug effect method in 1984[219], and this method has been applied to assess potential synergism among different drugs. This method takes the drug combination as a "single" and a "new" drug. Therefore, to test the concentration-survival curve of this new drug, the ratio of individual drugs should be fixed; that is to say, the relative effect of each drug in this ensemble is fixed. The mathematics of this method will not be introduced due to its complexity.

Combination therapy has achieved some success in cancer treatment when components in a combination have a favorable pharmacological interaction (same target, but different large-organ toxicities), as commented by Dr. Edward Sausville. However, the development of a drug combination is not an easy task, in the sense of the time and effort put before it could be clinically applied. Making the best out of preclinical models and overcoming intrinsic and extrinsic barriers of combination therapy are

the next step after we get a "good idea". Very often successful preclinical studies fail in clinical trials[220]. Poor concordance between preclinical and clinical results comes from: when molecular heterogeneity cannot be fully reflected by limited cell line models; when optimal dosing and sequencing of agents cannot be determined by limited attempts; and when the sensitivity or resistance cannot be completely determined by limited attempts[221]. Despite all the efforts made on developing these methods, none is perfect. Future work should not only rely on models, but also on more precise understandings of biological interactions between/among drugs.

1.6 Combination Chemotherapy of Cisplatin: A Literature Review

Cisplatin is a potent anti-cancer drug and one of the few curative agents of treating cancer. Current cancer chemotherapy often combines two or more drugs together to increase the therapeutic effect, to reduce chemo-resistance, and to limit the toxicity induced by each agent in the combination. To treat a certain kind of cancer, pre-clinical combination design first takes drugs that have been shown active in treating this cancer into consideration; in order to reduce toxicity and to circumvent cross-resistance, drugs targeting different mechanisms and cell cycles are frequently studied. Though combinations are designed rationally and some of them have been proved effective in the clinic, precise mechanisms are not always clear and therefore it is not easy to predict the efficacy of a designed combination regimen without being clinically confirmed. This section reviews pre-clinical and clinical studies investigating the effectiveness of Cisplatin combined with topoisomerases, antimetabolites, microtubule poisons, and antibodies.

1.6.1 Cisplatin Is Often Used in Combination

Being introduced into clinical practice in 1971 after preclinical trials[222], Cisplatin has achieved great success in treating a broad spectrum of cancers. Despite being such a potent and one of the few curative anticancer drugs, its clinical application is often restricted by its side effects[140] and drug resistance[185]. This inspires the discovery of other platinum-based agents[223]. Along with more clinical data and better understanding of Cisplatin, the expectation has evolved from "a less toxic but equally efficacious analogue", to a compound "possessing sufficient oral bioavailability", and finally to one "capable of circumventing Cisplatin resistance"[224], which gives birth to the second generation of platinum drug carboplatin that has a lower overall toxicity [225,226], and the third generation of that oxaliplatin that does not have cross-resistance with Cisplatin or carboplatin [227,228]. Moreover, supportive clinical measures and some protective agents, on the other hand, are proposed and applied to reduce Cisplatin-induced side

effects[140,229–233]. Though extensive studies have been carried out, the resistance of Cisplatin remains the major limitation in its clinical use. As a single agent, Cisplatin therapy normally gives an excellent initial response rate; however, there is a high rate of tumor recurrence in some cancers because of acquired resistance[184,234]. Combining two or more drugs is now the standard clinical cancer treatment. Attacking different targets or interfering with different parts of the cell cycle to achieve synergy, reducing drug resistance, and decreasing drug toxicity from each drug are all reasons for using multiple drugs to treat cancer and for designing drug combinations.

Here the combinations of Cisplatin and topoisomerases, antimetabolites, microtubule poisons, and antibodies are individually introduced.

1.6.2 Cisplatin in Combination with drugs targeting DNA-regulatory proteins

Chemotherapeutic agents targeting DNA regulatory proteins have been introduced in the previous section; and Cisplatin is often combined with these agents.

Irinotecan, as a semisynthetic camptothecin derivative, is a type I topoisomerase inhibitor that stabilizes topoisomerase I –DNA cleavable complexes[235–237]. Based on their different mechanisms of action[238], relatively different toxicity profiles[140,239], and lack of cross-resistance[240,241], Cisplatin and irinotecan have been used in combination to treat cancer.

Lung cancer is the leading cause of cancer death[242]. Cisplatin and irinotecan, both of them have been proved effective in treating lung cancer[243]. The combination of these two agents has also been confirmed synergistic both pre-clinically[244,240] and clinically[245]. Etoposide, a type II topoisomerase inhibitor, combined with Cisplatin (PE), used to be the standard treatment for small-cell lung cancer (SCLC); the response rate of which ranges from 60% to 90% and the median survival ranges from 8 to 11 months[246–248]. Compared with PE, the PI regimen is proved more effective shown in medium survival (12.8 months vs. 9.4 months), one-year survival (58.4% vs. 37.7%) and two-year survival (19.5% vs. 5.2%)[249]. The PI

34

combination regimen has also been assessed in elderly patients with extensive-disease SCLC and this regimen has been also confirmed effective[250]. A triplet combination regimen including Cisplatin, irinotecan, and etoposide (PIE) has been studied on extensive SCLC[251], the medium survival is increased to 15.1 months, suggesting that the PIE regimen is a more efficacious combination. Another triplet by adding another topoisomerase-I inhibitor, topotecan, to the standard PE regimen, has also been investigated but is shown not beneficial in enhancing response or survival in extended stage SCLC patients[252]. Furthermore, as a type of cancer that is sensitive to both chemotherapy and radiation therapy, limited-disease SCLC has been shown to be more responsive to the PI regimen combined with radiotherapy[253]. The PI regimen has also been tested and appears to be acceptable for the treatment for advanced thymic carcinoma, for which the optimal chemotherapeutic regimen is still being investigated[254].

Other combinations of topoisomerase inhibitors and Cisplatin, such as belotecan combined with Cisplatin to treat extensive stage SCLC[255], have also given promising results.

1.6.3 Cisplatin in Combination with Antimetabolites

Antimetabolites have been introduced in the previous section. The combination chemotherapy of Cisplatin and antimetabolites is a common regimen.

5-Fluorouracil (5-FU), as an analogue of uracil with a fluorine atom instead of hydrogen at the C-5 position, is first metabolized to its active forms (FdUMP, FdUTP, and FUTP), and these active metabolites could disrupt DNA/RNA synthesis and inhibit the action of thymidylate synthase that is a nucleotide synthetic enzyme[256]. The combination of 5-FU with Cisplatin has been extensively studied. Synergy is observed pre-clinically when Cisplatin is administered before 5-FU, as the first antimetabolite combined with Cisplatin[257–261]. Reasons for 5-FU potentiating the cytotoxicity of Cisplatin are attributed to the modulated repair of platinum-DNA adducts[257], increased levels of intracellular reduced folates[258,259], and increased DNA fragmentation[260]. It has been also shown that the ERCC1 gene encodes a protein

participating in the excision step in nucleotide excision repair (NER), through which the amount of platinated DNA could be increased[262]. Moreover, it has been found that if 5-FU exposure is given after Cisplatin, the increased gene expression responsible for the two drugs' resistances can be repressed; therefore, synergistic cytotoxicity is achieved[263].

Penis cancer is a rare cancer[264]. The response rate of penis cancer to Cisplatin is only 23%[265–267], and that of the PI combination regimen is reported to be 30.8%[268]. By combining Cisplatin and 5-FU (PF) to treat advanced squamous carcinoma of the penis, the average response rate is increased to 63%[269–271], which makes the PF regimen the standard treatment for penis cancer. This combination regimen is also used to treat advanced head and neck cancer: a 40% 9 months' survival is achieved by using the combination, compared to 24% of that by Cisplatin alone and 27% by 5-FU alone[272]. Moreover, the PF regimen has also been proved fairly active in treating SCCHN. Hypopharynx cancer, for example, has been treated with the PF regimen followed by radiation and this phase III trial has proved that this treatment could make larynx preservation feasible[273]. The PF regimen is also used to treat oropharyngeal cancer as a neoadjuvant chemotherapy followed by loco-regional treatment (radiotherapy and/or surgery), compared with loco-regional treatment alone. The overall survival is significantly prolonged from 3.3 years in the loco-regional treatment group to 5.1 years in the group with neoadjuvant chemotherapy[274].

Gemcitabine, a nucleoside analogue, has anti-tumor effect on various solid tumors[275,276] by incorporating itself into cellular DNA[277–279]. Synergy between Cisplatin and gemcitabine was first found on cell lines[280,281], and the mechanism was attributed to the effects of gemcitabine on intracellular Cisplatin pharmacokinetics[281]. Biliary tract cancer, being an uncommon cancer, often presents as an advanced disease when diagnosed. Though some agents have proved active, including Cisplatin[282], gemcitabine[283], and fluoropyrimidines[284,285], there is no consensus on the standard regimen for treating patients with locally advanced or metastatic biliary tract cancer,. A randomized phase II study was initially conducted to evaluate the combination regimen of Cisplatin with gemcitabine, because the

progression-free survival was prolonged this study was extended to a phase III study[286]. According to this study, the median overall survival is prolonged to 11.7 months by using Cisplatin combined with gemcitabine, compared to 8.1 months by using gemcitabine only, the progression-free survival is improved to 8.0 months from 5.0 months, and the tumor control rate is also increased from 71.8% to 81.4%; these results make the Cisplatin and gemcitabine combination regimen an option for treating patients with advanced biliary cancer.

A phase III study of the treatment of NSCLC comparing Cisplatin and gemcitabine with Cisplatin and pemetrexed has been conducted, showing that the overall survival of these two regimens are comparable (10.3 vs. 10.3 months). The Cisplatin and pemetrexed regimen works better in patients with adenocarcinoma and large-cell carcinoma histology (12.6 compared to 10.9 months) while the Cisplatin and gemcitabine regimen works better in patients with squamous cell histology (10.8 compared to 9.4 months)[287].

1.6.4 Cisplatin in Combination with Microtubule Poisons

Based on the different anti-cancer mechanisms of microtubule poisons and Cisplatin, they have been combined with the hope to achieve clinical synergy.

Ovarian cancer is the eighth most common cancer in women[242]. Due to its seldom early diagnosis it often progresses to advanced stage when diagnosed[288] and is the most lethal gynaecological cancer[289]. Chemotherapy is the first-line treatment after surgical cytoreduction for ovarian cancer. After Cisplatin's failure as a single-agent in treating ovarian cancer due to resistance, paclitaxel (Taxol) gained clinical attention as a single anti-cancer agent[290–292] by achieving an overall response rate of 37% in platinum-treated patients[293]. Further success was achieved by combining Cisplatin and paclitaxel to treat stage III and stage IV ovarian cancer, the response rate of which was 73%, and the median survival was 14 months longer than that of the previous combination of Cisplatin and cyclophosphamide (38 vs. 24 months)[294].

Besides ovarian cancer, the Cisplatin-paclitaxel combination has become the first-line chemotherapy for several other types of cancer, including advanced non-small-cell lung cancer[295], advanced gastric cancer[296], advanced breast cancer[297], and metastatic esophageal cancer[298].

Docetaxel, another kind of taxanes, is also applied in combination with Cisplatin to treat advanced ovarian cancer[299] and gastric carcinoma[300].

The triplet combination of Cisplatin, docetaxel, and 5-FU (TPF) used as induction chemotherapy has also been investigated. The activity of the PF regimen in SCCHN has been discussed earlier and the taxanes have also been confirmed effective in treating SCCHN as single agents. Therefore Cisplatin combined with 5-FU and docetaxel might be a possible combination for SCCHN and this triplet regimen has been proved effective in clinical trials[301,302].

1.6.5 Cisplatin combined with antibodies (targeted therapy)

Cetuximab is a chimeric monoclonal antibody (mouse/human) directed against the extracellular domain of the epidermal growth factor receptor (EGFR) that is overexpressed in one third of human cancers and has been shown to be related to tumor growth and progression. Due to its capability of binding to EGFR and disrupting its function, the antibody is proposed to possess anti-cancer activity[303]. Early clinical studies of cetuximab have been well reviewed[304].

Squamous cell carcinoma of the head and neck (SCCHN), a collective type of cancer that originated from the skin, nasal cavity, paranasal, sinuses, oral cavity, salivary glands, pharynx, and larynx, of which 90% are squamous cell carcinoma of the mucosal surfaces of the head and neck[305]. The expression of EGFR is almost invariably expressed in SCCHN and the overexpression of EGFR is often related to poor prognosis[306]. Therefore, cetuximab could be a candidate to treat SCCHN. Experiments on cell lines and xenografts have both confirmed the activity of cetuximab[307,308]. Moreover, it has been shown that Cisplatin's efficacy is enhanced by cetuximab[309] without affecting its pharmacokinetic profile[310]. Based

on these findings, the combination of Cisplatin and cetuximab is thought to have a better therapeutic effect on SCCHN. A phase IB clinical study of Cisplatin and cetuximab combination regimen has been conducted on patients who were pre-treated with Cisplatin and who showed resistance to Cisplatin therapy, and the result has shown this regimen effective[311]. A randomized phase III study in patients with metastatic and/or recurrent head and neck cancer has been conducted to investigate the efficacy of the combination of Cisplatin and cetuximab. The result shows that patients receive weekly cetuximab plus a Cisplatin-cetuximab combination every 4 weeks have an objective response rate of 26% and a median survival of 9.2 months, compared to 10% and 8.0 months of that by Cisplatin mono-therapy[312]. Additionally, the Cisplatin and cetuximab combination regimen has also been suggested as a possible second-line treatment after progression on platinum-based chemotherapy. A phase II study of the combination chemotherapy of Cisplatin and cetuximab in patients with recurrent and/or metastatic SCCHN has been conducted to confirm the efficacy of this regimen[313]. A response rate of 10% and a median survival of 183 days are achieved, compared to 2.6% and 103 days in patients with advanced SCCHN progressed on platinum-based treatment[314].

Recent clinical studies have tried to combine cetuximab, Cisplatin, and another anti-cancer agent to enhance the chemotherapeutic effect. A phase III clinical study shows that the response rate is increased from 20% (Cisplatin and 5-FU) to 36% (Cisplatin with 5-FU and cetuximab), the progression-free survival is increased from 3.3 months to 5.6 months, and the overall survival is prolonged from 7.4 months to 10.1 months[315], making Cisplatin with 5-FU and cetuximab the standard systemic treatment for R/M (recurrent or metastatic) SCCHN. Furthermore, pemetrexed as a folic acid inhibitor has also been tried in combination with Cisplatin and cetuximab, but no improvement is achieved compared with the standard treatment, and on the other hand this regimen is shown to have a higher treatment-related death rate (7.6%)[316].

1.6.6 Discussion of Cisplatin-Based Combination Chemotherapy

In spite of the better and deeper understanding of the nature and causes of cancer, and various therapies to treat cancer, chemotherapy remains a required treatment in many situations. Cisplatin, as an "old" but one of the most widely prescribed anticancer drugs, is still of great clinical importance. As one of the most effective chemotherapeutic drugs used in the clinic, Cisplatin is often used in combination with topoisomerase inhibitors, antimetabolites, microtubule poisons, and antibodies. In order to design rational combinations, synergy is attempted by targeting different cellular mechanisms, interfering with different parts of the cell cycle, and using drugs with confirmed activity in treating certain types of cancer. Also, relatively distinct toxicity profiles and not being cross-resistant should be considered.

Some proposed rules/principles have been helpful in investigating combinations to treat cancer. Cisplatin as an alkylating-like agent acts similarly with the alkylating agent cyclophosphamide. Therefore, the combination of Cisplatin and paclitaxel, which act more distinctly, should be more effective. These two combinations of Cisplatin with cyclophosphamide and Cisplatin with paclitaxel have been compared to treat stage III and stage IV ovarian cancer. The results have shown the latter combination is superior in terms of both response rate (73% vs. 60%) and median survival (38 months vs. 24 months)[294].

Though Cisplatin-based combination chemotherapy has achieved some success in the clinic, issues remain for further investigation. First, from the perspective of combination design, macroscopic guidance does not always guarantee clinical success. For example, the triplet combination including Cisplatin, etoposide, and irinotecan significantly enhances the therapeutic effect, whereas a similar triplet combination including topotecan plus the PE (Cisplatin and etoposide) regimen does not[251,252]. Drugs are normally combined because both/all of them are active in treating a certain kind of cancer and therefore it is anticipated that the combined effect will be enhanced. But this is not always confirmed by clinical trials. Second, most of these combinations are dependent on the types of cancer, drug sequence, and the population selected for study. For example, the combination of paclitaxel and Cisplatin shows synergy in

treating ovarian cancer whereas not in treating SCLC[317]. The same combination regimen, administered in different sequences, sometimes gives opposite conclusions. Clinical trials comparing the effectiveness of PE and PI regimens in treating SCLC by the Japanese Cooperative Oncology Group (JCOG) and by Nasser Hanna et al. give different answers[249,318]. Contradictory results could be explained by the difference between Asian and Western populations. Moreover, recent studies have confirmed that no superiority is observed in extensive-stage SCLC patients treated with PI compared with PE in Western patients[319,320]. In addition, it has also been demonstrated that survival could be different depending on the histological type of a certain cancer[287]. Besides, combining drugs sometimes introduces additive toxicity. For example, with the PIE regimen in treating extensive SCLC, the addition of the third agents induces myelosuppressions[251]. Another example is that the combination of Cisplatin with cetuximab and pemetrexed has been proved to have a higher rate of drug-related deaths[316]. Though the initial hope is to reduce the dose and toxicity from each individual agent, it is not surprising that additive toxicity is observed in some combinations if all agents are toxic.

To achieve the best chemotherapeutic effect of a combination, the dosing of each agent is crucial, which involves the balance between maximizing efficacy and minimizing toxicities. Taking the combination of Cisplatin and topoisomerase inhibitors as an example, the commonly used dose of Cisplatin is 80-100 mg/m^2, and that of a topoisomerase inhibitor is 0.4 mg/m^2/d. While in the combination of Cisplatin and belotecan[255], the dose of Cisplatin is 60 mg/m^2 and that of belotecan is 0.5 mg/m^2/d. The reason for lowering the dose of Cisplatin is to reduce its toxicity. The increase of the dose of belotecan is due to the fact that belotecan as a single agent has been proved highly active against SCLC. On the other hand, possible increase of hematologic toxicity of this combination is the primary concern.

Efforts, money, time, and hundreds of lives of patients are all used in each clinical trial. The trials to compare the chemotherapeutic effect of two different combination regimens often result in no or only a little improvement of several months more survival. Combinations including "similar anti-cancer agents"

sometimes give different results. It seems like there is chance behind the mechanisms. Likely the low

success rate of combination designs is due to the poor understanding of each agent in a combination.

1.7 Project Motivation and Theory: A Novel Combination Chemotherapy of Cisplatin and Rhodamine-B

Although Cisplatin-based cancer treatment has achieved success in the clinic, our understanding of its activity is not deep enough. The inaccurate and incomplete understanding of the great anti-cancer drug Cisplatin prevents patients from taking the most advantage of it. Here we are going to propose a Cisplatin-based combination chemotherapy regimen based on its precise mode of action.

1.7.1 Understanding of Cisplatin's Anticancer Activity

In this section, a brief review of the current research status of Cisplatin and its anticancer activity will be given. In particular, molecular processes taking place before Cisplatin molecules bind to the DNA will be emphasized.

1.7.1.1 Cellular Response to Cisplatin

Before entering the cell, Cisplatin molecules react with proteins like serum albumin[321]; as a result, its bioavailability is limited by the extracellular environment. Cisplatin enters the cell by both passive diffusion[322] and active transport[323], including carrier-mediated import via OCTs (organic cation transporters) and Ctr1 (copper transporter 1), and endocytosis[321]. Once entering the cell, only 1% of intracellular Cisplatin molecules can reach the nuclear DNA[324]. The majority of Cisplatin molecules react with other cellular biomacromolecules. For example, thiol-containing molecules deactivate Cisplatin molecules before reaching nuclear DNA[325]. Among those thiol-containing molecules, glutathione (GSH, tri-peptide gamma-glutamyl-cysteine-glycine) is the most important sulfhydryl compound that leads to Cisplatin resistance[326], as discussed previously.

43

Besides, more recent studies have suggested that mitochondria might be another important target of Cisplatin[327].

1.7.1.2 DNA Lesions Caused by Cisplatin

It has been believed that DNA is the major target of Cisplatin[328]. Studies of the mechanism of Cisplatin suggest that its anti-cancer activity comes from the covalent modification of DNA, which induces distortions in the structure of DNA, and finally triggers cell death events[329].

Competition studies have indicated that Cisplatin preferentially reacts with guanine bases[330,331]. DNA of salmon sperm treated by Cisplatin has been quantitatively analyzed, showing Cisplatin mainly forms intra-strand 1,2-GG adducts (60-65%) and intra-strand 1,2-AG

Figure 1-8: Cisplatin-DNA cross-links[334].

adducts (20-25%), with the remaining being inter-strand G-G cross-links and intra-strand cross-links between non-adjacent G bases[332,333]. Crystal structure of Cisplatin-DNA adducts and the resultant DNA bending and unwinding have been demonstrated by x-ray crystallography study[334], as shown in Figure 1-8. The structure of these adducts has also been verified by NMR study[335]. Furthermore, other studies have suggested that Cisplatin-DNA adducts are recognized by high-mobility group (HMG) containing proteins[336,337], which shield the repair of DNA cross-links via the nucleotide excision repair (NER) pathway[338,339], as introduced in Section 1.4.2.2.

1.7.1.3 Hydrolysis of Cisplatin

The final products from the interactions of Cisplatin with DNA have been identified, but the molecular reactions still need to be investigated. As the structures indicate, before binding to DNA, a Cisplatin molecule needs to lose its two chlorine atoms.

It has been long believed that an aquation process must occur before Cisplatin molecules can modify DNA[340]. The process involves a sequential replacement of two chlorine atoms by two water molecules. The resultant aqua-complexes bind to purines and cause DNA damage[332, 334, 341], which blocks cell division and results in apoptosis. Cellular biological processes of Cisplatin are shown in Figure 1-9[342] and the one interferes with DNA is highlighted:
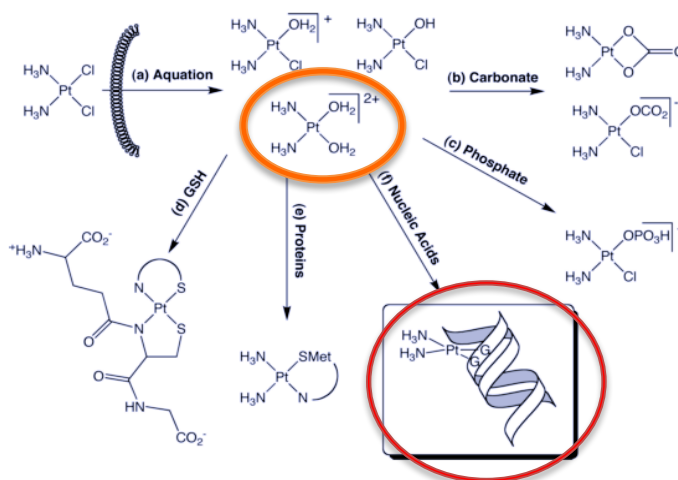
Figure 1-9: Cellular biological processes of Cisplatin[342].

Although the hydrolysis process has been widely accepted, some questions remain unanswered. Dr. Lu has challenged this mechanism from different aspects[343]. First and foremost, this hydrolysis mechanism cannot explain the sequence-selective binding of Cisplatin to DNA. Second, the main product of the hydrolysis of Cisplatin is $[PtCl(H_2O)(NH_3)_2]^+$ that cannot bind to two neighboring guanine bases; while the species that can form DNA cross-links, $[Pt(H_2O)_2(NH_3)_2]^{2+}$, is very difficult to form under

physiological conditions and has been considered "the least important of all the potential hydrolysis products available to bind to replicating DNA at pH=7.4" [344,345]. Moreover, it has been estimated that the rate constant for Cisplatin hydrolysis is only about $10^{-4} \, M^{-1} s^{-1}$ [344], at low Cl^- concentrations and a higher temperature (45°C), and in solvents such as $HClO_4$ and $NaClO_4$. It is reasonable to infer that the reaction rate would be even lower under physiological conditions (37°C, water environment) [344]. All these considerations indicate that there may exist another mechanism that is responsible for the chloride-bond breaks.

1.7.2 DET Mechanism of Cisplatin and Its DET-based Combination Chemotherapy

In contrast to the conventional approach to synthesize and screen a huge number of Cisplatin-like compounds, our group attempted to apply fs-TRLS to unravel the precise molecular mechanism of Cisplatin.

First, Dr. Lu[346] discovered the molecular mechanism explaining why low-dose Cisplatin can significantly enhance the therapeutic efficacy of radiotherapy, and found that it was due to the extremely effective dissociative electron transfer (DET) reaction of Cisplatin with the generated pre-hydrated electron (e_{pre}^-):

$$e_{pre}^- + Pt(NH_3)_2Cl_2 \rightarrow [Pt(NH_3)_2Cl_2]^{*-} \rightarrow Pt(NH_3)_2Cl^{\bullet} + Cl^-$$

$$e_{pre}^- + Pt(NH_3)_2Cl \rightarrow [Pt(NH_3)_2Cl]^{*-} \rightarrow Pt(NH_3)_2^{\bullet} + Cl^-$$
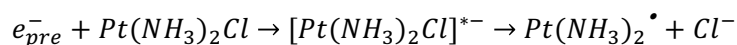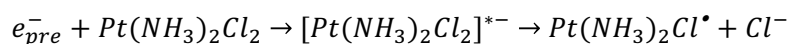
The resultant cis-$Pt(NH_3)_2$ radical very effectively leads to DNA strand breaks[346]. Second, we showed that for chemotherapy, Cisplatin indeed preferentially attracts two electrons from two neighboring guanine bases in DNA, since guanine is the most favored electron donor in DNA[343]:

$$G + Pt(NH_3)_2Cl_2 \rightarrow G^+ + [Pt(NH_3)_2Cl_2]^{*-} \rightarrow G^+ + Pt(NH_3)_2Cl^{\bullet} + Cl^-$$

$$G + Pt(NH_3)_2Cl \rightarrow G^+ + [Pt(NH_3)_2Cl]^{*-} \rightarrow G^+ + Pt(NH_3)_2{}^{\bullet} + Cl^-$$
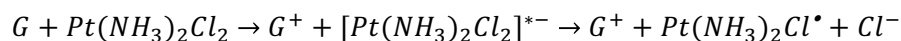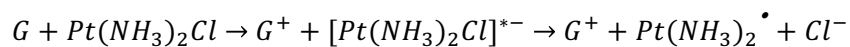
In contrast, a weaker DET reaction of Cisplatin with DNA base A and no DET reactions with C and T were observed. This DET mechanism has uncovered the long-existing mystery of why Cisplatin results in a preferential binding of the cis-Pt(NH$_3$)$_2$ to two neighboring G bases in DNA[343]. Subsequently, this EDT mechanism of Cisplatin has been confirmed both experimentally by Kopyra et al. [347] in studying dissociative attachments of nearly 0 eV electrons to gas-phase Cisplatin, and theoretically by Kuduk-Jaworska[348] et al. in their quantum chemical studies of the reaction between the pre-hydrated electron (e_{pre}^-) and aqueous Cisplatin. This new mechanistic insight has great potential to improve existing therapies using Cisplatin and enable novel combination treatments for challenging cancers.

Taking advantage of our discovery of the dissociative-electron-transfer (DET) mechanism of Cisplatin as a chemotherapeutic drug[343] and its combination with radiotherapy[346], we aim to identify effective molecular promoters (PMs) to enhance the cytotoxicity of Cisplatin, to overcome the drug resistance, and to widen the application of Cisplatin to other cancers such as breast cancer that are insensitive to Cisplatin. In view of the extremely high electron reactivity of Cisplatin we hypothesize that the DET reaction of an electron-donating agent with Cisplatin will generate the reactive radical and thus enhance the cytotoxicity of Cisplatin. Therefore, we have rationally identified several molecular promoters that have a high potential to result in a synergistic effect with Cisplatin. Notably, these compounds must be electron donors, biocompatible, and essentially non-toxic. A free PMx molecule is expected to react with Cisplatin via the DET reaction inside the cancer cell:

$$PMx + Pt(NH_3)_2Cl_2 \rightarrow PMx^+ + [Pt(NH_3)_2Cl_2]^{*-} \rightarrow PMx^+{:}Cl^- + Pt(NH_3)_2Cl^{\bullet}$$
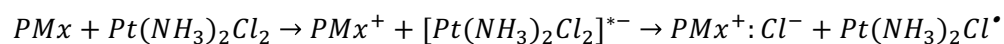
The resultant Pt(NH$_3$)$_2$Cl$^{\bullet}$ or Pt(NH$_3$)$_2{}^{\bullet}$ (by further reaction with another PM molecule) radical can lead to DNA strand breaks[346], adding to the intra-strand cross-links induced by Cisplatin alone. It is well

47

known that among various forms of DNA damage the most dangerous is the DNA double-strand break (DSBs), which is difficult to repair and is a potent inducer of mutations and cell death.

We have tested one such compound, tetramethyl-*p*-phenylenediamine (TMPD), in combination with Cisplatin and obtained very encouraging results from measurements of DNA strand breaks, cell viability, cytotoxicity, DNA fragmentation, cell cycle checkpoint induction, and apoptosis[349]. These preliminary studies suggest a very promising femtomedicine strategy and strongly motivate us to continue this direction of research towards a final goal of developing highly effective combination chemotherapies. This novel and innovative approach may offer a highly effective and economical strategy to develop combination therapies for use in the clinic.

TMPD is a well-known biochemical electron donor used in biological system[349], but it also shows some toxicity. In addition, the enhanced anti-cancer activity relies on its solvent ethanol. These limitations may make this combination clinically intolerable and/or ineffective. Thus, our new goal is to find better PMs that have no or little toxicity in its "effective concentration range" when combined with Cisplatin.

1.7.3 Combination Chemotherapy of Cisplatin and Rhodamine-B

This thesis aims to investigate a novel combination chemotherapy of Cisplatin with Rhodamine-B (RDM-B). Oxidation of Rhodamine-B has been well studied in the literature. Particularly, photo-induced electron transfer from Rhodamine-B has been discovered[350–353]. The chemical structure of Rhodamine-B is shown in Figure 1-10:
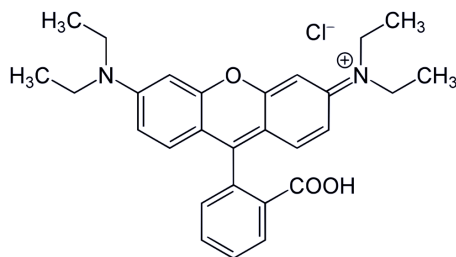
Figure 1-10: Chemical structure of Rhodamine-B

And the mechanism for the proposed combination is shown in Figure 1-11:
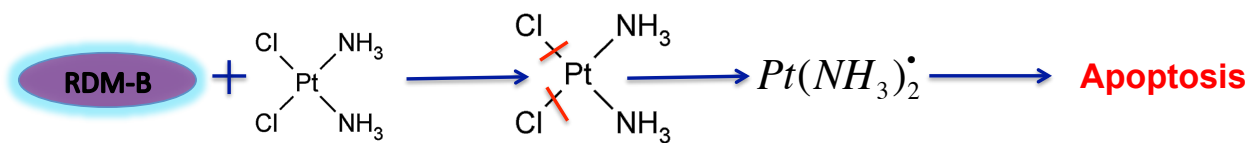
Figure 1-11 Mechanism of DET-based combination chemotherapy of Cisplatin and Rhodamine-B.

As the schematic figure shows, Cisplatin can capture two electrons from Rhodamine-B and its two chlorine atoms will then leave the molecule; the resultant radical can attack DNA and induce apoptosis.

This project will perform in-depth *in vitro* and *in vivo* studies of the novel combination therapy of Rhodamine-B and Cisplatin against various cancers, and will provide spectroscopic evidence of the electron transfer reaction between these two molecules. These results will be presented and discussed in later Chapters.

Chapter 2
Cisplatin Intrinsically Induce Double-Strand Breaks

It is well-known that Cisplatin induces cross-links in DNA and they are believed to be responsible for the cytotoxicity of Cisplatin. DNA double-strand breaks (DSBs) induced by Cisplatin have been observed but were considered to arise from the repair process of DNA cross-links. In this Chapter we investigate the formation of Cisplatin-induced DNA DSBs. First we expose human cervical (HeLa) cancer cells to Cisplatin and monitor the formation of DNA DSBs by labeling the phosphorylation of histone H2AX, a marker of DNA DSBs. Our observations confirm the formation of DNA DSBs in HeLa cells. Second, by applying agarose gel electrophoresis, plasmid DNA damage induced by Cisplatin is analyzed. Since no repair process could be involved in the extracted and purified plasmid DNA, our results prove that DNA DSB could be a result of a *direct* interaction between Cisplatin and DNA, rather than an intermediate step of the repair process of DNA cross-links.

2.1 Introduction

Cisplatin forms covalent adducts with various cellular macromolecules, while DNA is its principal target[354]. Extensive studies of Cisplatin's mechanism of action have shown that the cytotoxicity of Cisplatin arises from its capacity to damage DNA, by forming Cisplatin-DNA adducts[332,334,341]: intra-strand 1,2-d(GpG) adducts (65% of the total adducts) and intra-strand 1,2-d(ApG) (25%) with small percentages of 1,3-d(GpNpG) intra-strand cross-links and inter-strand cross-links. Being the major lesion induced by Cisplatin, much attention has been given to the formation of DNA cross-links, especially its cellular/molecular mechanism. In contrast, DNA double-strand break (DSB), the most lethal form of DNA damage, has not drawn attention in previous studies of Cisplatin. Previous observations have proved the formation of DNA DSBs induced by Cisplatin in replicating yeast, *E. coli*, and in mammalian

50

cells[355,356]. However, the formation of DNA DSBs were thought to be an intermediate step during the repair process of DNA cross-links, rather than a result of *direct* Cisplatin-DNA interaction.

In this Chapter, we show that Cisplatin can *intrinsically* induce DSBs, by a *direct* interaction with DNA.

2.2 Experimental Methods

2.2.1 Chemicals, Cell Lines, Culture Conditions, and Assay Kit

Cis-Diammineplatinum (II) dichloride used in this study to treat cells and plasmid DNA was purchased from Sigma-Aldrich (Sigma-Aldrich Canada Ltd., Oakville, ON, Canada) without further purification. A 3 mM stock solution of Cisplatin was prepared in ultrapure water (resistivity > 18.2 MΩ/cm, TOC < 1 ppm) obtained from the Barnstead Nanopure (Thermo Scientific, Dubuque, IA, USA) water system and stored in the dark at 4℃.

Cell culture minimum essential medium Eagle (MEM) was purchased from Sigma-Aldrich. Penicillin-streptomycin antibiotics (PS), fetal bovine serum (FBS), phosphate buffered saline (PBS), and trypsin-EDTA (0.5 g/L porcine trypsin and 0.2 g/L EDTA·4Na in Hank's Balanced Salt Solution with phenol red) were purchased form Hyclone Laboratories (Logan, UT, USA). The human cervical cancer (HeLa) cell line (ATCC#: CCL-2™) was directly obtained from the American Type Culture Collection (ATCC, Manassas, VA, USA). HeLa cells were cultivated with MEM supplemented with 10% FBS (v/v), 100 units/mL penicillin G and 100 µg/mL streptomycin. Cells were incubated at 37℃ in a humidified atmosphere containing 5% CO_2.

HCS DNA Damage Kit used in *in vitro* DNA double-strand breaks measurements was purchased from Invitrogen (Invitrogen, Life Technologies Inc., Burlington, ON, Canada).

Agarose and ethidium bromide (EtBr) used in the gel electrophoresis experiment were purchased from Sigma-Aldrich.

2.2.2 DNA Double-Strand Breaks Measurement using the HCS DNA Damage Kit

DNA double-strand break is the most lethal DNA damage due to its difficulty to repair[357]. The failure of repairing or mis-repairing of DNA DSBs may induce cell death[358]. Whether or not a treatment can induce DNA DBSs is important in evaluating its efficacy.

DNA double strand breaks (DSBs) measurements were performed by using the HCS DNA Damage Kit (Invitrogen). The main purpose of this kit is to detect and quantitate *in vitro* genotoxicity, specifically DNA DSBs, using pH2AX mouse monoclonal antibodies (1 mg/mL from the manufacturer) to label phosphorylated histone variant H2AX, which is involved in the DSB repair process. The visualization is achieved by using a secondary fluorescent antibody Alexa Fluor® 555 goat anti-mouse IgG (H+L) (2 mg/mL from the manufacturer). Another purpose of this kit is to evaluate *in vitro* cytotoxicity by Image-iT® Dead Green™ (1 mM in DMSO from the manufacturer) viability staining. Only cells with serious injuries are permeable to this DNA-binding dye and therefore be stained. This kit also includes Hoechst 33342 (10 mg/mL from the manufacturer) nuclear staining.

The mechanism is shown in Figure 2-1:
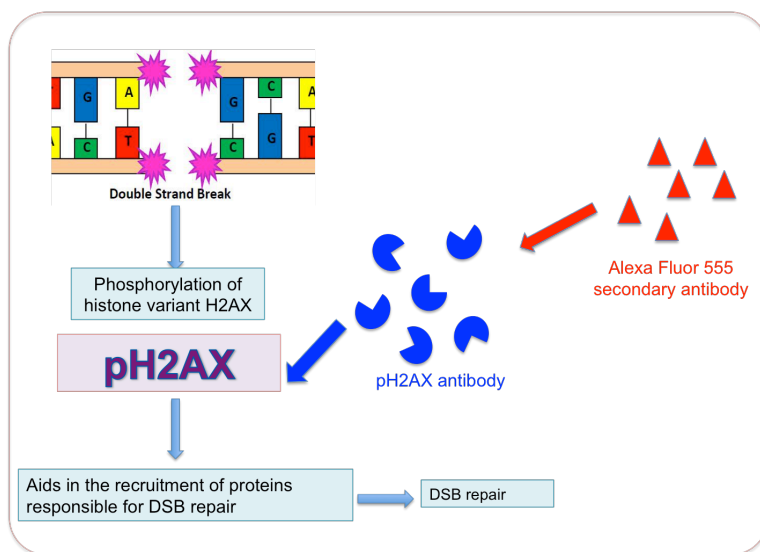
Figure 2-1: The detection of DNA double-strand breaks (DSBs) using γH2AX labeling.

   3000 cells were seeded into 96-well black tissue culture 96-well plates (BD Falcon™) and they were allowed an overnight incubation before treatment to ensure that cells had been well attached. At the end of the treatment (with 100 μL of cell culture medium), 50 μL of Image-iT® Dead Green™ viability stain working solution was added to each well at a final concentration of 0.3 μM. After 30 minutes' incubation, the medium was removed and cells were fixed (100 μL fixative solution, 4% paraformaldehyde (PF), 15 minutes), permeabilized (100 μL permeabilization solution, 0.25% v/v Triton® X-100 in PBS, 15 minutes), and blocked (100 μL blocking buffer, 10 mg/mL bovine serum albumin, 1hour), with sufficient PBS washing between sequential steps. Then cells were stained with the primary antibody solution (final concentration at 1 μg/mL, 1hour), secondary antibody and counterstain solutions (final concentrations at 1 μg/mL and 1.67 μg/mL, respectively, 1hour, protected from light). After each staining, cells were washed 3 times with PBS; and 100 μL PBS was added to each well before taking images. Images were taken on a Nikon Eclipse TS100/TS100-F microscope with filters set to Ex/Em of BP510-560/LP590 nm for Alexa Fluor®, BP330-380/LP420 nm for Hoechst 33342, and BP450-490/LP520 nm for Image-iT® Dead

Green™. Exposure time for each fluorophore was set the same for each image. The software ImageJ was used to perform quantitative analysis.

2.2.3 Plasmid DNA Gel Electrophoresis

Agarose gel electrophoresis is a standard method to directly measure plasmid DNA damage. Three conformations of plasmid DNA are: intact/supercoiled (SC), relaxed circular with single-strand break (SSB), and linear with double-strand break (DSB). This experiment is designed to observe and quantitate the amounts of SC, SSB, and DSB DNA after a certain treatment through the DNA migration in an agarose gel with an electric potential difference.

Agarose gel was prepared by mixing 0.4 g of agarose powder with 4 mL 10× TAE (Tris-Acetate-EDTA) buffer (48.4 g/L Tris base, 1.14% glacial acetic acid v/v, and 3.7 g/L EDTA disodium salt) and 36 mL ultrapure water, and heating up the solution using microwave twice for 20 s and 10 s, with a gentle shake in between. After the solution was cooled down to 50-60℃, 4 μL ethidium bromide stock solution was added (5 mg/mL) to the gel solution to make a final EtBr concentration of 0.5 μg/mL. The apparatus is shown below in Figure 2-2:
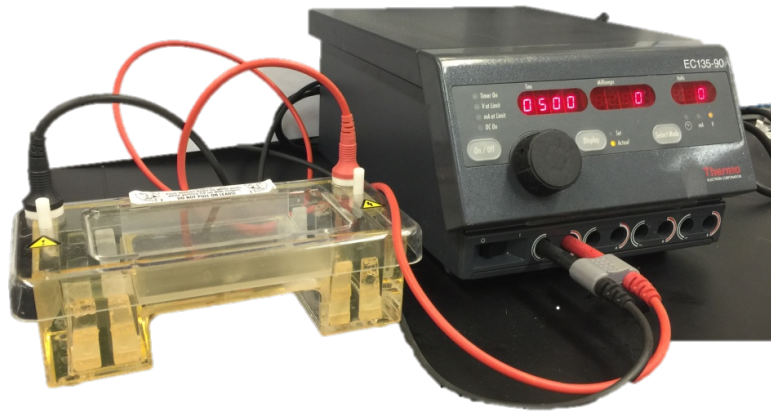
Figure 2-2: Apparatus for plasmid DNA agarose gel electrophoresis.

As can be seen, it consists of a power supply across the transparent plastic chamber, a small gel box placed in the middle of the chamber, a comb used to form DNA loading wells in the gel, and two black stoppers to prevent gel solution from flowing out before it is solidified. Gel solution was poured into the gel box and allowed for a further cooling to room temperature and to form a solid gel. After the gel was solidified, ~250 mL 1×TAE buffer was poured into the chamber and to cover the gel. DNA samples were then loaded with 6× DNA loading dye (8 μL DNA sample + 1.6 μL DNA loading dye). DNA molecules are negatively charged at a neutral pH, and when the power supply is on, a potential difference is given; therefore, DNA molecules will migrate from the cathode to the anode. Their migration speeds in the agarose gel are different due to their shape difference and these speeds have the relation SC DNA >DSB DNA >SSB DNA. According to the migration speed difference, molecules with different conformations can be separated after traveling a certain distance. After being labeled by ethidium bromide that is fluorescent under UV radiation, bands of DNA molecules with different shapes (with different damages) can be visualized.

Gel electrophoresis experiments in this thesis were all set to the same conditions: 200 ng of DNA per well was loaded, 75 V was set for the power supply, DNA molecules were allowed to run for 2 hours before images were taken. The gel images were taken on a FluoChem imaging station (Alpha Innotech) and the software AlphaEase FC was used to perform quantitative analysis.

2.3 Results

2.3.1 *In Vitro* Double Strand Breaks Measurements

The phosphorylation of histone variant H2AX is the key step in the repair process of DNA double-strand breaks (DSB). To study whether Cisplatin could induce DSBs in cells, we detected pH2AX in HeLa cells treated with Cisplatin. As is shown in Figure 2-3, after being treated with Cisplatin for 12 h, significant DSBs were induced in HeLa cells, which was evidenced from the increased red fluorescence as the Cisplatin concentration increased.
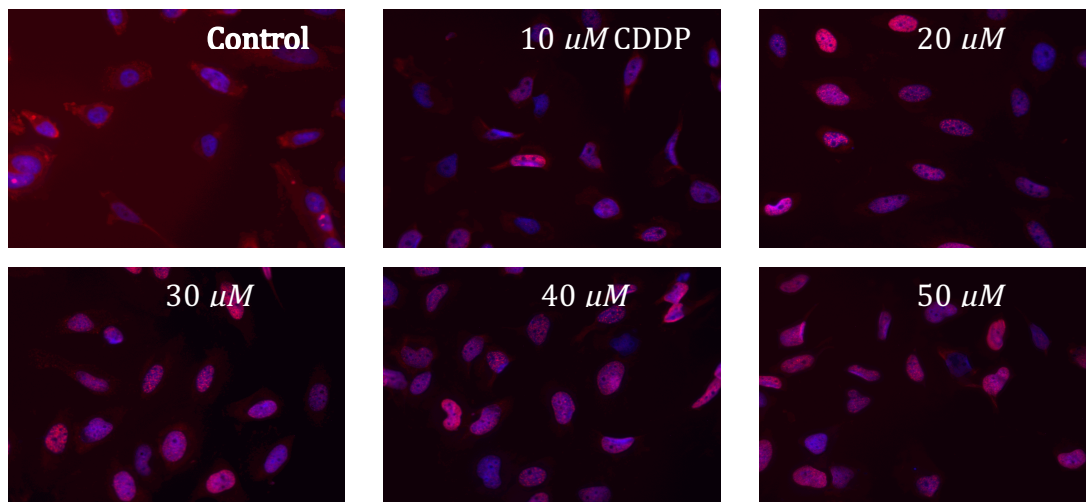
Figure 2-3: Representative images of Cisplatin-treated HeLa cells labeled by Alexa Fluor and Hoechst 33342 for DNA double strand breaks detection.

Images were merged from those taken at Ex/Em of BP510-560/LP590 nm for Alexa Fluor® (double-strand break labeling) and those taken at BP330-380/LP420 nm for Hoechst 33342 (nucleic labeling). As can be seen from the images, control cells were stained blue. As the concentration of Cisplatin increased, more cells were stained pink (merged from red and blue), indicating more double-strand breaks were induced in cells. After the concentration reached 30 µM, the percentage of pink-stained cells and their brightness did not change significantly, indicating a plateau was reached.

ImageJ was used to do quantitative analysis:
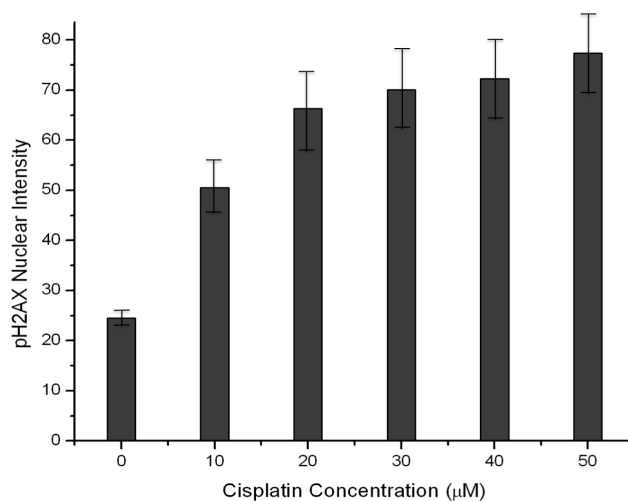
Figure 2-4: Amount of cellular DNA double-strand breaks in HeLa cells treated with Cisplatin.

2.3.2 Gel Electrophoresis

To examine whether the formation of Cisplatin-induced DNA DSBs was intrinsic instead of an intermediate step during the repair of DNA cross-links, we conducted agarose gel electrophoresis to measure damage in plasmid DNA treated by Cisplatin. The gel image and the yields of DNA DSBs in

plasmid DNA incubated with Cisplatin at various concentrations for 150 minutes (37 ℃) are shown in

Figure 2-5 and Figure 2-6, respectively:
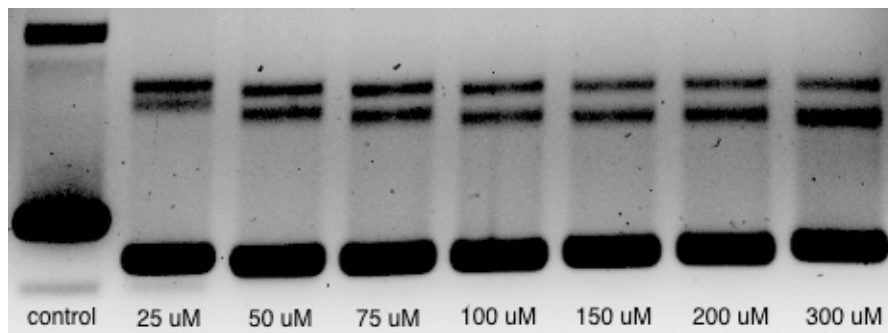
Figure 2-5: Picture of the agarose gel of plasmid DNA treated with Cisplatin.

DNA DSB yields in each band were determined by calculating the integrated density values. Platinated

DNA is not visible in the gel image since the fluorescence emission of the DNA-binding dye (EtBr) is

quenched. It is notable that no DNA repair could be involved in the extracted and purified plasmid DNA,

this result shows that Cisplatin directly induced DSBs in the plasmid DNA.

Quantitative analysis of the gel image is shown in the graph below:
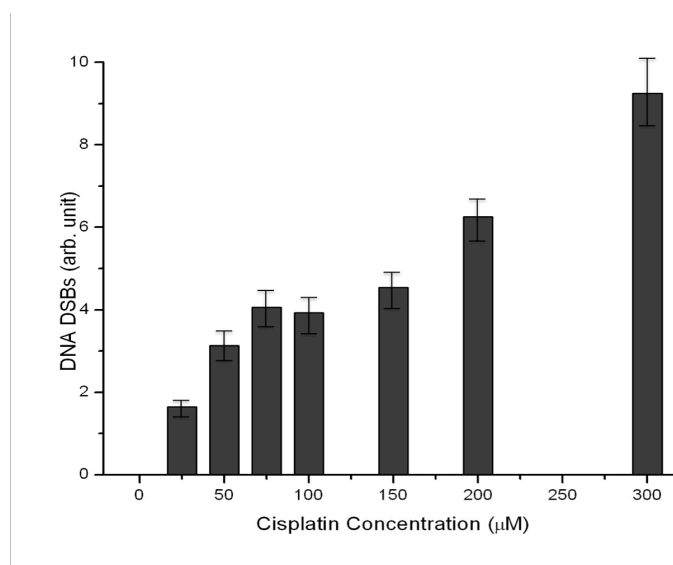
Figure 2-6: Yields of double-strand breaks in Cisplatin-treated plasmid DNA as a function of Cisplatin concentration.

2.4 Discussion and Conclusion

Despite the potent anticancer effect of Cisplatin, its application is limited to its severe side effects and resistance. Only by accurately knowing the mechanism of Cisplatin could we find ways to overcome its limitations. Much attention has been drawn to the cross-links induced by Cisplatin but little to this most lethal form of DNA damage, DNA double-strand breaks (DSBs).

In this Chapter we confirmed the formation of DNA DSBs induced by Cisplatin in HeLa cells. Additionally, we showed evidence that DNA DSBs could be induced by Cisplatin without cellular signaling processes; they could be a result from a *direct* interaction between Cisplatin and DNA, independent of the repair process of DNA cross-links. Nevertheless, we do *not* claim that there is no relationship between the formation of DNA DSBs and the repair process of DNA cross-links. Cisplatin *may* induce DNA DSBs via more than one pathway.

The relationship between the formation of DNA DSBs and the cellular responses to DNA cross-links in cells treated by various compounds/treatments have been reported[359–365], it would be of great interest for us to further investigate the molecular mechanism of the formation DNA DSBs induced by of Cisplatin and other agents.

Our observations confirmed that Cisplatin could induce DNA DSBs in human cervical (HeLa) cancer cells. More remarkably, our gel electrophoresis experiments showed that these DSBs were induced by Cisplatin intrinsically, rather than by an intermediate step during the repair process of DNA cross-links, since no repair process could take place in the extracted and purified plasmid DNA in this experiment.

Chapter 3

In Vitro Studies of the Combination of Cisplatin and Rhodamine-B

3.1 Objective of This Chapter

Before a new drug can be used to treat patients in the clinic, it takes an average time of 12-15 years and a mean cost of about $1.8 billion from its discovery[366]. The process consists of basic research, preclinical tests, clinical tests, and post-marketing surveillance.

Figure 3-1 shows an overview of screening assays in early drug discovery[366]:
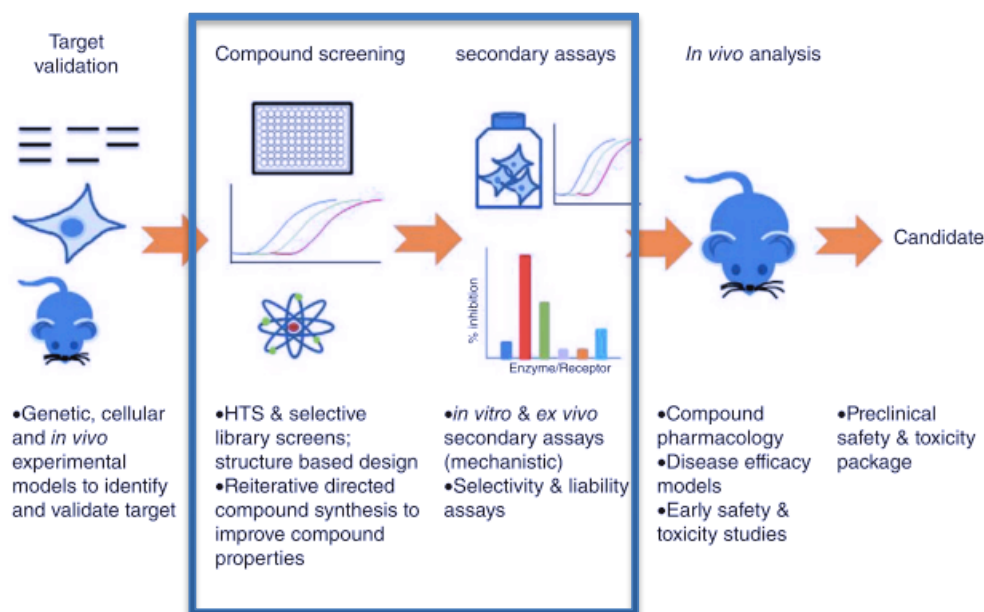
Figure 3-1: Scope of this Chapter: compound screening and secondary assays, with the summary of early drug discovery screening processes/assays[366].

In this project, rather than to test a newly designed anti-cancer drug, we aim to verify the effectiveness of a combination regimen of an FDA-approved anti-cancer drug, Cisplatin. So, instead of target validation, the starting point of our studies is compound screening. In this Chapter the results of compound screening and secondary assays are presented and discussed.

In Chapter 1 the rationale to combine Rhodamine-B with Cisplatin to treat cancer has been introduced. In this Chapter, *in vitro* cell-based and extracted plasmid DNA-based experiments are performed to test if the combination of Cisplatin and Rhodamine-B can enhance the chemotherapeutic effect, as compared with Cisplatin monotherapy.

Various cancer cell lines: human cervical cancer (HeLa and ME-180), human non-small-cell lung cancer (A549), human ovarian cancer (NIH:OVCAR-3), and normal human fibroblast (GM05757) cell lines are tested in this Chapter. Cell survival, important cellular processes such as apoptosis and the formation of DNA double-strand breaks (DSBs) are studied. Direct damage to plasmid DNA extracted from *E.Coli* is also measured.

Questions to be answered in this Chapter include the following:

(1) Is the proposed combination effective in killing cancer cells?

(2) Is the proposed combination toxic to normal cells?

(3) How does the combination kill a cell?

3.2 Materials and Experimental Techniques

3.2.1 Chemicals, Cell Lines, and Assay Kits

Rhodamine-B (RDM-B) and cis-Diammineplatinum(II) dichloride (Cisplatin, CDDP) used in the current study were purchased from Sigma-Aldrich (Sigma-Aldrich Canada Ltd., Oakville, ON, Canada) without further purification. A 3 mM stock solution of Cisplatin and a 24 mM stock solution of Rhodamine-B were both prepared in ultrapure water (resistivity > 18.2 MΩ/cm, TOC < 1 ppm) obtained from the Barnstead Nanopure (Thermo Scientific, Dubuque, IA, USA) water system and stored in the dark at 4℃. Cell culture media, including minimum essential medium Eagle (MEM), nutrient mixture F12 Ham

Kaighn's modification (F-12K), Mccoy's 5A Medium Modified, and RPMI-1640 medium were purchased from Sigma-Aldrich. Penicillin-streptomycin antibiotics (PS), fetal bovine serum (FBS), phosphate buffered saline (PBS), and trypsin-EDTA (0.5 g/L porcine trypsin and 0.2 g/L EDTA·4Na in Hank's Balanced Salt Solution with phenol red) were purchased form Hyclone Laboratories (Logan, UT, USA). Human cervical cancer HeLa cell line (ATCC#: CCL-2™), human cervical cancer ME-180 cell line (ATCC#: HTB-33™), human non-small-cell lung cancer A549 cell line (ATCC#: CCL-185™), and human ovarian cancer NIH:OVCAR-3 (ATCC# HTB-161™) cell line were obtained from the American Type Culture Collection (ATCC, Manassas, VA, USA) directly. Human skin diploid fibroblast GM05757 cell line was obtained from the Coriell Cell Repository directly. HeLa and GM05757 cells were cultivated in MEM supplemented with 10% FBS (v/v), 100 units/mL penicillin G and 100 μg/mL streptomycin. ME-180 cells were cultivated in Mccoy's 5A medium with 10% FBS, 100 units/mL penicillin G and 100 μg/mL streptomycin. The complete growth medium for A549 cells was the F-12K medium with 10% FBS, 100 units/mL penicillin G and 100 μg/mL streptomycin. The complete medium for NIH:OVCAR-3 cells was RPMI-1640 supplemented with 20% FBS, 100 units/mL penicillin G and 100 μg/mL streptomycin. Cells were incubated at 37°C in a humidified atmosphere containing 5% CO_2.

MTT (3-(4,5-dimethylthiazol-2-yl)-2,5-diphenyltetrazolium bromide, MW=414 g/mol) and SDS (sodium dodecyl sulfate, MW=288 g/mol) used in the MTT cell viability assay were purchased from Sigma-Aldrich. A 12 mM MTT stock solution was prepared by dissolving 50 mg of MTT powder in 10 mL sterile PBS. The SDS-HCl solution was prepared by dissolving 1 g of SDS powder in 10 mL 0.01M HCl. Crystal violet and glutaradehyde used in the clonogenic assay were purchased from Sigma-Aldrich. The staining solution was prepared at 0.5% (w/v) of crystal violet and 6.0% (v/v) of glutaradehyde in ultrapure water.

The CellEvent® Caspase-3/7 Green Detection Reagent and the HCS DNA Damage Kit used in the *in vitro* apoptosis detection and DNA double-strand breaks measurement were purchased from Invitrogen (Invitrogen, Life Technologies Inc., Burlington, ON, Canada). The Annexin V-FITC Apoptosis Detection Kit was purchased from Sigma-Aldrich.

Agarose and ethidium bromide (EtBr) used in the gel electrophoresis experiment were purchased from Sigma-Aldrich.

3.2.2 Experimental Techniques

3.2.2.1 MTT Cell Viability Assay

The MTT cell viability assay is a popular and fast assay that measures cell survival/cell-killing efficacy of a given treatment through a direct determination of the cell number by using standard microplate absorbance readers.

Figure 3-2: MTT assay performed in cells in a 96-well plate, and the plate reader.

The 96-well plate with different numbers of cells and the plate reader are shown in Figure 3-2.

5000-8000 cells were seeded into 96-well transparent tissue culture plates (BD Falcon™, Corning Inc., NY, USA). Treatment was given after overnight incubation to ensure that cells had been well attached and adapted to the environment. For each well, cell culture medium was replaced after the desired treatment

time period with 10 µL MTT stock solution with 100 µL regular complete cell culture medium (without phenol red). The light-yellow water soluble MTT was reduced by the mitochondria of a living cell to an insoluble purple-blue formazan, which was then dissolved in the SDS-HCl solution after 3-4 hours' incubation. After 4-18 hours' further incubation, the concentration of the solubilized formazan was determined by measuring its absorbance at 570 nm with a Multiscan GO microplate spectrophotometer (Thermo Scientific, Mississauga, ON, Canada), and the cell number should be proportional to the absorbance.

The principle of the MTT assay is shown in Figure 3-3:
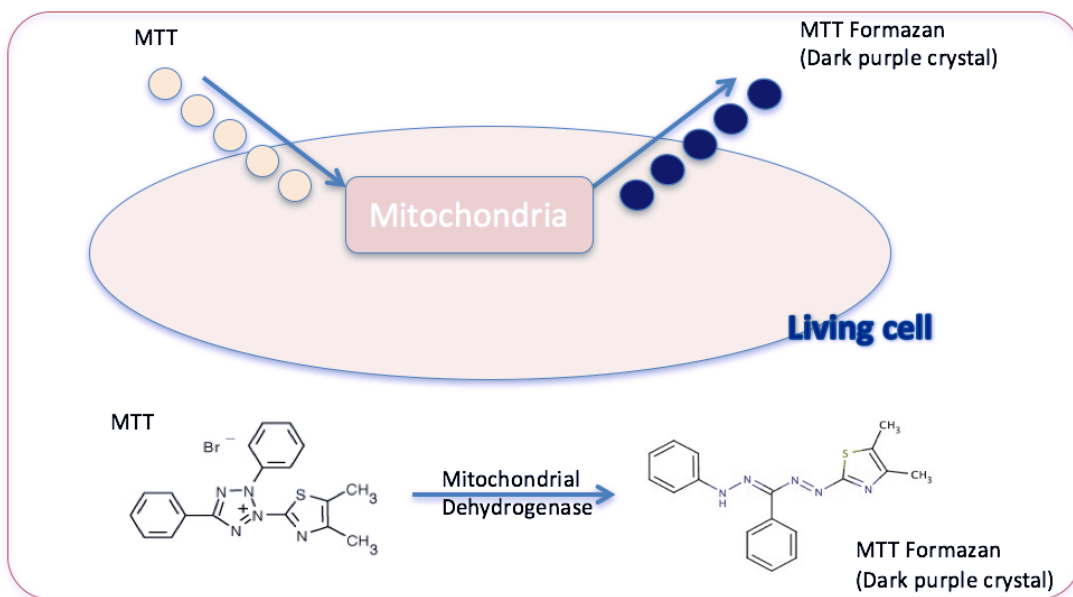
Figure 3-3: Principle of the MTT assay.

For all MTT experiments in this thesis at least three replicates were set for any concentration of treatment. Cell viability was represented by the percentage of the untreated (control) cells and the error bars represented the standard deviations of the replicates.

3.2.2.2 Clonogenic Assay

Clonogenic assay is considered as a more sensitive cell viability measurement assay that was first designed to study radiation effects.

Cells were uniformly plated onto 100×100 mm tissue culture dishes (Thermo Scientific), and they were allowed at least 5 hours' incubation before treatment to ensure that cells had been well attached. At the end of the incubation period, cell culture medium was removed to terminate treatment. Tissue culture dishes were washed by sterile PBS, after that fresh complete cell culture medium was added. Cells were further incubated for 10-14 days until clones were big enough to be counted.

Dishes were washed with PBS before being stained and fixed by crystal violet and glutaradehyde. After staining at room temperature for 30 minutes, staining/fixation solution was removed and dishes were washed with ice-cold deionized water to remove residual color. When dishes were dried out, clones were counted. 50-100 clones per dish were desirable for accuracy.

A picture of a six-well tissue culture dish with countable clones is shown in Figure 3-4:
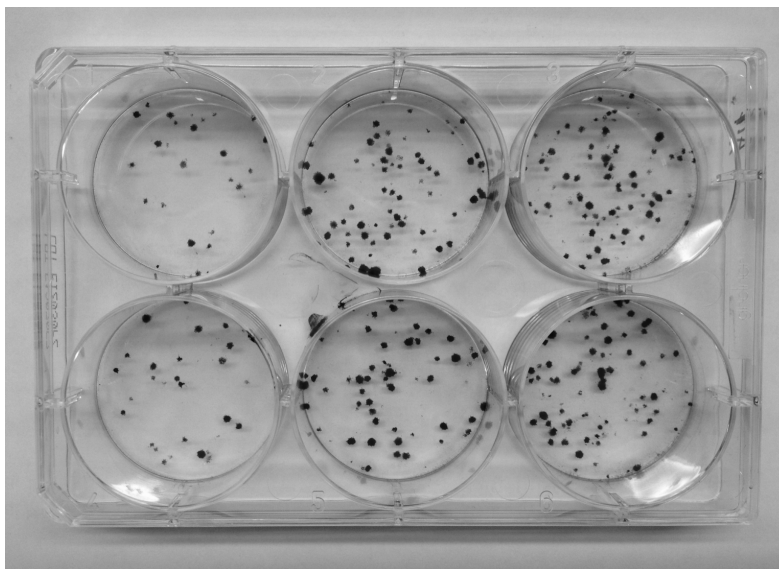
Figure 3-4: Representative picture of a 6-well plate with clones for counting.

For all clonogenic experiments in this thesis, three replicates for each group were set and the cell viability was represented by the percentage of the untreated (control) cells, and the error bars represented the standard error of the mean (s.e.m.) of the replicates.

3.2.2.3 Apoptosis Detection using the CellEvent® Caspase-3/7 Green Detection Reagent staining

Apoptosis, or programmed cell death, is characterized by distinct morphological alterations and energy-dependent biochemical mechanisms[367]. Chemotherapy may induce DNA damage and therefore *p-53* dependent apoptotic death. Caspases are primary mediators of apoptosis; therefore, detecting the activation of caspases provides us information on how a cell is killed by a given treatment. In this project, apoptosis detection is performed by using the CellEvent® Caspase-3/7 Green Detection Reagent staining, which is a fluorogenic substrate for activated caspase 3/7. A four amino acid peptide (DEVD) is conjugated to a nucleic binding dye to form this non-fluorescent and non-DNA binding substrate. In caspase 3/7-activated cells, however, the DEVD peptide is cleaved, and therefore the dye is enabled to bind to DNA and to produce fluorescence. The absorption/emission peaks of this reagent are 502/530nm. The concentration of the CellEvent® Caspase-3/7 Green Detection Reagent is 2.0 mM in DMSO from the manufacturer. The principle is shown in Figure 3-5.

1500-3000 cells were seeded into 96-well black tissue culture 96-well plates (BD Falcon™) and they were allowed an overnight incubation before treatment to ensure that cells had been well attached. After the incubation with treatment, the old medium was removed and the CellEvent® Caspase-3/7 Green Detection Reagent was added with 100 µL fresh complete cell culture medium to a final concentration of 5 µM (2-10 µM recommended by the manufacturer). After 30 minutes' incubation, images were taken on

a Nikon Exlipse TS100/TS100-F microscope with the filter set to Ex/Em of BP450-490/LP520 nm.

Quantitative analysis of caspase-activated (apoptotic) cells was performed by the software Image J.
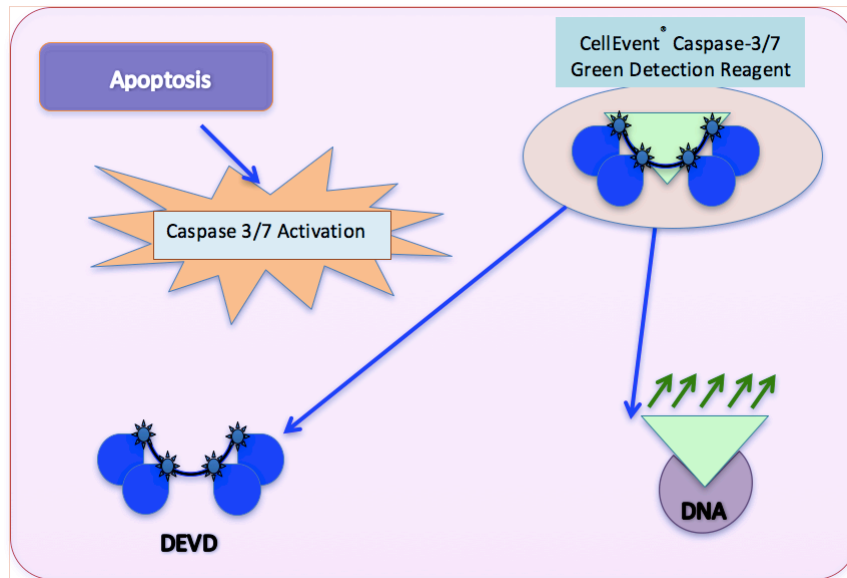
Figure 3-5: Mechanism of the detection of apoptotic cell through CellEvent® Caspase-3/7 Green Detection Reagent labeling.

3.2.2.4 Early/Late Apoptosis Differentiation Using the Annexin V-FITC Apoptosis Detection Kit by Flow Cytometry

Apart from Caspase activation, apoptosis is also characterized by morphologic changes, including the loss of cell membrane asymmetry and attachment, blebbing, cytoplasm and nucleus condensation, and DNA fragmentation[367]. In cells undergoing early apoptosis, one important feature is the loss of membrane asymmetry. In "healthy" cells, an enzyme, aminophospholipid translocase, helps to locate phospholipid phosphatidylserine (PS) to the inside of the cell membrane[368]. In apoptotic cells, the membrane PS translocates itself from the inner leaflet to the outer of the cell membrane. Therefore, apoptotic cells can be detected by labeling the external cellular environment-exposed PS. Annexin V is a phospholipid-binding protein (in the presence of calcium)[369,370], with a high affinity for PS. In this kit, Annexin V is

conjugated with the fluorochrome fluorescein isothiocyanate (FITC) so that by detecting the fluorescence signal of FITC, early apoptotic cells can be identified. Late apoptotic cells undergo the loss of membrane integrity. In this kit, a vital dye propidium iodide (PI) is used as a marker of late apoptosis: only dead and/or damaged cells are permeable to PI. Therefore, after performing this double staining process, with fluorescent microscopy/flow cytometry, cells can be visualized: "healthy" cells will be stained both Annexin V and PI negative (no external PS exposure with intact membrane), early apoptotic cells will be stained Annexin V positive but PI negative (with external PS exposure and intact membrane), late apoptotic/dead cells will be stained both Annexin V and PI positive (with external PS exposure and damaged membrane), and necrotic cells will be stained Annexin V negative but PI positive.

In this experiment, fluorescence detection was performed by flow cytometry. Flow cytometry is a technique utilizing a flow cytometer (BD FACSAria™ Fusion) to perform optical/fluorescence detection of single cells. A typical flow cytometer is composed of five parts: a light source (laser), a flow cell, illumination optics, collection optics, and a detection system.

A simplified schematic is shown below in Figure 3-6:
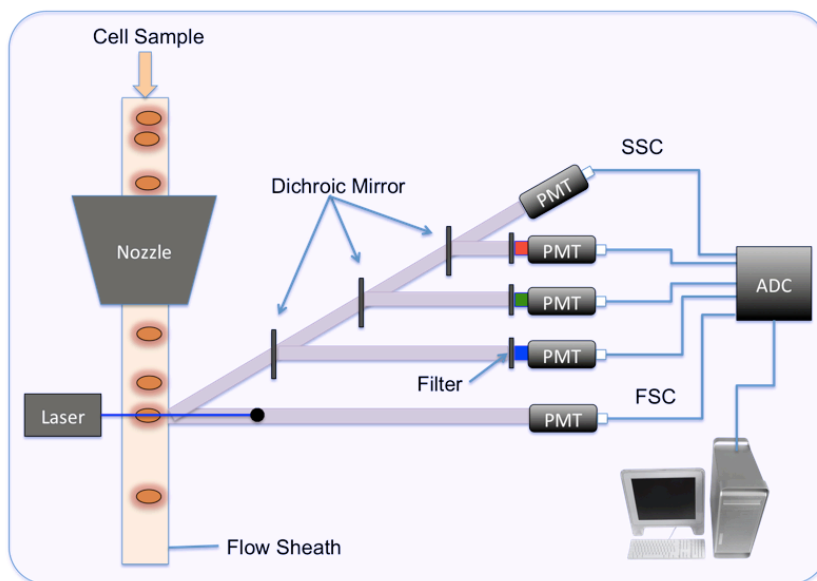
Figure 3-6: Schematic diagram of a flow cytometer.

In this experiment, the laser wavelength was chosen as 488 nm, by which both FITC and PI can be excited. According to the DB FACSAria ™ III User's Guide, the emission spectra of some commonly used fluorochromes are shown in the figure below:
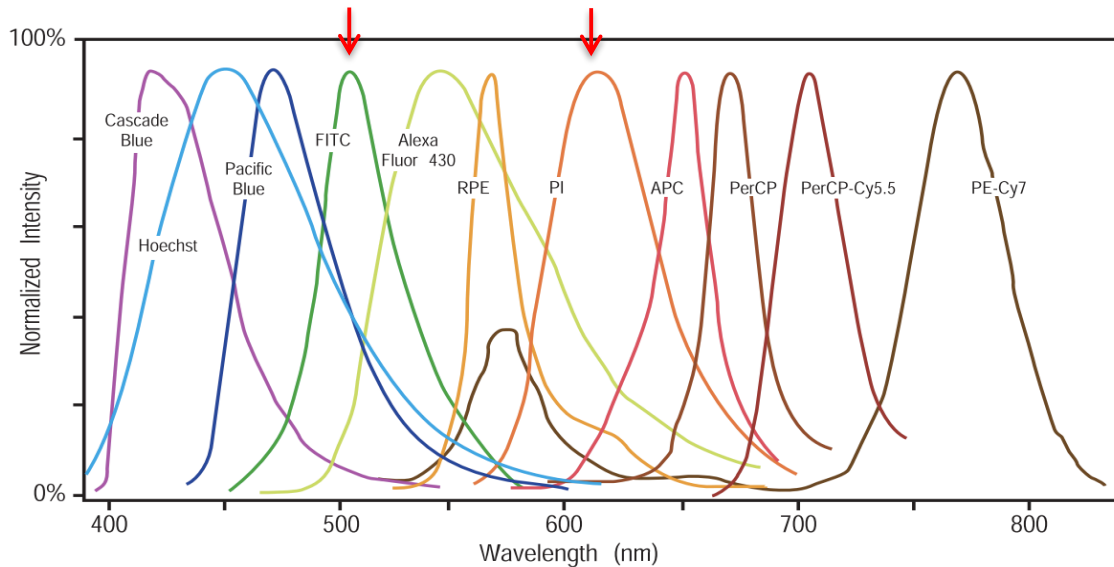
Figure 3-7: Fluorescence spectra of some common fluorophores. Spectra of FITC and PI are indicated by red arrows.

As can be seen from the spectra, fluorescence signals from FITC and PI (red arrows) can be well separated without significant overlap. Therefore, signals from these two channels can be analyzed individually without interfering with one another.

5×10^5 cells were seeded into T25 flasks, allowing an overnight incubation to ensure cells had been well attached. Treatment was given when cells reached 50% confluence. After the treatment incubation, cells were collected (including floating cells in the cell culture medium) by trypsinization. After being centrifuged, cells were washed 3 times with PBS and resuspended in 500 μL binding buffer. Then cells were labeled by 5 μL Annexin V FITC conjugate and 10 μL PI solution. After ten minutes of incubation

69

protected from light, cells were analyzed by a flow cytometer. In each experiment, one unstained sample (without treatment and without any staining) and two positive samples (FITC only and PI only) were prepared to help with gating. Quantitative analysis was performed by the software FlowJo to detect apoptotic cells.

3.2.2.5 Double-Strand Breaks Measurement Using the HCS DNA Damage Kit

The experimental method of using DSC DNA Damage Kit to measure *in vitro* DNA double-strand breaks (DSBs) has been described in Chapter 2.

3.2.2.6 Plasmid DNA Gel Electrophoresis

The experimental method of applying gel electrophoresis to study strand breaks of plasmid DNA in *E. Coli.* has been described in Chapter 2.

3.3 Experimental Results

3.3.1 *In Vitro* Cytotoxicity and Toxicity Studies of Rhodamine-B

The *in vitro* cytotoxicity and toxicity were studied using the MTT cell proliferation assay. Cytotoxicity study of Rhodamine-B on human cervical cancer (HeLa and ME-180), human non-small-cell lung cancer (A549), and human ovarian cancer (NIH:OVCAR-3) cell lines were conducted. Toxicity of Rhodamine-B on a normal human skin diploid fibroblast (GM05757) cell line was also tested.

5000-8000 cells were seeded into 96-well plates, after overnight incubation, old medium was replaced by fresh cell culture medium with different concentrations of Rhodamine-B (RDM-B). Cells were all

treated for 24 hours before the MTT assay was performed. Concentrations of Rhodamine-B were set the same for all tested cell lines: 0 to 80 μM with a 10 μM increment.

The result is shown in Figure 3-8:

RDM-B Toxicity/Cytotoxicity Profiles
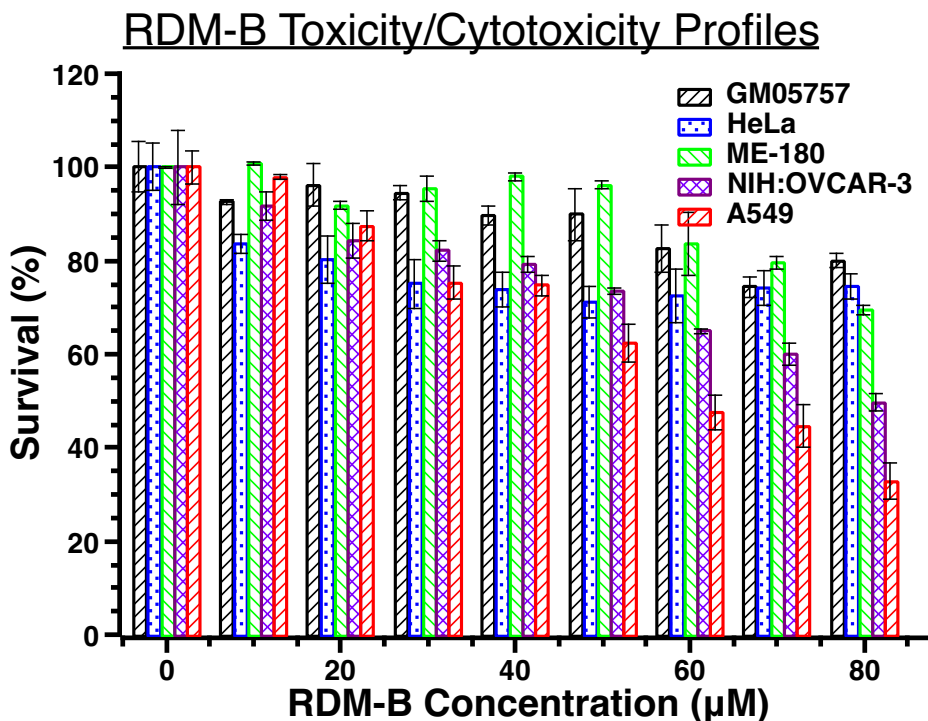
Figure 3-8: Toxicity and cytotoxicity profiles of Rhodamine-B. Drug-dose response curves obtained from MTT assay in GM05757, HeLa, ME-180, NIH:OVCAR-3, and A549 cells.

It can be seen that the normal GM05757 cells were almost the least sensitive to Rhodamine-B treatment. In contrast, cancer cells especially A549 and NIH:OVCAR-3 cells were highly responsive.

This MTT viability test shows that Rhodamine-B selectively killed more cancer cells than normal cells, which makes Rhodamine-B an ideal candidate for our electron-transfer-based combination with Cisplatin.

3.3.2 *In Vitro* Survival Studies of the Combination of Cisplatin and Rhodamine-B

First, MTT proliferation assay was performed to test the cell-killing efficacy of the combination of Cisplatin and Rhodamine-B. All experiments in this section were designed to compare the survivals of cells treated by Cisplatin only and its combination with Rhodamine-B.

5000-8000 cells were seeded into 96-well plates and allowed for overnight incubation. Cells were treated with various concentrations of Cisplatin with/without Rhodamine-B. The concentrations of Rhodamine-B for different cell lines were chosen at values that can kill 10-20% of cells by Rhodamine-B only. Incubation time for all MTT experiments was 24 hours.

In HeLa cells, Rhodamine-B was tested at 20 μM and 40 μM, with Cisplatin of 0~40 μM. The MTT assay results for HeLa cells are shown below:
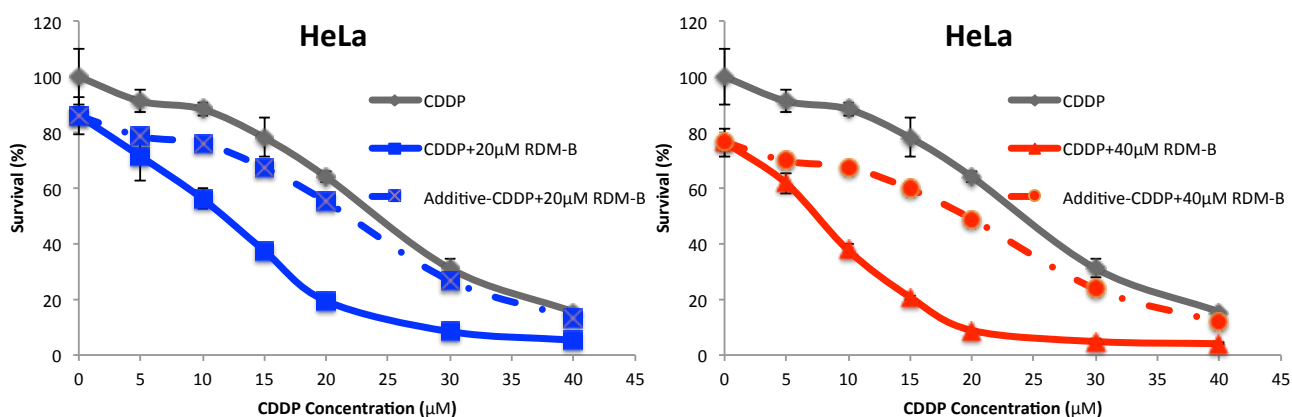
Figure 3-9: Drug-dose response for cell survival of HeLa cells treated by Cisplatin and its combination with Rhodamine-B. In each graph, the dashed line represents the calculated additive survival of the combination of Cisplatin and Rhodamine-B. Data points at 0 μM CDDP represent the survivals by the treatment of RDM-B only.

In Figure 3-9, additive or expected survivals were calculated based on the fractional effect method that has been introduced in Chapter 1. As we can see from the figures, actual survivals of the combination of

Cisplatin and Rhodamine-B were significantly lower than that of the calculated additive. That is to say, Cisplatin and Rhodamine-B killed HeLa cells *synergistically*.

MTT survival assay was also performed on three other human cancer cell lines: ME-180, A549, and NIH:OVCAR-3. Results for these four cell lines are summarized in Figure 3-10:
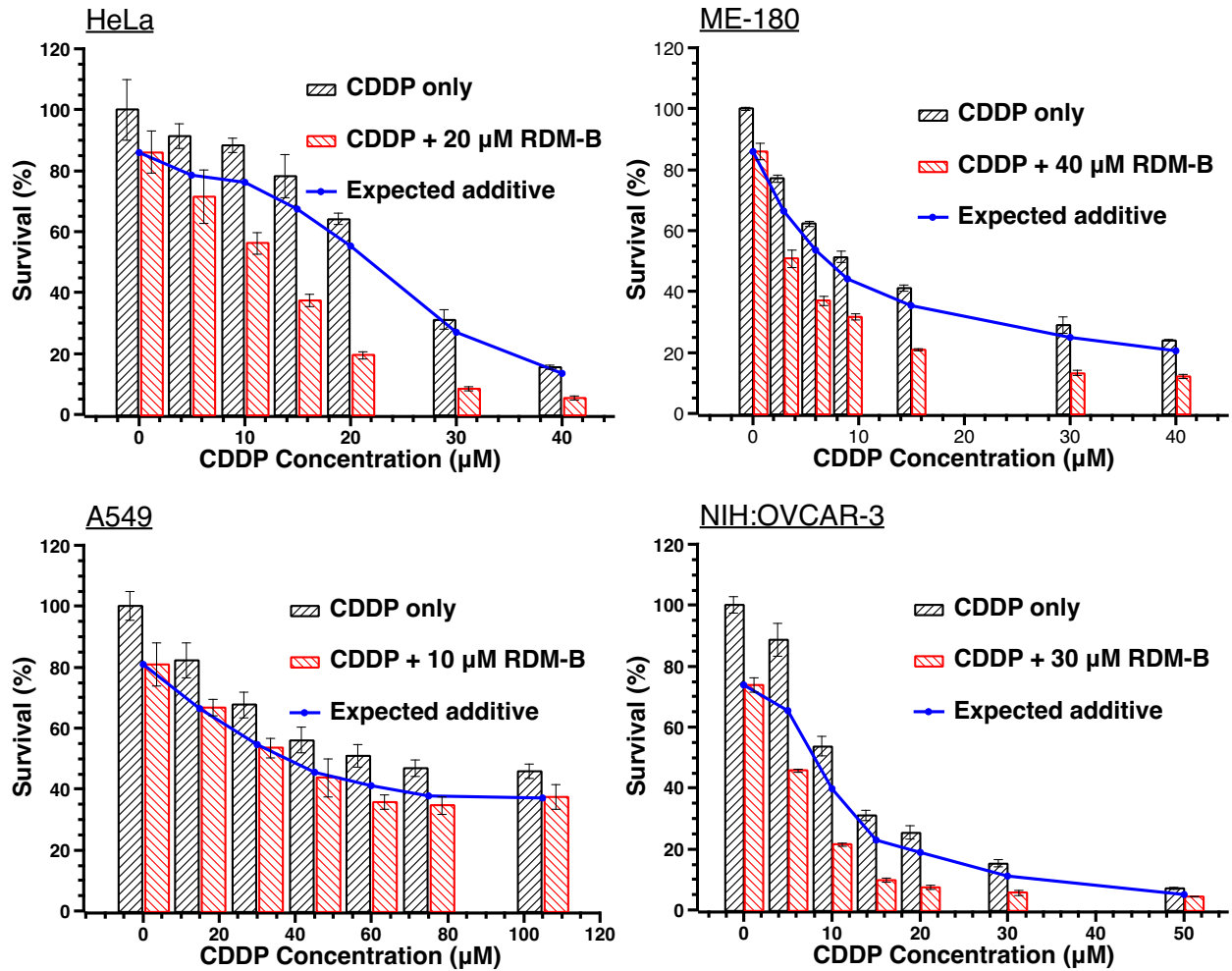
Figure 3-10: Drug-dose response curves obtained from MTT assay for cell survival of different human cancer cell lines: HeLa, A549, NIH:OVCAR-3, and A549; they were treated with Cisplatin and its combination with Rhodamine-B. Blue lines represent calculated additive survivals of the combination of Cisplatin and Rhodamine-B.

As can be seen from the graphs, in HeLa and ME-180 cells, the observed survival curves were significantly lower than that of the additive survivals of this combination. In each graph, multiplying the survival at a constant Rhodamine-B concentration only and those at corresponding Cisplatin concentrations gave the expected additive survival curve. Strong synergistic effect was observed in cervical HeLa and ME-180 cells. In NIH:OVCAR-3 cells, moderate synergy was also observed. In A549 cells, however, the additive and the observed curves showed no significant difference.

Second, clonogenic assay was conducted to further confirm the *in vitro* synergistic effect of the combination of Cisplatin and Rhodamine-B. Cells were seeded at numbers sufficient to produce 50-200 clones. Cells were treated by various of concentrations of Cisplatin with/without Rhodamine-B. Incubation time for all clonogenic experiments was set the same as 2 hours. At the termination of the treatment, in order to sufficiently remove residual Cisplatin and Rhodamine-B, tissue culture dishes were washed with PBS and then fresh medium was added. After that, cells were incubated for 10-14 days for cells to form clones. After staining/fixation, clones were counted with the naked eye.

Clonogenic assay results in semi-log graphs are shown in Figure 3-11.As can be seen from the results, strong synergy was observed in A549, NIH:OVCAR-3, and ME-180 cells. At higher concentrations, the combination of Cisplatin and Rhodamine-B killed 10 times more cells than Cisplatin only did. Synergy was less significant in HeLa cells but also observed.
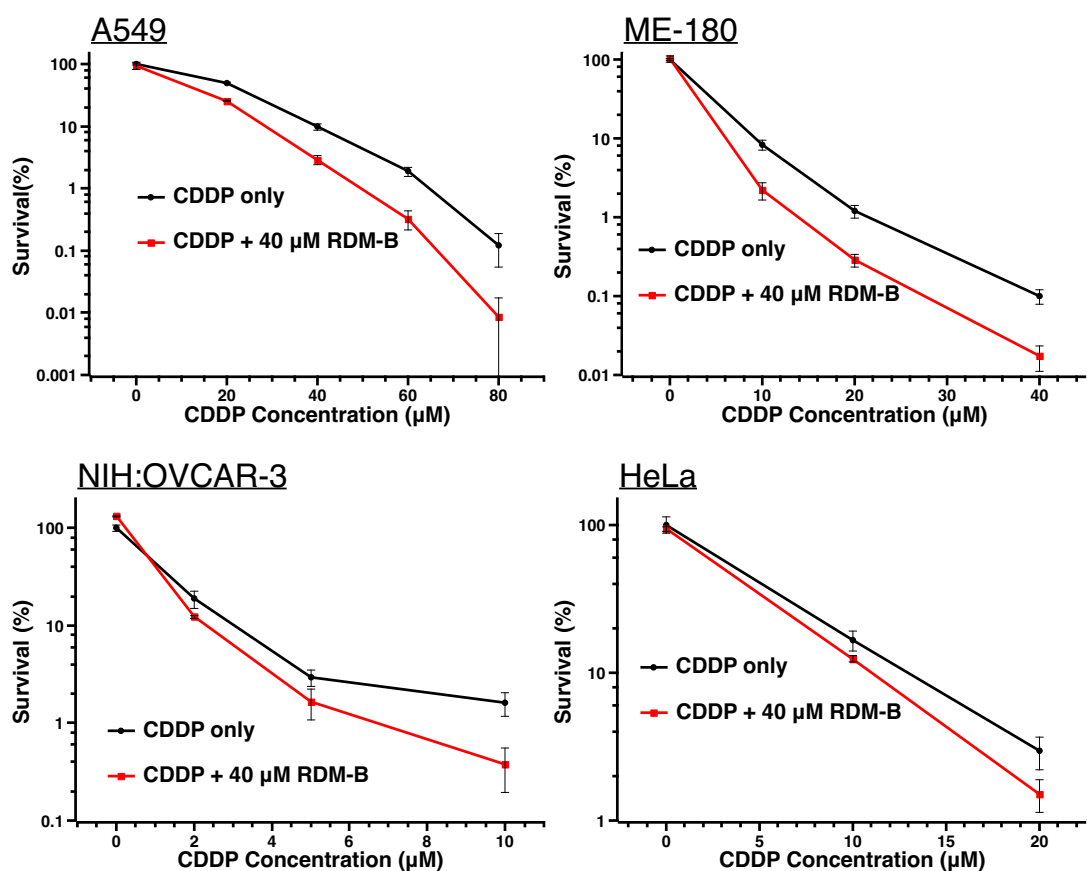
Figure 3-11: Drug-dose response curves obtained from clonogenic assay for cell survival of different human cancer cell lines: HeLa, A549, NIH:OVCAR-3, and A549; cells were treated by Cisplatin and its combination with Rhodamine-B. All graphs were plotted as semi-log graphs.

After we confirmed the synergistic *in vitro* cytotoxicity of the combination of Cisplatin and Rhodamine-B on cancer cell lines, we needed to determine whether or not this combination would give additive/synergistic toxicity. Therefore, the MTT survival assay was performed in normal GM05757 cells to answer this question.

The result is shown in Figure 3-12:

75
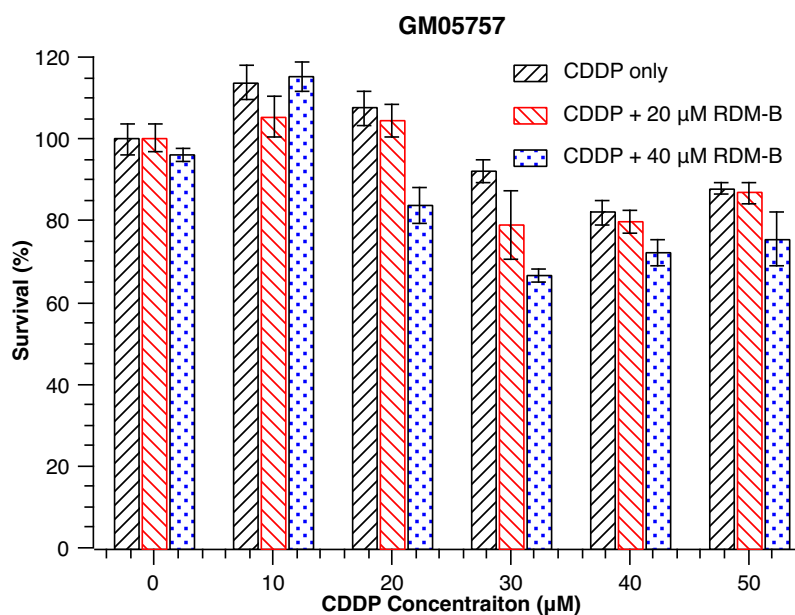
Figure 3-12: Drug-dose response curves obtained from MTT assay for cell survival of GM05757 cells treated by Cisplatin and its combination with Rhodamine-B.

GM05757 cells were treated with 0-50 μM Cisplatin with/without 20 μM and 40 μM Rhodamine-B for 24 hours. As can be seen from the graph, little additional toxicity was observed. The combination of Cisplatin and Rhodamine-B did not kill GM05757 cells as effectively as it did in killing other cancer cells.

3.3.3 *In Vitro* Apoptosis Detection of the Combination of Cisplatin and Rhodamine-B

CellEvent[®] Caspase-3/7 Green Detection Reagent was used to detect *in vitro* apoptosis in HeLa cells. 3000 cells were seeded into a black 96-well plate and allowed for overnight incubation. Treatments of 0, 10, and 30 μM of Cisplatin with/without 10 μM Rhodamine-B were given and the incubation time was 12 hours. Images were taken after 30 minutes of CellEvent[®] Caspase-3/7 Green Detection Reagent incubation.

The images are shown in Figure 3-13:
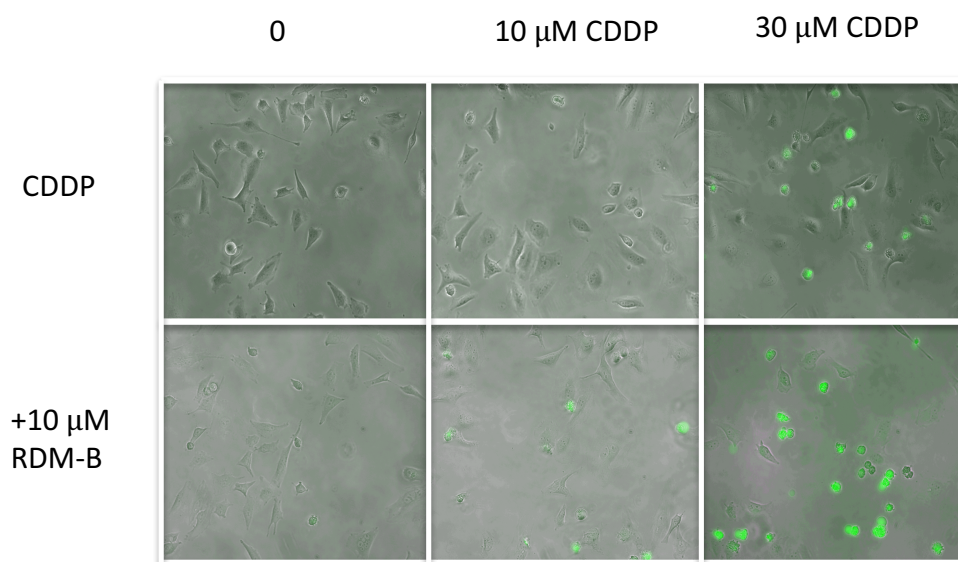
Figure 3-13: Representative images of HeLa cells treated by Cisplatin and its combination with Rhodamine-B labeled by CellEvent® Caspase-3/7 Green Detection Reagent.

These images were merged from pictures taken at Ex/Em of BP450-490/LP520 nm and those taken under bright field. Green cells represent Caspase 3/7 activated cells, i.e. apoptotic cells. By comparing the two images in the 0 μM CDDP column we can see that Rhodamine-B only almost did not induce any apoptotic cells at the concentration of 10 μM. However, when 10 μM Rhodamine-B was combined with 10 μM and 30 μM Cisplatin, it induced many more Caspase 3/7 positive (apoptotic) cells, compared to Cisplatin only.

Quantitative analyses were performed by counting the number of green (apoptotic) cells and the total number of cells in each image, and the result was represented by the percentage of apoptotic cells in each image, the graph is shown in Figure 3-14:
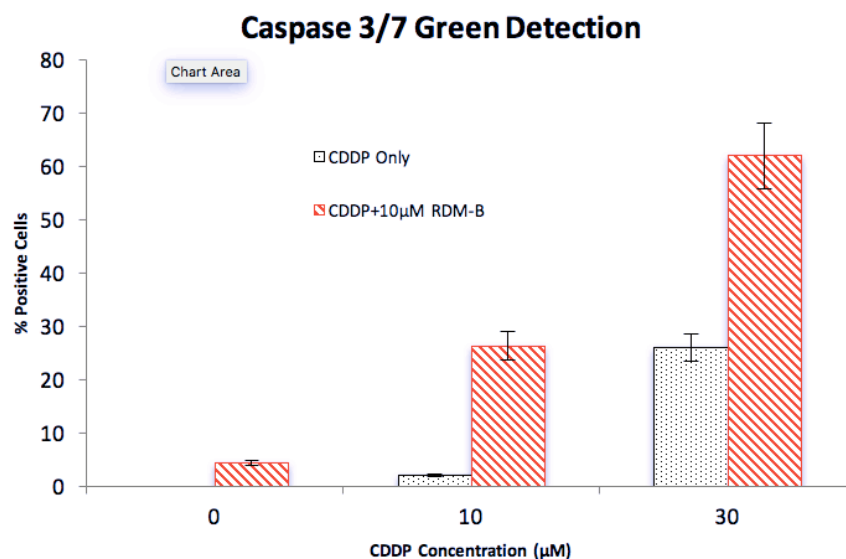
Figure 3-14: Percentages of caspase 3/7 activated HeLa cells as a function of Cisplatin concentration. HeLa cells were labeled by CellEvent® Caspase-3/7 Green Detection Reagent.

Apoptosis is also characterized by its morphological difference from healthy cells. Images taken under bright field are shown in Figure 3-15:
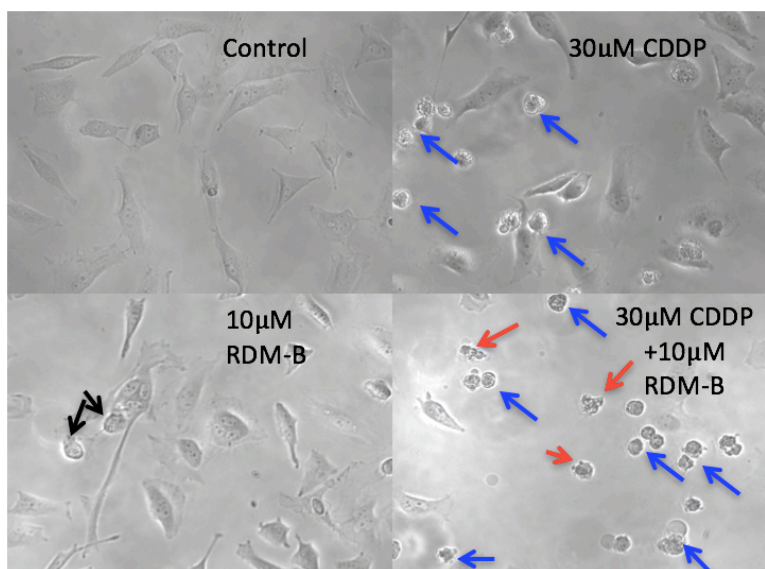
Figure 3-15: Representative pictures of HeLa cells treated by Cisplatin and its combination with Rhodamine-B. Pictures were taken using a camera under the microscope.

Apoptosis is visually characterized by cell shrinkage and fragmentation into membrane-bound apoptotic bodies[371, 372]. As we can see from above pictures, control cells were expanded, well-attached and well-shaped with clear boundaries. For cells treated with 10 μM Rhodamine-B, though almost no caspase 3/7 activated cell was observed, cell shape was changed to some extend (black arrows) without significant cell shrinkage. This observation was consistent with previously shown MTT viability result: about 15% of HeLa cells were killed after 24 hours' 10 μM Rhodamine-B treatment. When 30 μM Cisplatin was given, cell shrinkage was induced to treated cells; round and brighter cells (due to detachment) were observed (blue arrows). The combination of Cisplatin and Rhodamine-B induced many more apoptotic cells (blue arrows); furthermore, cell membrane blebbing and smaller cell capsules (red arrows) were observed, indicating cell fragmentation.

3.3.4 *In Vitro* Double-Strand Breaks Measurement of the Combination of Cisplatin and Rhodamine-B.

In vitro double-strand break measurement was performed using the HSC DNA Damage Kit. This assay was done on human cervical cancer (HeLa), human non-small-cell lung cancer (A549), and human ovarian cancer (NIH:OVCAR-3) cell lines. For all experiments, 3000 cells were seeded into black 96-well plates, after overnight incubation, cells were treated with various concentrations of Cisplatin with/without Rhodamine-B for 12 hours before the assay was performed. For HeLa cells, concentrations of Cisplatin were 0, 1 μM, and 10 μM, and the concentration of Rhodamine-B was 20 μM.

First, *in vitro* genotoxicity induced by the treatment was evaluated by phosphorylated H2AX (γH2AX) labeling. Images were merged from those taken at Ex/Em of BP510-560/LP590 nm for Alexa Fluor® (double-strand break labeling) and those taken at BP330-380/LP420 nm for Hoechst 33342 (nucleic labeling). The images of HeLa cells treated by Cisplatin and its combination with Rhodamine-B are shown in Figure 3-16:
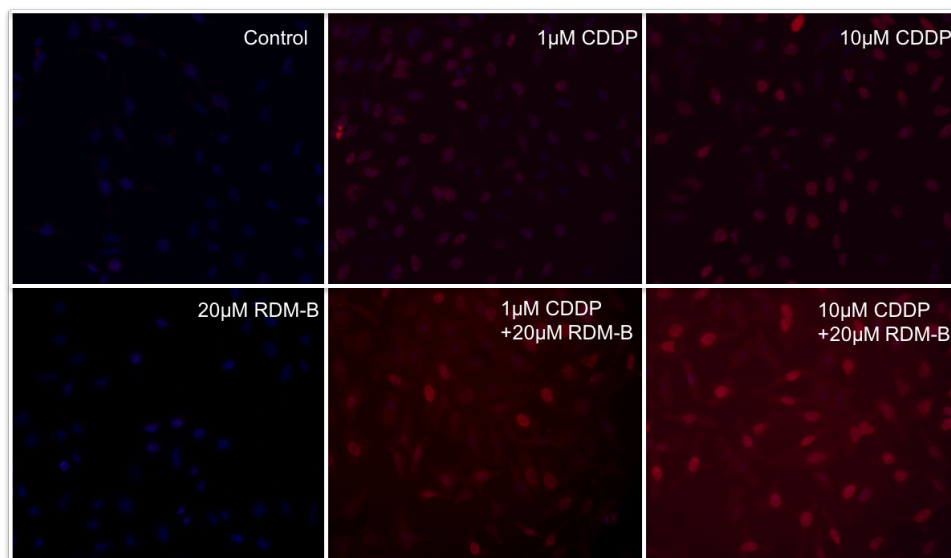
Figure 3-16: Representative images of HeLa cells treated by Cisplatin and its combination with Rhodamine-B using the HCS DNA damage kit. Cells were double stained with Alexa Fluor® 555 (red) and Hoechst 33342 (blue)

Red cells were cells that had phosphorylated H2AX (with double strand breaks) labeled. It can be seen that 20 μM Rhodamine-B almost did not induce double-strand breaks. 1 μM and 10 μM Cisplatin induced DNA DSBs and these damages were dramatically enhanced by combining Cisplatin with 20 μM Rhodamine-B. ImageJ software was applied to quantitatively analyze the amount of induced DNA DSBs. The result is shown in Figure 3-17:
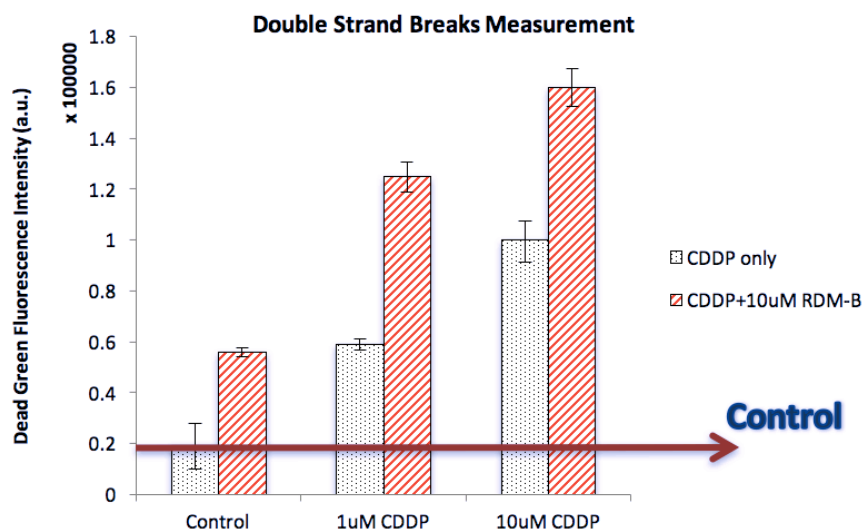
Figure 3-17: Integrated Alexa Fluor® 555 fluorescence intensity per cell as a function of Cisplatin concentration in HeLa cells using the HCS DNA damage kit.

Second, cytotoxicity of this combination was also evaluated using this kit from images taken at BP450-490/LP520 nm for Image-iT® Dead Green™ staining. Only dead cells allow Image-iT® Dead Green™ reagent enter cells through damaged cell membrane and labels the DNA. The concentrations of Cisplatin and Rhodamine-B were both 10 µM.

Images of HeLa cells are shown in Figure 3-18. Green cells represent cells with serious membrane damage. It can be seen that 10 µM Rhodamine-B did not affect the cell membrane integrity. Cells treated with 10 µM Cisplatin were weakly stained by Image-iT® Dead Green™, and cells treated by 10 µM Cisplatin combined with 10 µM Rhodamine-B were very strongly stained, which can be seen from the bright green color in these cells.
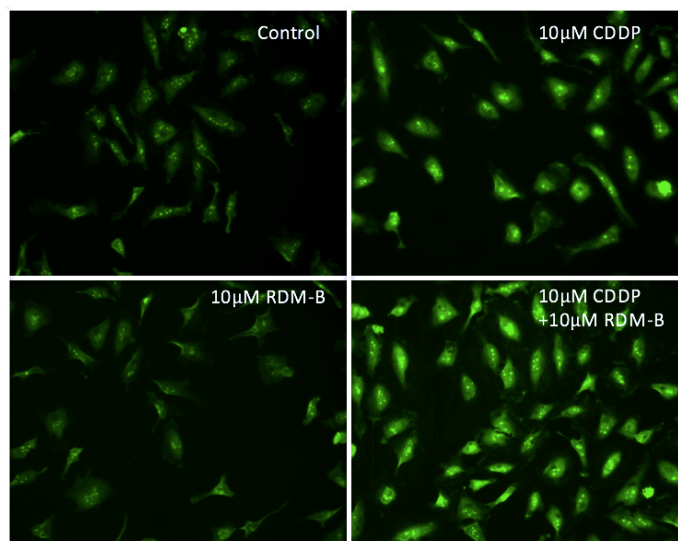
Figure 3-18: Representative images of HeLa cells treated by Cisplatin and its combination with Rhodamine-B for cytotoxicity evaluation using the HCS DNA damage kit. Cells were stained with Image-iT® Dead Green™.

ImageJ software was applied to quantitatively analyze the amount of Image-iT® Dead Green™ taken by HeLa cells and the result is shown in Figure 3-19:
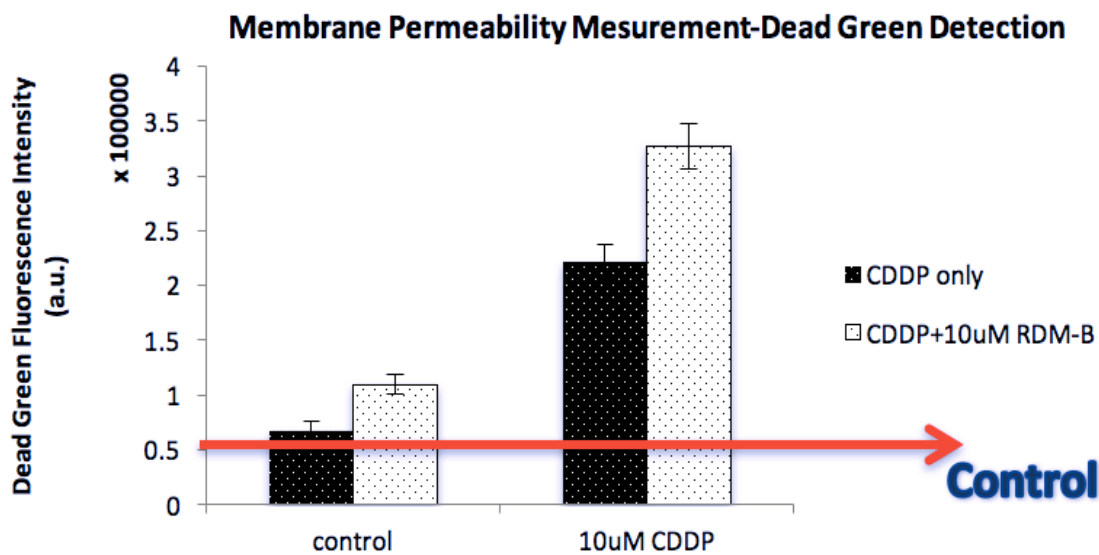
Figure 3-19: Integrated Image-iT® Dead Green™ fluorescence intensity per cell in HeLa cells treated by Cisplatin and its combination with Rhodamine-B using the HCS DNA damage kit.

This assay was also performed in human lung cancer A549 cells to measure DNA DSBs and to evaluate cell membrane integrity (cytotoxicity).

Images are shown in Figure 3-20, followed by the quantitative analysis in Figure 3-21:
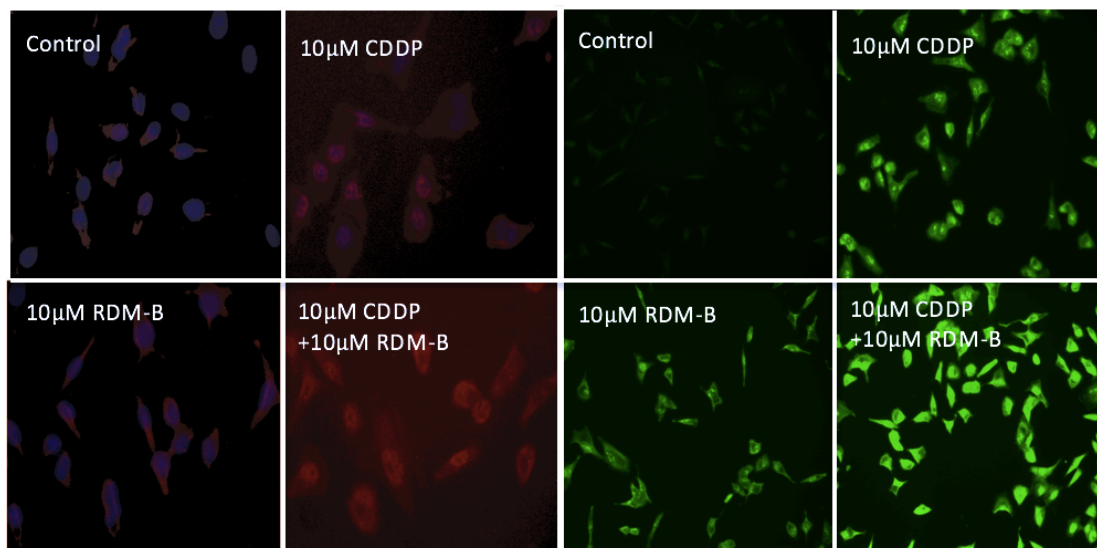
Figure 3-20: Representative images of A549 cells treated by Cisplatin and its combination with Rhodamine-B for DNA DSBs detection and cytotoxicity evaluation using the HCS DNA damage kit. Cells were stained with Alexa Fluor® 555 (red), Hoechst 33342 (blue), and Image-iT® Dead Green™ (green).
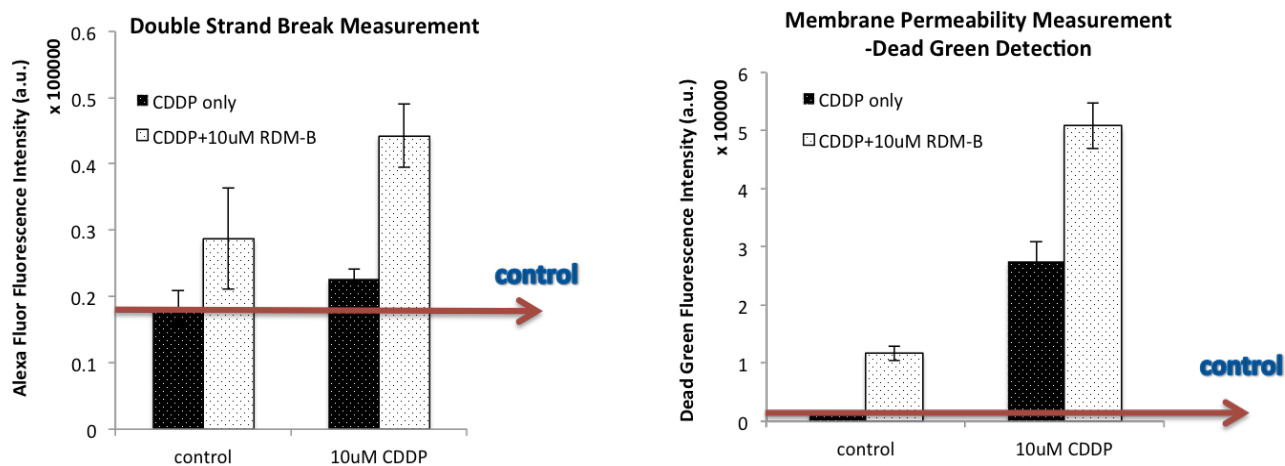
Figure 3-21: Integrated Alexa Fluor® 555 and Image-iT® Dead Green™ fluorescence intensities per cell in A549 cells treated by Cisplatin and its combination with Rhodamine-B using the HCS DNA damage kit.

This assay was also applied in human ovarian cancer NIH:OVCAR-3 cells to measure double strand breaks and to evaluate cell membrane integrity. Images are shown in Figure 3-22, followed by their quantitative analyses:
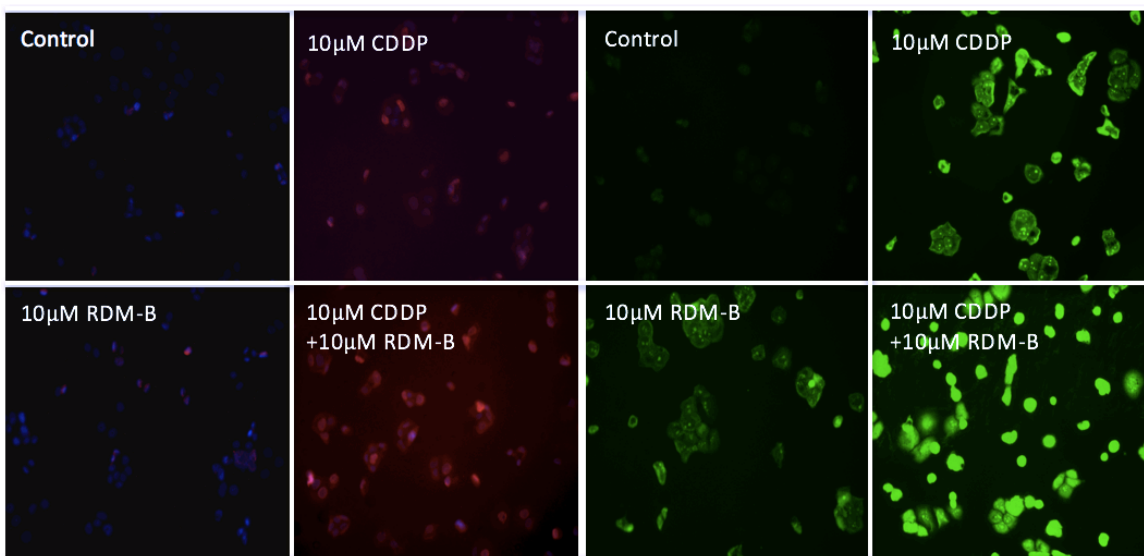
Figure 3-22: Representative images of NIH:OVCAR-3 cells treated by Cisplatin and its combination with Rhodamine-B using the HCS DNA damage kit. Cells were stained with Alexa Fluor® 555, Hoechst 33342 (blue), and Image-iT® Dead Green™ (green).
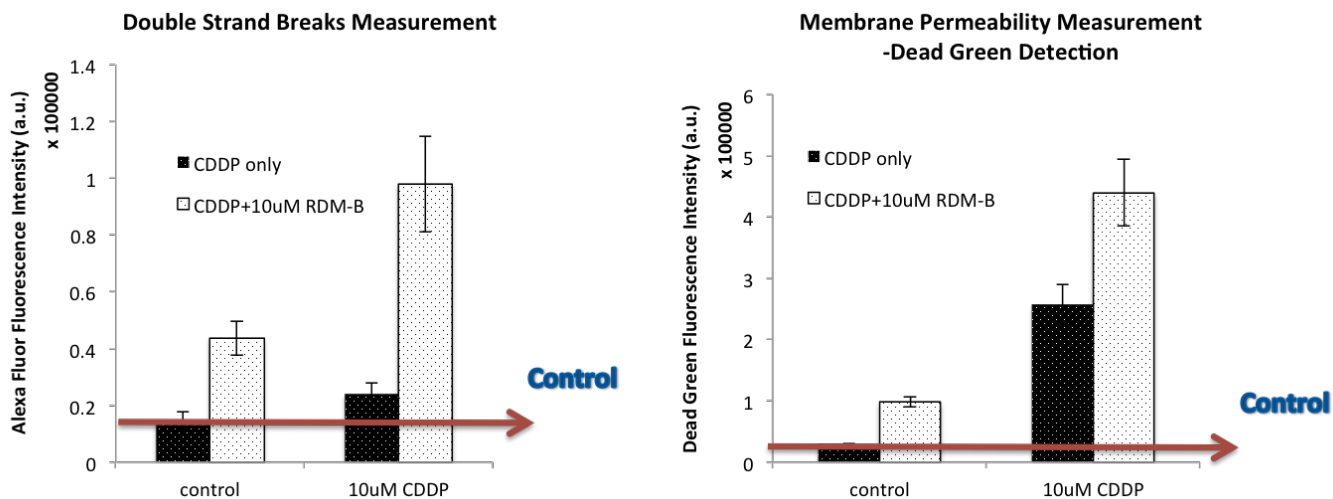
Figure 3-23: Integrated Alexa Fluor® 555 and Image-iT® Dead Green™ fluorescence intensities per cell in NIH:OVCAR-3 cells treated by Cisplatin and its combination with Rhodamine-B using the HCS DNA damage kit.

3.3.5 Early/Late Apoptosis and Necrosis Differentiation

Cisplatin is a known apoptosis inducer, which has been confirmed by our Caspase 3/7-activation experiment. This current early/late apoptosis and necrosis differentiation experiment was performed in human cervical (HeLa) and human lung cancer (A549) cells using the Annexin V-FITC Apoptosis Detection Kit.

HeLa cells were seeded into T25 cell culture flasks at 5×10^5 cells/flask. Overnight incubation was allowed to make sure cells had been well attached. Cells were treated with 0, 20, and 40 µM Cisplatin with/without 20 µM Rhodamine-B. One unstained and two positive controls (PI/FITC single stained) were prepared for the purpose of flow cytometer setup. Positive controls were prepared by HeLa cells treated by 25 µM of Cisplatin. The Annexin V-FITC Apoptosis Detection Kit was performed on the 9 flasks of cells after 18 hours of treatment; the protocol from the manufacturer was followed without modification.

Before staining with fluorochromes, collected cells were washed with PBS for 3 times to remove residual Rhodamine-B and trypsin as much as possible, to minimize overlapped fluorescence signal with PI. After adding the binding buffer, cells were filtered through 70 μm nylon cell strainers to get rid of cell clumps. After that, cells were stained with PI and Annexin V-FITC, and then cells were analyzed by the BD FACSAria™ Fusion flow cytometer. Quantitative analysis was performed using the software FlowJo.

Since two fluorochromes, PI and FITC, were used to stain cells, 2 dimensional graphs were plotted to display the staining, and 4 quadrants were used to represent 4 staining combinations: PI−/FITC−, PI+/FITC−, PI−/FITC+, and PI+/FITC+. The vertical and horizontal lines used to separate cell populations were estimated from the single fluorochromes staining (PI/FITC only) of the two positive controls. The graphs are shown in Figure 3-24:
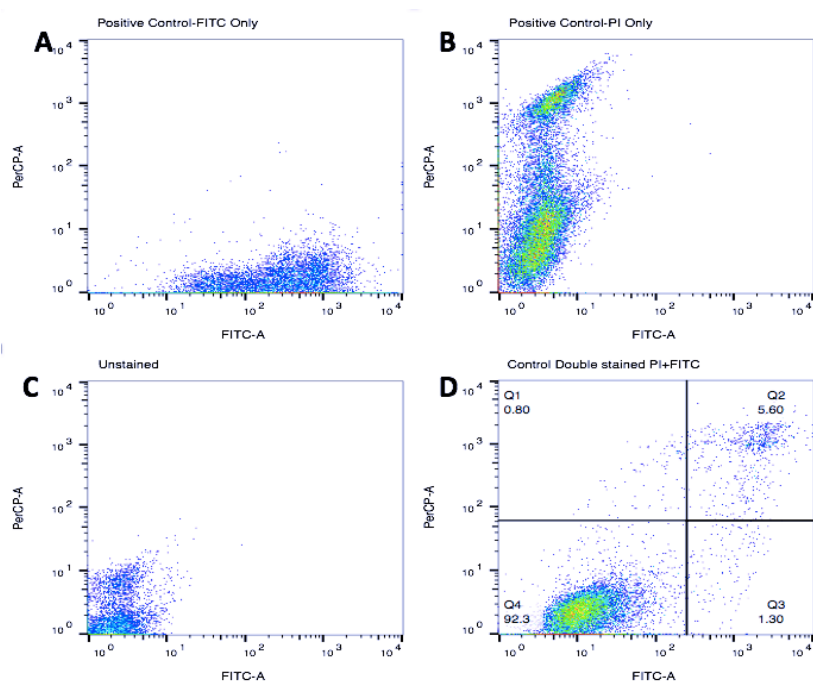
Figure 3-24: (A) and (B): Flow cytometry cell distributions in pre-treated apoptotic HeLa cells stained with Annexin V-FITC only (A) and PI only (B). (C): Unstained and untreated HeLa cells. (D): Untreated HeLa cells double stained with Annexin V-FITC and PI.

For the double stained control sample, the line separating FITC+/− was chosen at 266, and the line separating PI+/− was chosen at 59. These two values were used as reference (approximately) in separating cell populations in the double-stained treated samples.

The graphs of treated samples that were both PI and FITC stained and they are shown in Figure 3-25.

In these graphs, each dot represents a cell. Dots in Q4 represent healthy cells (FITC− and PI−), dots in Q3 represent early apoptotic cells, dots in Q2 represent late apoptotic cells, and dots in Q1 represent necrotic cells.

By comparing the left column graphs (control and Cisplatin only) with the right column graphs (with Rhodamine-B), it can be seen that the major population of cells (healthy) in the right column graphs moved collectively upwards to the PI-positive direction. This was caused by residual Rhodamine-B *inside* cells, which has overlapped excitation and fluorescence spectra with the fluorochrome PI. Although collected cells were washed three times with PBS before staining, Rhodamine-B molecules that had entered cells cannot be removed. However, this did not affect the analysis, since the PI-positive population determined from the positive control that was single stained with PI located at a value around 1000, which was much higher than that of the upwards-moved population (lower than 100). Therefore, these upwards-moved cells were not PI-positive cells. It is notable that for all samples treated with Rhodamine-B, its concentration was fixed at 20 μM, and therefore further upwards-moved cells should be considered as necrotic. This observation actually provides evidence that Rhodamine-B can enter the cell during incubation and it provides chance for the reaction of Cisplatin and Rhodamine-B to occur inside the cell.
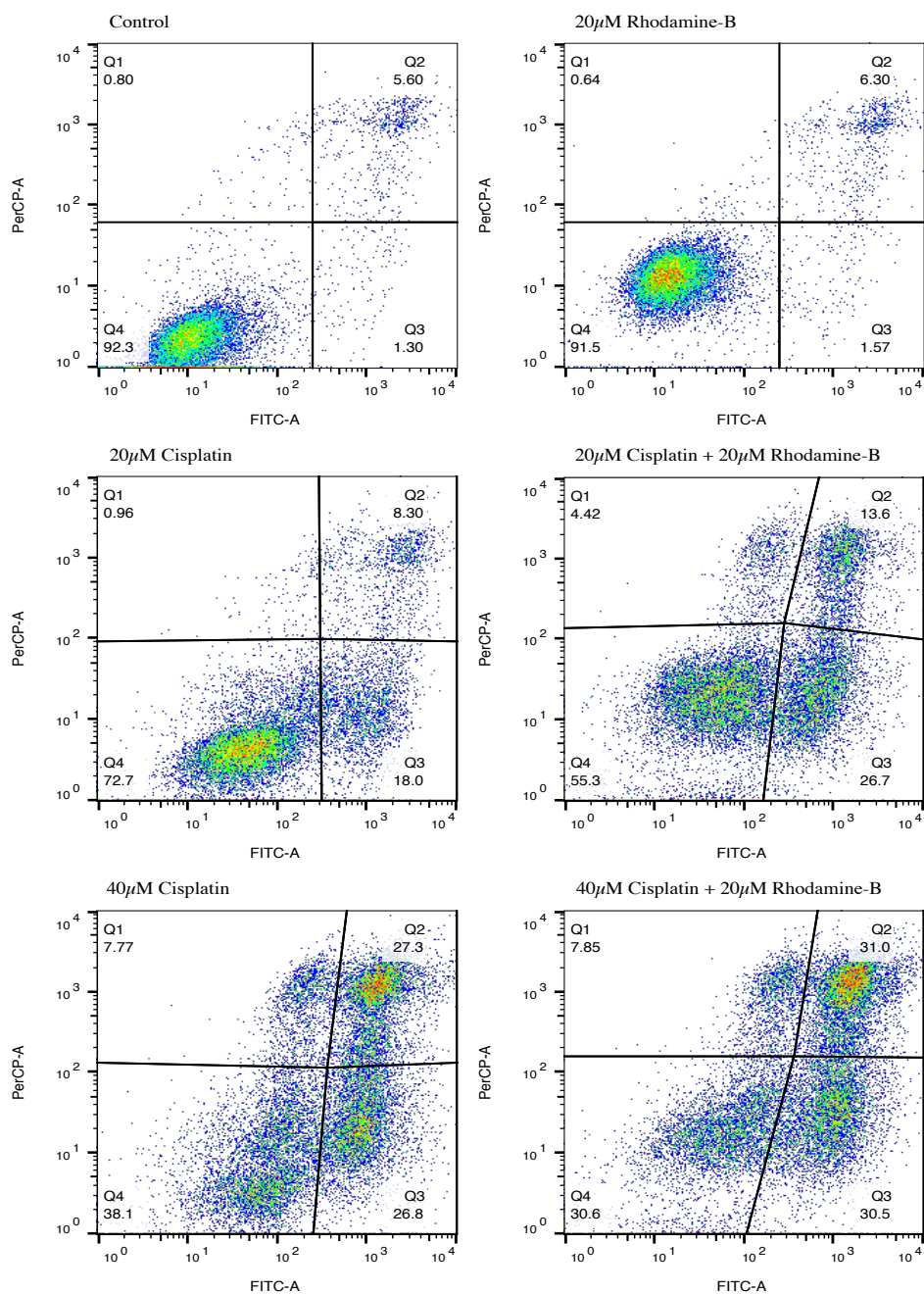
Figure 3-25: Annexin V-FITC Apoptosis Detection in HeLa cells treated by Cisplatin and its combination with Rhodamine-B. Cell populations: healthy (FITC−/PI−: lower-left), early apoptotic (FITC+/PI−: lower-right), late apoptotic (FITC+/PI+: upper-right), and necrotic (FITC−/PI+: upper-left). HeLa cells were treated by 0, 20, 40 μM Cisplatin with (left column)/without (right column) 20 μM of Rhodamine-B. All cells were double stained with Annexin V-FITC and PI.

Percentage of cells in different conditions are indicated in the above graphs and are plotted below in Figure 3-26 and Figure 3-27:
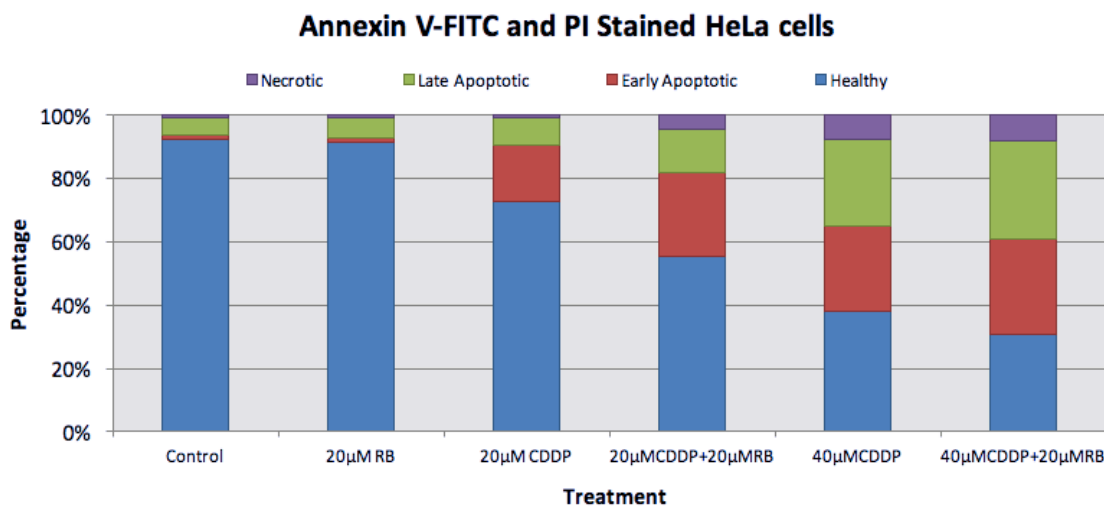
Figure 3-26: Percentages in 100% stacked graph of HeLa cells in different conditions (healthy, early apoptotic, late apoptotic, and necrotic) treated by Cisplatin and its combination with Rhodamine-B.
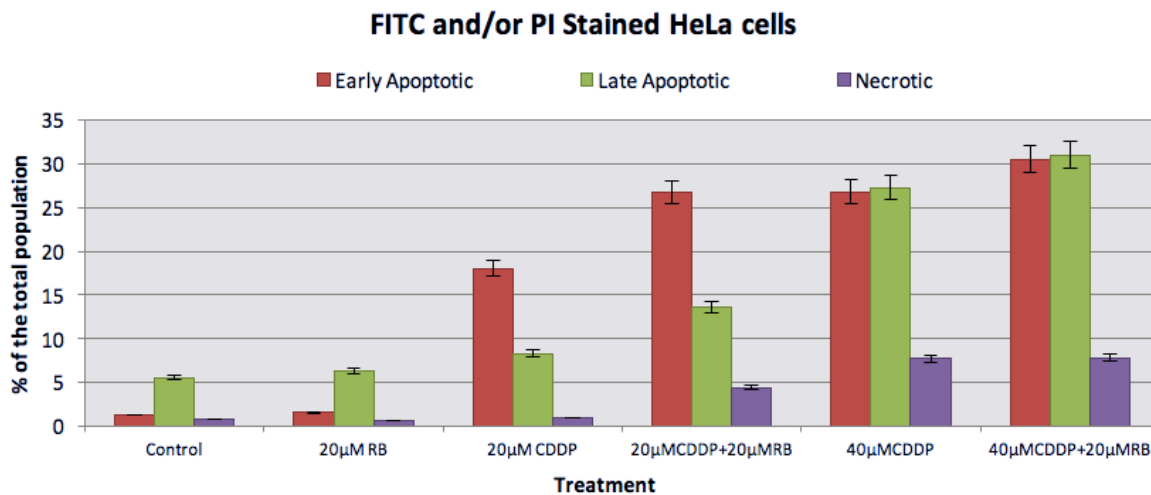
Figure 3-27: Percentages of early/late apoptotic and necrotic HeLa cells treated by Cisplatin and its combination with Rhodamine-B.

As can be seen from the graphs, 20 µM Rhodamine-B did not induce early/late apoptosis and necrosis by itself. However, when it was combined with Cisplatin, many more early and late apoptotic cells were induced, and so were necrotic cells.

The same assay was performed in A549 cells treated with 25 µM and 50 µM Cisplatin with/without 20 µM Rhodamine-B. Results are shown in Figure 3-28.

As can be seen from the graphs, 20 µM Rhodamine-B did not induce more apoptotic or necrotic cells, compared to the control group. When Rhodamine-B was combined with Cisplatin to treat A549 cells, the population of early apoptotic cells increased dramatically. The percentages of late apoptosis and necrosis did not change significantly among the control and all treated groups.

These results were consistent with that of MTT assay. For short time incubation (12/24 hours), HeLa cells were more sensitive to not only Cisplatin but also the combination of Cisplatin and Rhodamine-B, compared to A549 cells. That is why we see a clear population migration from early apoptosis to late apoptosis/necrosis in HeLa cells, but not in A549 cells.
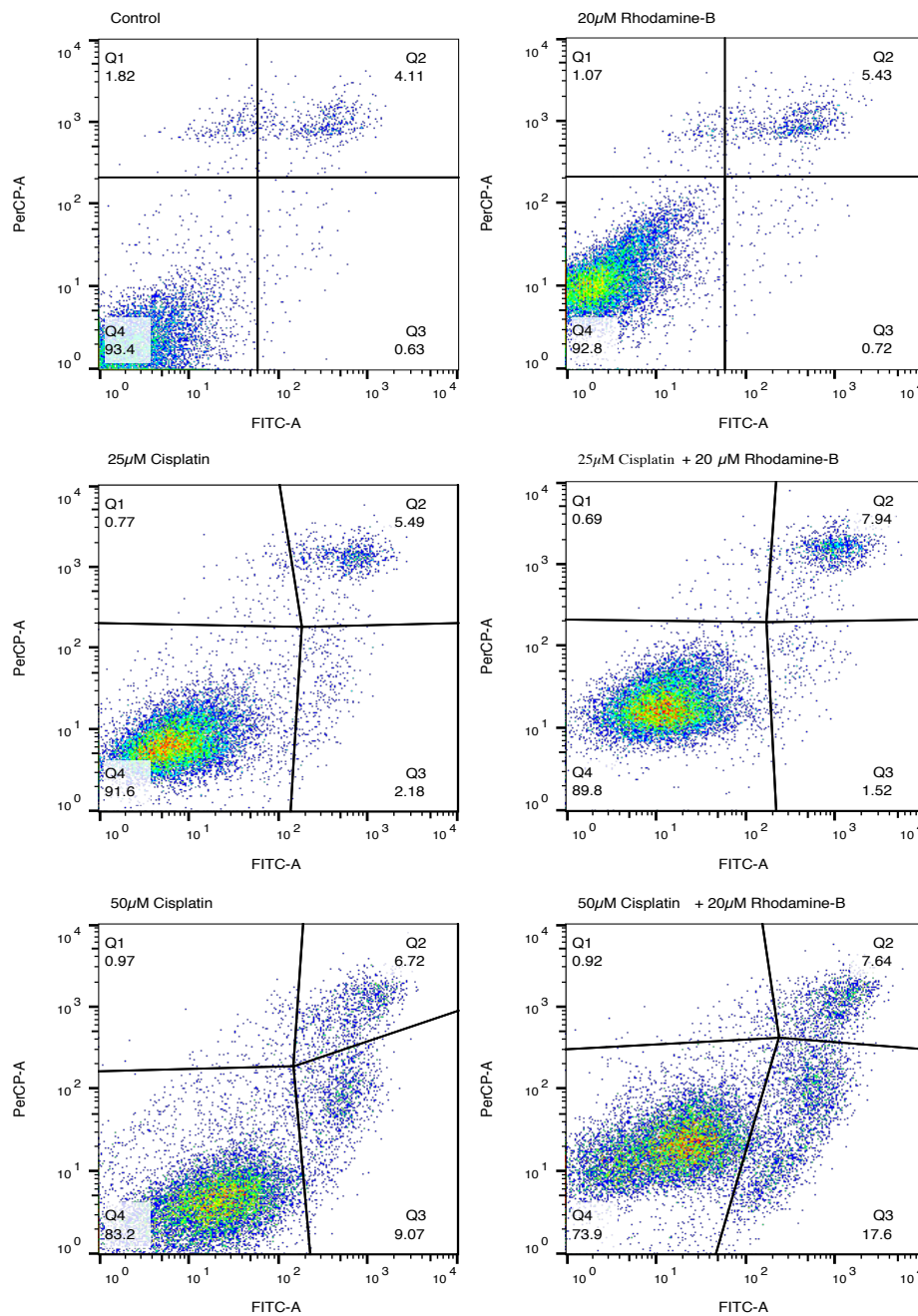
Figure 3-28: Annexin V-FITC Apoptosis Detection in A549 cells treated by Cisplatin and its combination with Rhodamine-B. Cell populations: healthy (FITC−/PI−: lower-left), early apoptotic (FITC+/PI−: lower-right), late apoptotic (FITC+/PI+: upper-right), and necrotic (FITC−/PI+: upper-left). HeLa cells were treated by 0, 25, 50 μM Cisplatin with (left column)/without (right column) 20 μM of Rhodamine-B. All cells were double stained with Annexin V-FITC and PI.

91

Percentages of cells in the four quadrants are plotted in the two figures below:
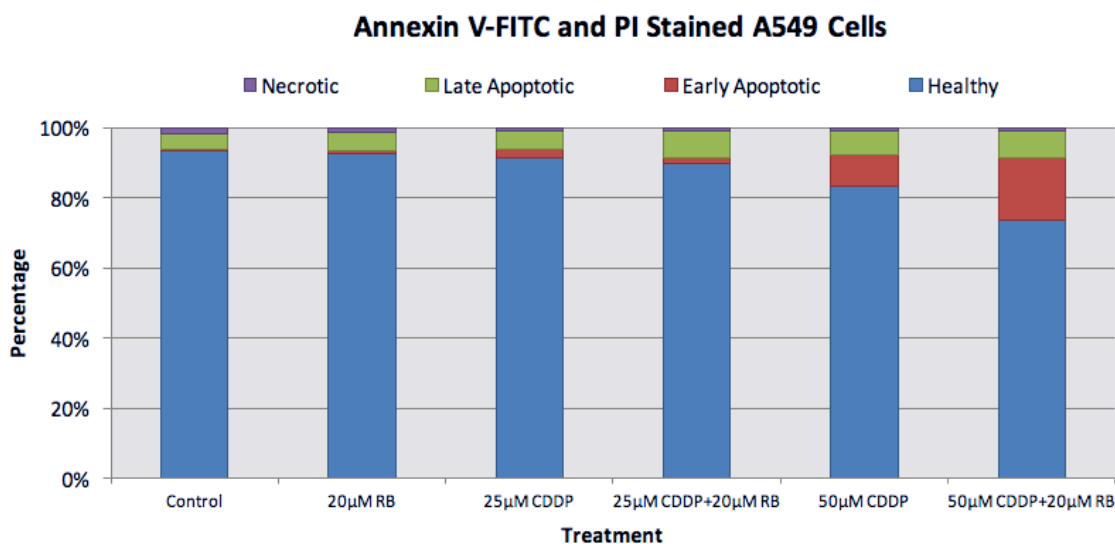
Figure 3-29: Percentages in 100% stacked graph of A549 cells in different conditions (healthy, early apoptotic, late apoptotic, and necrotic) treated by Cisplatin and its combination with Rhodamine-B.
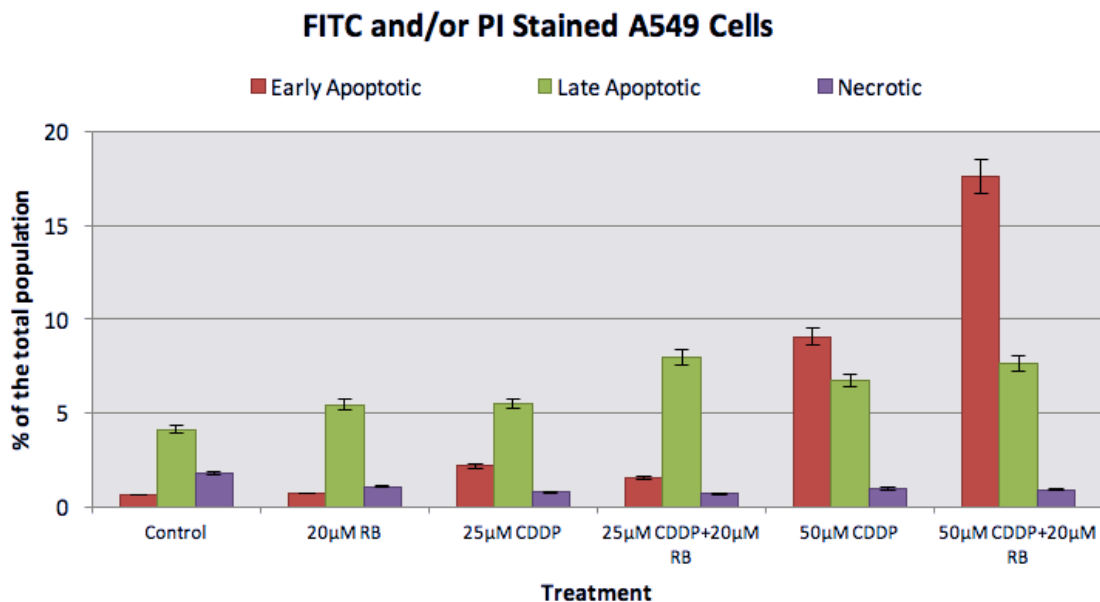
Figure 3-30: Percentages of apoptotic/necrotic A549 cells treated by Cisplatin and its combination with Rhodamine-B.

3.3.6 Plasmid DNA Gel Electrophoresis

Gel electrophoresis was performed in plasmid DNA from *E. Coli* to test the direct damage induced by Cisplatin and the combination of Cisplatin and Rhodamine-B.

The major lesion in DNA caused by Cisplatin is thought to be 1,2-d(GpG) intra-strand cross-links, as introduced in Chapter 1. It has been shown in Chapter 2 that Cisplatin can also intrinsically induce DNA double-strand breaks (DSBs). This experiment is designed to study if the combination of Cisplatin and Rhodamine-B can enhance the formation of DNA DSBs in plasmid DNA.

In this experiment, plasmid DNA (Pgem 3Af(-), 3197kbp) was extracted from *Escherichia Coli* JM109 and purified using the GeneJET Plasmid Miniprep Kit (#K0502) (Thermo Scientific). 5 µL frozen (−80℃) concentrated *E. Coli* was added to 50 mL autoclaved LB medium (10 g/L tryptone, 5 g/L yeast extract, 10 g/L NaCl, and 100 µg/mL Ampicillin sodium salt). *E. Coli* were allowed 16 hours of growth at 37℃ on a shaking plate at 200 r/min before the kit was applied to extract and purify plasmid DNA. The protocol from the manufacturer was followed without modification.

DNA samples were prepared in water at a concentration of 25 µg/mL, incubated with 0, 20, 50, 100, and 200 µM Cisplatin with/without 10 µM Rhodamine-B. Samples were incubated at 37℃ for 150 minutes and then the agarose gel electrophoresis was performed on these treated plasmid DNA samples.

The gel image is shown in Figure 3-31. The amount of DNA in each band on the image was determined from the band peak area. The yields of the undamaged DNA and DNA with DSBs, as functions of Cisplatin concentration, are presented in Figure 3-32.
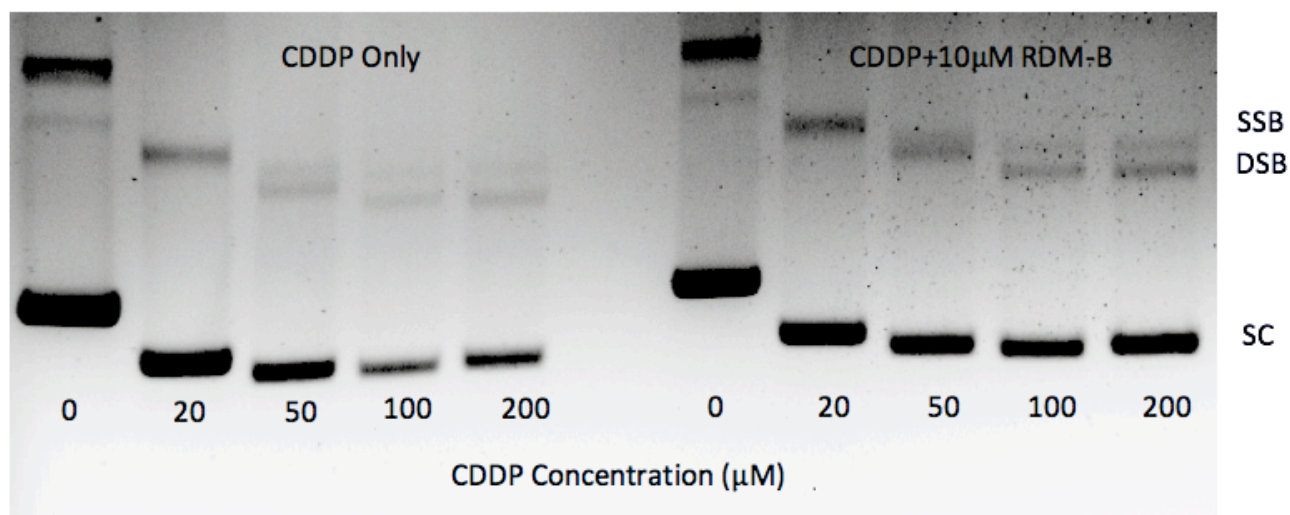
Figure 3-31: Gel electrophoresis image of plasmid DNA treated with 0, 20, 50, 100, and 200 μM of Cisplatin with (right)/without (left) 10μM of Rhodamine-B. Three separated bands from top to bottom represent DNA molecules with single-strand breaks (SSB), double-strand breaks (DSB), and supercoiled (SC) DNA. The gel image seemed over exposed, as the ratios of SSB to SC at 0 μM CDDP appeared to be large.

As shown in Figure 3-32, the presence of Rhodamine-B increased the DNA DSB yields by approximately three times, compared to that by Cisplatin only. Due to the fact that CDDP-DNA adducts formed from intra-strand cross-linking were invisible in the gel image (the fluorescence emission of the DNA-binding EtBr was quenched), the amount of SC DNA decreased as the concentration of Cisplatin increased.

Interestingly, as shown in Figure 3-32 (B), compared to Cisplatin only, the amount of intact (SC) plasmid DNA was *increased* by the addition of Rhodamine-B. That indicates *decreased* formation of Cisplatin-DNA cross-links; it further suggests that Cisplatin molecules were involved in other reactions and therefore fewer free Cisplatin molecules were available to bind to DNA. Moreover, the increased DNA double-strand breaks should be induced by the product(s) from the reaction between Cisplatin and Rhodamine-B, that is, the Cisplatin radicals.
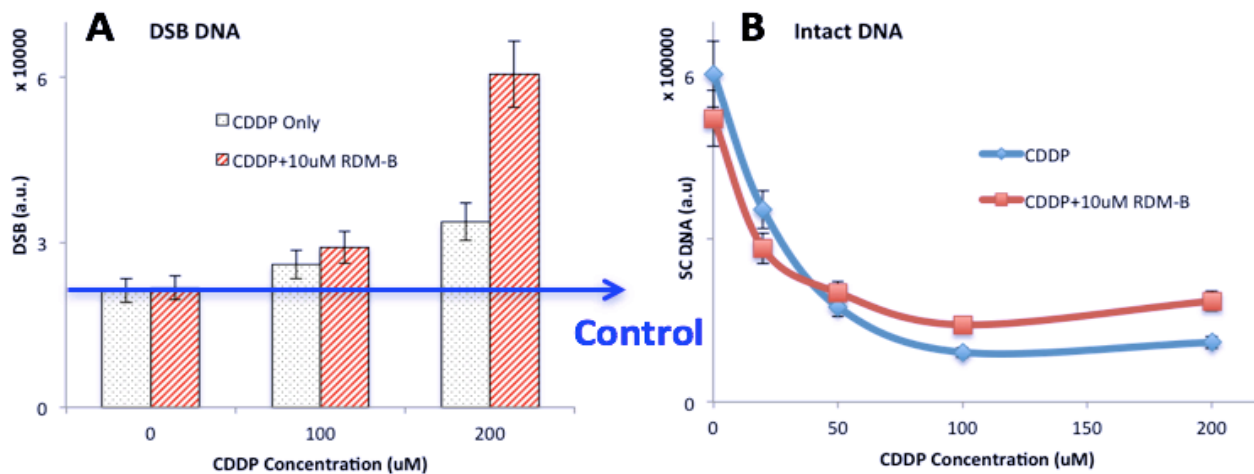
Figure 3-32: Amounts of DNA molecules with DSBs (A) and intact supercoiled DNA (B) treated by Cisplatin and its combination with Rhodamine-B as functions of Cisplatin concentration.

3.4 Conclusion

This Chapter aimed to verify the effectiveness of the combination of Cisplatin and Rhodamine-B in treating various cancer cells.

The *in vitro* chemotherapeutic effect of the combination of Cisplatin and Rhodamine-B was studied through cell survival assays, MTT assay and clonogenic assay. Our results strongly supported that the cell-killing efficacy of Cisplatin was dramatically enhanced by the addition of Rhodamine-B on various cancer cell lines. However, the cell survival was not significantly affected by the addition of Rhodamine-B on the normal GM05757 cell line. Survival assays showed that our combination had a level of selectivity between cancer cell lines and the normal cell line.

Cellular processes leading to the death of cancer cells were studied by several experiments: immunofluorescence microscopy, flow cytometry, and DNA gel electrophoresis. DNA gel electrophoresis directly showed that by adding Rhodamine-B, more double-strand breaks were induced by Cisplatin. Caspase 3/7 activation measurement and Annexin V-FITC labeling flow cytometry experiment proved that cancer cells were more effectively killed by the combination of Cisplatin and Rhodamine-B via inducing more apoptosis. γH2AX staining demonstrated that by the addition of Rhodamine-B, Cisplatin-induced DNA double-strand breaks were greatly enhanced.

To conclude, our studies in this Chapter have proved our combination, Cisplatin and Rhodamine-B, effective in the '*compound screening and secondary assays*' step of early drug development, and this combination is therefore ready to be tested *in vivo*.

Chapter 4

In Vivo Studies of the Combination of Cisplatin and Rhodamine-B

4.1 Objective of This Chapter

The results from cell/DNA-based *in vitro* experiments presented in Chapter 3 have encouraged us to perform further preclinical studies through *in vivo* mouse experiments. This is schematically shown in Figure 4-1[366]:
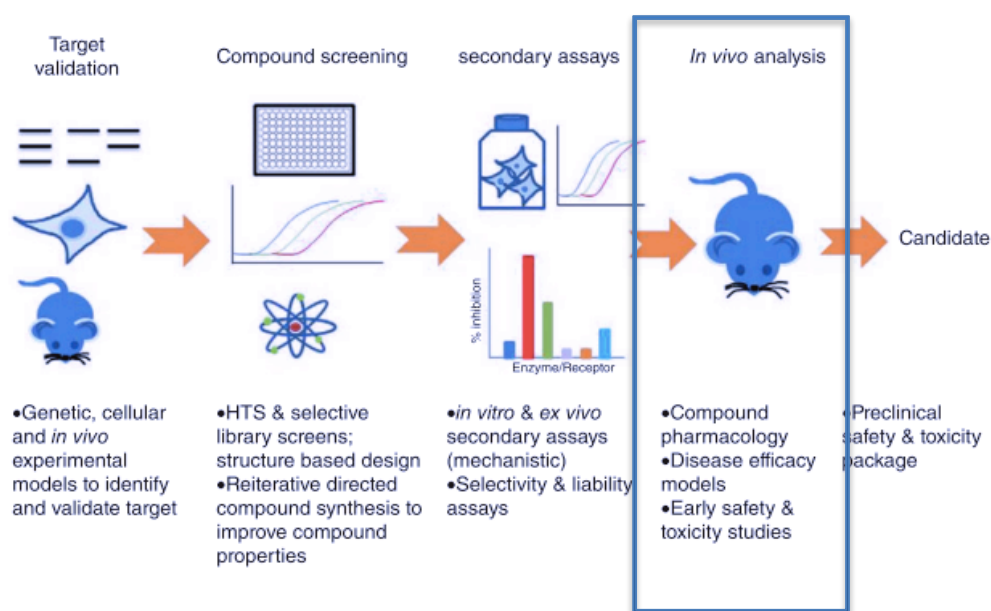
Figure 4-1: Scope of Chapter 4: *in vivo* analysis of the combination of Cisplatin and Rhodamine-B, with the summary of early drug discovery processes/assays[366].

In this Chapter, xenograft mouse models bearing various cancers: lung cancer, ovarian cancer, and cervical cancer are developed to test the *in vivo* anti-cancer effect of the combination of Cisplatin and Rhodamine-B. Tumor growth and tumor samples are studied for chemotherapeutic information; serum samples and gut samples are tested for toxicity profiles.

In this Chapter, questions to be answered are:

(1) Is the proposed combination effective in tumor inhibition, or even tumor shrinkage?

(2) How tumor cells are killed *in vivo* by our combination?

(3) Does the proposed combination cause any additional *in vivo* toxicity?

4.2 Experimental Techniques and Methods

4.2.1 Chemicals, Cell Lines, Assay Kit, Mice and their Conditions

Rhodamine-B and cis-Diammineplatinum (II) dichloride for *in vivo* mouse studies were purchased form Sigma-Aldrich (Sigma-Aldrich Canada Ltd., Oakville, ON, Canada) without further purification. A 0.5 mg/mL solution of Cisplatin and a 3.2 g/mL solution of Rhodamine-B were both prepared in sterile saline (0.9% Sodium Chloride Injection USP) purchased from Baxter (Baxter Co., Mississauga, ON, Canada) and stored in the dark at 4°C. Matrigel used in tumor cell injection was purchased from Sigma-Aldrich.

Xenograft mouse models were used to study the *in vivo* effect of the combination of Cisplatin and Rhodamine-B. The models were developed by injecting cultured cancer cells into the left flank in mice. Detailed information on the three cancer cell lines used in *in vivo* studies: human non-small-cell lung (A549), human ovarian (NIH:OVCAR-3), and human cervical (ME-180) cancer cell lines and their cell culture media with cell growth condition has been introduced in Chapter 3.

In vivo apoptosis detection was performed using the DeadEnd™ Colorimetric TUNEL System (purchased from Promega, Madison, WI, USA).

Female mice with severe combined immunodeficient disease (SCID) aged 6-8 weeks were obtained from Charles River Lab. One-week acclimatization was allowed after mice arrived. Mice were allocated to 5 mice/cage.

4.2.2 Xenograft Mouse Models

Xenograft mouse models of A549, NIH:OVCAR-3, and ME-180 cells were studied. Here the development of the non-small-cell lung cancer (A549) mouse model is introduced in detail and the other two models were built following the same procedure.

A549 cells were cultured in their normal culturing conditions in T75 flasks. Cells were rinsed (PBS), trypsinized, centrifuged, and resuspended in completed F-12K cell culture medium before being counted. Collected concentrated cell solution was diluted by 100 times, and 75 µL of which was pipetted into the Moxi Z™ (ORFLO® Technologies) Mini Automated Cell Counter to be counted. The concentrated cell solution was then diluted in completed cell culture medium, in order that after mixing with the same volume of Matrigel the final concentration was 5×10^6 cells per 100 µL. The mixing process was performed in the biosafety cabinet on ice.

The cell solution was placed on ice and then transferred to the SCID room for injection.

Before tumor injection, the left flank area of mice was shaved for a better visualization of tumors. Mice were injected under anesthesia through Isoflurane inhalation (carried by oxygen). The Central Animal Facility (CAF) at the University of Waterloo provided the apparatus, which is shown in Figure 4-2. As can be seen from the picture, the anesthesia system consists of a gas supplier connected to two compressed gas cylinders (Isoflurane and oxygen), an anesthesia chamber, a fixed nozzle, and two tubes from the pre-injection anesthesia chamber and the nozzle that can be switched when mice were transferred from the chamber to the nozzle. Mice were ear-notched (numbered) before injection at the nozzle. 100 µL cell solution containing 5×10^6 of A549 cells was injected in the left flank to each mouse through subcutaneous injection.

Figure 4-2: Apparatus for mice anesthesia.

Before injection, the Isoflurane pressure (in the chamber) was set to 5% and during the injection it was set to 2-2.5%. Oxygen was continuously given before and during the injection at 1 L/min.

Xenograft mouse models of NIH:OVCAR-3 and ME-180 were built following the same procedure, except that the injected cell numbers were different: 6×10^6 cells per mouse (NIH:OVCAR-3), and 2×10^6 cells per mouse (ME-180).

4.2.3 Chemotherapy Treatment

Mice with tumor volume reached the desirable starting point of treatment, 200 mm^3 for A549 and ME-180 models and 150 mm^3 for NIH:OVCAR-3 model, were randomly allocated into 4 groups: control, Cisplatin, Rhodamine-B, and combination groups. For A549 and NIH:OVCAR-3 models, each group had 7 mice; and for the ME-180 model, each group had 5 mice. The two extra mice from each group in A549 and NIH:OVCAR-3 models were euthanized 24 hours after the last treatment for acute toxicity analysis.

Mice from the control group received saline injection to eliminate the deviation caused by the injection itself. All injections were performed as intraperitoneal (IP) injections.

KMR® powder was purchased from the pet store and it was given to mice as a nutrition supplement when necessary. Vetoquinol Laxatone lubricant was purchased from Shoppers and applied to mice to ameliorate constipation. Polysporin® original antibiotic cream was purchased from Shoppers to treat tumor ulceration.

4.2.4 Tumor Volume Measurement

Approximately, mice were weighed and tumors were measured three times a week after treatments, and twice a week after two weeks after the first treatment (Day 1). The tumor (and surrounding) area was shaved before each measurement to eliminate measurement error caused by the fur.

Tumors were typically ellipsoid, the lengths of the longest axis (L) and that of the axis perpendicular to it (W) were measured by calipers. The volume of a tumor was calculated using the well-accepted formula[373, 374]:

$$V = \frac{L \times W^2}{2}$$

When multiple tumors were observed, the tumor size was calculated as the summation of individual small tumors.

4.2.5 *In Vivo* Apoptosis Detection Using the TUNEL Assay

DNA is degraded into 180-200 bp fragments before a cell dies, this fragmentation has been verified as a component of (late) apoptosis[375–377]. The DeadEnd™ Colorimetric TUNEL System is designed to label

fragmented DNA *in situ* and therefore it is used to detect *in vivo* tumor cell apoptosis. TUNEL is short for terminal deoxynucleotidyl transferase (TdT) dUTP nick end labeling.

Two mice from each group were euthanized 24 hours after the last treatment. The tumor and gut tissues were persisted in formalin for further analysis. These tissues were sectioned and fixed on glass slides in the University of Guelph Animal Health Laboratory and the DeadEnd™ Colorimetric TUNEL System was performed in these sections to detect apoptosis.

In this experiment, some required materials/chemicals were not included in the assay kit. Phosphate buffered saline (PBS) was purchased from Hyclone. Hydrogen peroxide, sodium chloride, formalin, and DNase I were purchased from Sigma-Aldrich. Ethanol was bought from the ChemStore at the University of Waterloo. Coplin jars were purchased from Fisher.

The experimental procedure is briefly introduced below.

The tissue sections were prepared as paraffin-embedded sections. Theses tissue sections were deparaffinized and rehydrated by being immersed in ethanol with decreasingly graded concentrations: 100%, 95%, 85%, 70%, and 50%. After being washed with 0.85% NaCl and PBS, tissue sections were fixed in 10% buffered formalin. After another wash with PBS, 100 μL Proteinase K solution (20 μg/mL) was added on top of the tissue section to make it permeabilized. After 20 minutes' incubation, tissue sections were washed with PBS, and re-fixed in 10% buffered formalin. Slides were washed twice with PBS; excess liquid was removed by tapping with Kimwipes. 100 μL Equilibration Buffer was added on the slide to cover the tissue, and allowed for 10 minutes' incubation. At the end of equilibration, Kimwipes were used to blot around the equilibrated areas. 100 μL rTdT reaction mix (98 μL Equilibration Buffer, 1 μL Biotinylated Nucleotide Mix, and 1 μL rTdT enzyme) was added on the tissues, and they were covered by coverslips and then incubated at 37°C for 60 minutes in a humidified incubator. After the incubation, 2×SSC was applied to terminate the reaction, and 0.3% hydrogen peroxide was used to block

the endogenous peroxidase. 100 μL Streptavidin HRP (1:500 dilution) was added on tissue sections and allowed for a 30 minutes' incubation. After being washed in PBS, 100 μL DAB solution was added on the tissue until a light brown background could be observed (~ 10 minutes). After being rinsed with deionized water a few times, slides were ready to be observed under the microscope. Apoptotic cells were stained with dark brown color.

4.2.6 *In vivo* Acute Toxicity Analysis in Xenograft Mouse Models

Two mice from each group were euthanized 24 hours after the last treatment for acute toxicity study.

Blood samples were collected through a terminal cardiac puncture in the mice. After 30-60 minutes' upright standing for natural clotting, blood samples were centrifuged for 10 minutes at 6,000 revolutions per minute (rpm) using a Mimi centrifuge Sprout™ (Fisherbrand). The supernatant (serum) was collected, labeled, and stored in cryovials at −20℃.

Serum samples were analyzed to study hepatotoxicity and nephrotoxicity.

Xenograft mouse models provide useful and reliable information on the hepatotoxicity of a given treatment[378]. Exposure of drugs or xenobiotics may induce the dysfunction or damage of liver, which is called hepatotoxicity[379]. Serum alanine aminotransferase (ALT), alkaline phosphatase (ALP), and total bilirubin (TBL) are all biomarkers of hepatotoxicity[380]. ALT participates in the metabolism and gluconeogenesis of amino acids by catalyzing the reductive transfer of an amino group from L-alanine to α-ketoglutarate, the products of this reaction are pyruvate and L-glutamate[380]. When hepatocytes are damaged, ALT will be released to the extracellular space and introduced into the circulation system; as a result, elevated serum level of ALT will be detected. The serum ALT activity has been considered the gold standard to detect liver injury. ALP is an enzyme catalyzing hydrolysis reactions to remove phosphate groups from proteins, nucleotides, and alkaloids at an alkaline pH[381]. Bile can eliminate ALP,

but liver damage inhibits the excretion of bile[378]. As a result, elevated serum ALP level is an indicator of hepatobiliary effects and cholestasis (impaired bile glow)[382], and it is also a marker of hepatotoxicity. Bilirubin is an "orange-yellow pigment derived from senescent RBCs (red blood cells)"[383], which is moved from the blood to the liver by binding to albumin. After the dissociation on the hepatocytes' membrane, bilirubin is transported into the cell. Bilirubin must be conjugated to form bilirubin monoglucuronide and diglucuronide before being excreted to the bile[384]. Bilirubin test is used to assess the liver's ability to clear endogenous/exogenous substances from the circulation. The level of bilirubin indicates how capable the liver is in moving bilirubin into the bile from plasma[379]. Elevated level of bilirubin in serum also serves as a biomarker of cholestasis and hetatotoxicity[380].

Acute nephrotoxicity (renal toxicity) was studied by measuring the serum urea and serum creatinine levels. Urea and creatinine are both end products from nitrogenous metabolism, the metabolism of protein (mainly dietary) nitrogen, and the catabolism of muscle creatine, respectively[385]. Both urea and creatinine are excreted through glomerular filtration[386]. When abnormal kidney function occurs, the glomerular filtration rate (GFR) is decreased, and therefore less urea/creatinine is removed from the body with urine. As a result, an increased serum urea/creatinine is an indicator of renal dysfunction. In this project, urea and creatinine levels in mice serum samples were measured to detect possible nephrotoxicity caused by our treatment. Nephrotoxicity also causes electrolyte disturbances. In this project, serum electrolytes levels were also measured.

4.2.7 Animal Experiments Guidelines and Humane Endpoints

All animal experiments in this project were performed in agreement with the University of Waterloo's Guidelines for the Care and Use of Animals in Research and Teaching (AUPP #13-30), the Animals for

Research Act of Ontario, and the Guide to the Care and Used Experimental Animals for the Canadian Council on Animal Care.

According to the animal experiment protocol, the humane endpoint is reached if any of the following is observed:

1. Bodyweight loss > 20% from the first day of treatment;

2. Diameter of the longest axis of the tumor > 17mm;

3. Body condition score (BCS) < 2;

4. Deep tumor ulceration.

Mice were euthanized when the humane endpoint was reached.

4.3 Results and Discussion

4.3.1 Tumor Growth Inhibition/Shrinkage Study

4.3.1.1 Lung Cancer (A549) Xenograft Mouse Model

When the tumor volume reached 200 ($\pm$20) mm^3 mice were randomly allocated into 7/group with 5 for tumor growth measurement and 2 for acute toxicity study.

Mice in the control group received saline injections. Mice in the Cisplatin group received 3 treatments of 2.5 mg/kg Cisplatin, mice in the Rhodamine-B group received 3 treatments of 8 mg/kg Rhodamine-B, and mice in the combination group received 3 treatments of 2.5 mg/kg CDDP and 8 mg/kg with 15-20 minutes between two injections (in the order: Cisplatin, and then Rhodamine-B). All solutions were prepared in saline and all injections were IP injections. Treatments were given on days 1, 3, and 5.

The tumor growth graph is shown in Figure 4-3:
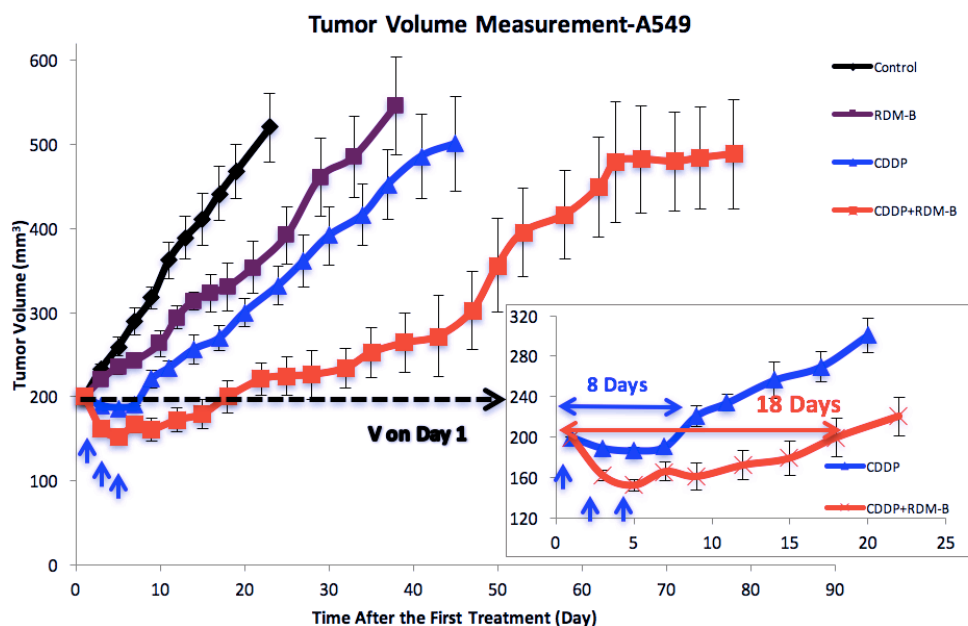
Figure 4-3: Tumor growth curves of mice bearing A549 tumors receiving different treatments: saline (black), Rhodamine-B (purple), Cisplatin (blue), and Cisplatin combined with Rhodamine-B (red). Error bars represent the standard error of the mean (s.e.m.) of measurements on the same day in each group. The inset shows the tumor shrinkage observed in the Cisplatin group and the combination group.

As can be seen from the curves, three 8 mg/kg Rhodamine-B treatments weakly inhibited the tumor growth. Three 2.5 mg/kg Cisplatin treatments induced tumor shrinkage (lowest point to ~180 mm³) during the treatment period (day 1-5) and it took 3 more days to grow back to the initial volume. Three combination treatments induced a more significant tumor shrinkage (lowest point to ~145 mm³) and the tumor shrinkage continued for 13 more days after the treatment. Compared to the Cisplatin group, the combination group prolonged the tumor shrinkage duration from 8 days to 18 days. The subsequent tumor growth curves also showed a dramatic difference between Cisplatin and combination groups.

4.3.1.2 Ovarian Cancer (NIH:OVCAR-3) Xenograft Mouse Model

When the tumor volume reached 150 ($\pm$20) mm^3 mice were grouped the same as the lung cancer (A549) xenograft mouse model.

The treatment dosages were the same as that of the lung cancer (A549) xenograft mouse model; however, instead of 3 treatments, 1 additional was given. Totally 4 treatments were given: each one on days 1, 3, 5, and 7.

The tumor growth graph is shown in Figure 4-4.
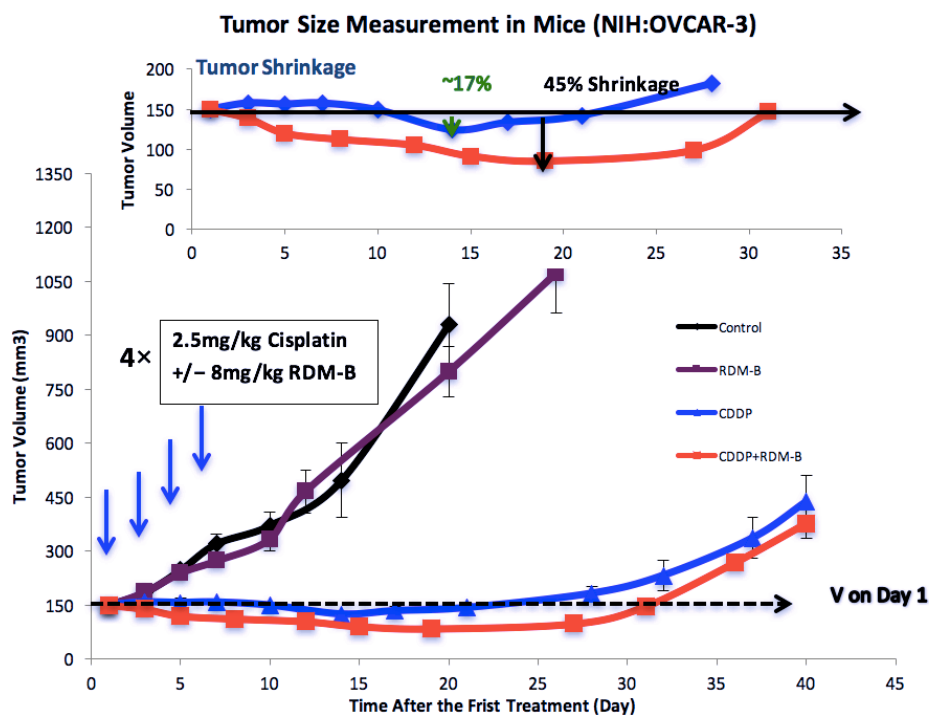
Figure 4-4: Tumor growth curves of mice bearing NIH:OVCAR-3 tumors receiving different treatments: saline (black), Rhodamine-B (purple), Cisplatin (blue), and Cisplatin combined with Rhodamine-B (red). Error bars represent the standard error of the mean (s.e.m.) of measurements on the same day in each group. The inset shows the tumor shrinkage observed in the Cisplatin group and the combination group.

107

As shown in Figure 4-4, the tumor growth curve of the control group and that of Rhodamine-B treatment group increased at almost the same speed and no significant difference was observed. The combination $4 \times$ [2.5 mg/kg Cisplatin$+8$ mg/kg Rhodamine-B] treatments induced tumor shrinkage during the treatments (Days 1-7) while the 4×2.5 mg/kg Cisplatin treatments did not. After the treatment, the averaged tumor volume in the combination group kept decrease (lowest point on day 18 to ~ 80 mm^3, $> 45\%$ tumor shrinkage) and it took approximately 25 more days to grow back to the treatment-starting volume 150 mm^3. The averaged tumor volume in the Cisplatin group unexpectedly decreased from day 10 to day 17, the possibility of measuring error on day 14 was not excluded. Even though the tumor shrinkage was questionable in the Cisplatin group, the tumor growth inhibition was very significant (approximately 15 days before apparent tumor volume increase), compared to the control/Rhodamine-B group.

Photos of mice with tumors were taken on Day 22. They are shown below in Figure 4-5:

108

CDDP only-Day 22

CDDP + Rhodamine-B-Day 22
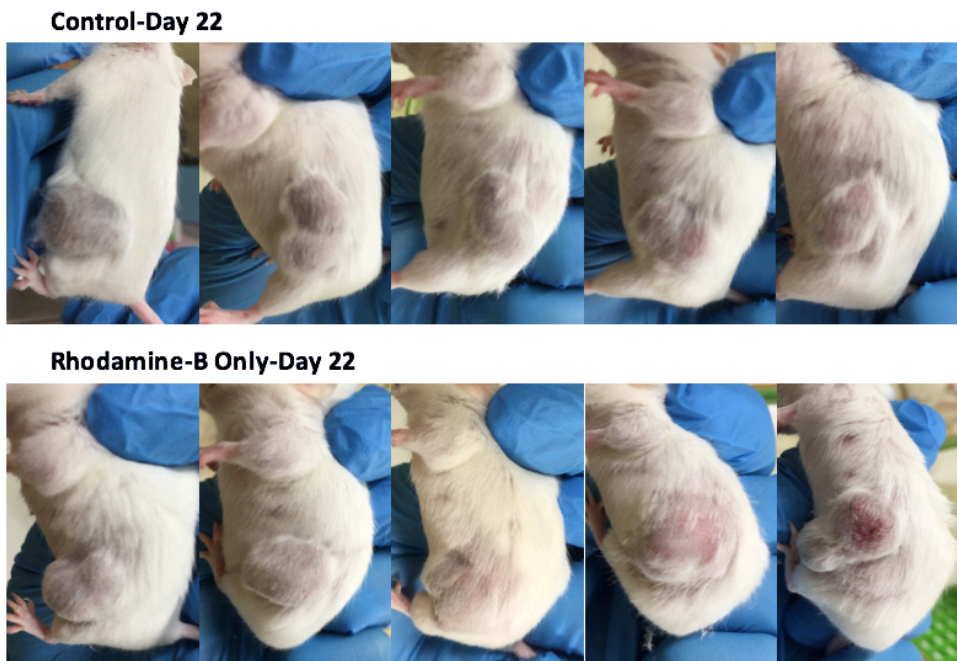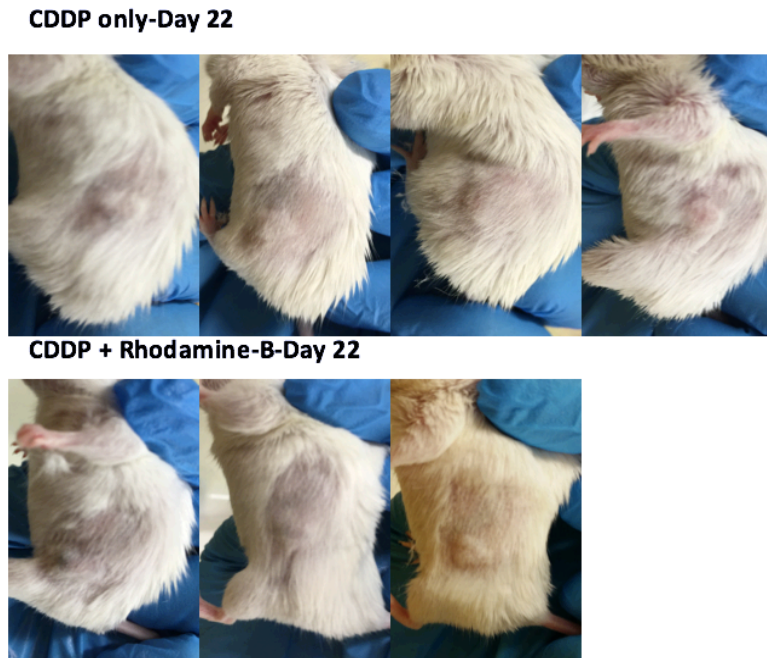
Figure 4-5: Pictures of mice bearing NIH:OVCAR-3 tumors receiving different treatments.

As can been seen from the photos, Rhodamine-B did not significantly affect tumor growth; the tumor size from the control group and Rhodamine-B only group did not show a big difference. However, when Rhodamine-B was combined with Cisplatin, the tumor growth inhibition was greatly enhanced.

4.3.1.3 Cervical Cancer (ME-180) Xenograft Mouse Model

When the tumor volume reached 200 ($\pm$20) mm^3 mice were randomly allocated into 5/group for tumor growth inhibition study. (Acute toxicity study was performed on the other two models)

Treatments were the same as that of lung cancer (A549) xenograft model, but the dose of Cisplatin was given at 2.0 mg/kg instead of 2.5 mg/kg. 3 treatments were given on day 1, 3, and 5.

The tumor growth graph is shown in Figure 4-6. As the figure shows, ME-180 cells were more sensitive to the 8 mg/kg Rhodamine-B treatment, compared to the other two models. Tumor growth was inhibited by single agent treatment either Rhodamine-B or Cisplatin, with a weak superiority observed in the

Cisplatin group. The combination of Cisplatin of Rhodamine-B more significantly inhibited the tumor growth. Tumor-volume-tripling (600 mm^3) growth time was 12 days of the control group, 16 days of the Rhodamine-B group, 17 of the Cisplatin group, and 26 days of the combination group.
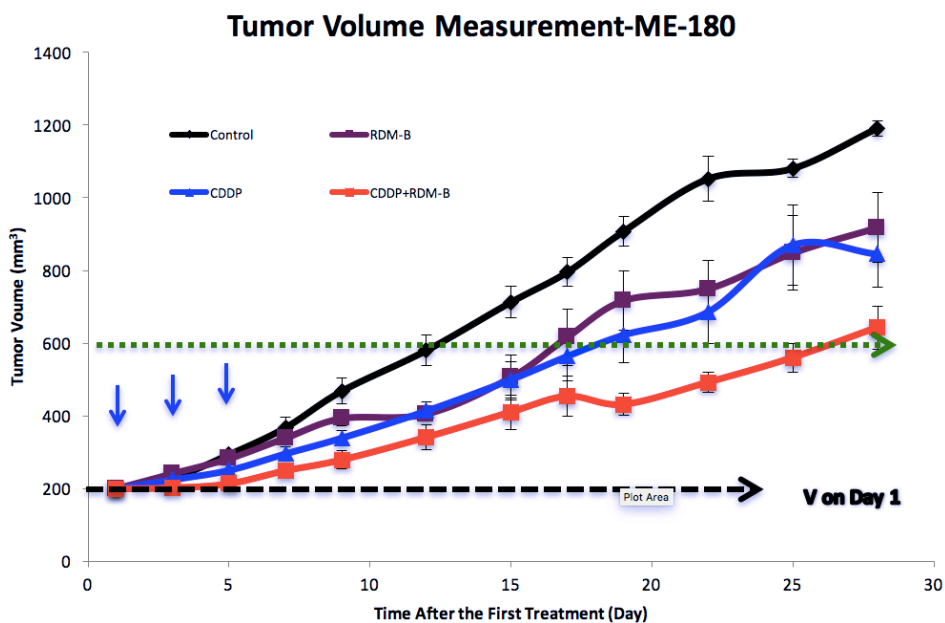
Figure 4-6: Tumor growth curves of mice bearing ME-180 tumors receiving different treatments: saline (black), Rhodamine-B (purple), Cisplatin (blue), and Cisplatin combined with Rhodamine-B (red). Error bars represent the standard error of the mean (s.e.m.) of measurements on the same day in each group. The dashed green line represents the tripled volume from day 1, i.e. 600 mm^3.

4.3.2 *In Vivo* Apoptosis Detection in Tumors

Tumor samples were collected 24 hours after the last treatment and were stored in formalin. Paraffin-embedded sections were prepared and to be analyzed. After being processed as the procedure described previously, slides were observed under microscope and pictures were taken by a Nikon Cloopix 8400 camera. Apoptotic cells were stained with dark brown color and non-apoptotic cells were stained blue. For each slide, at least 4 pictures were taken.

Images of NIH:OVCAR-3 tumor samples from mice are shown below in Figure 4-7.
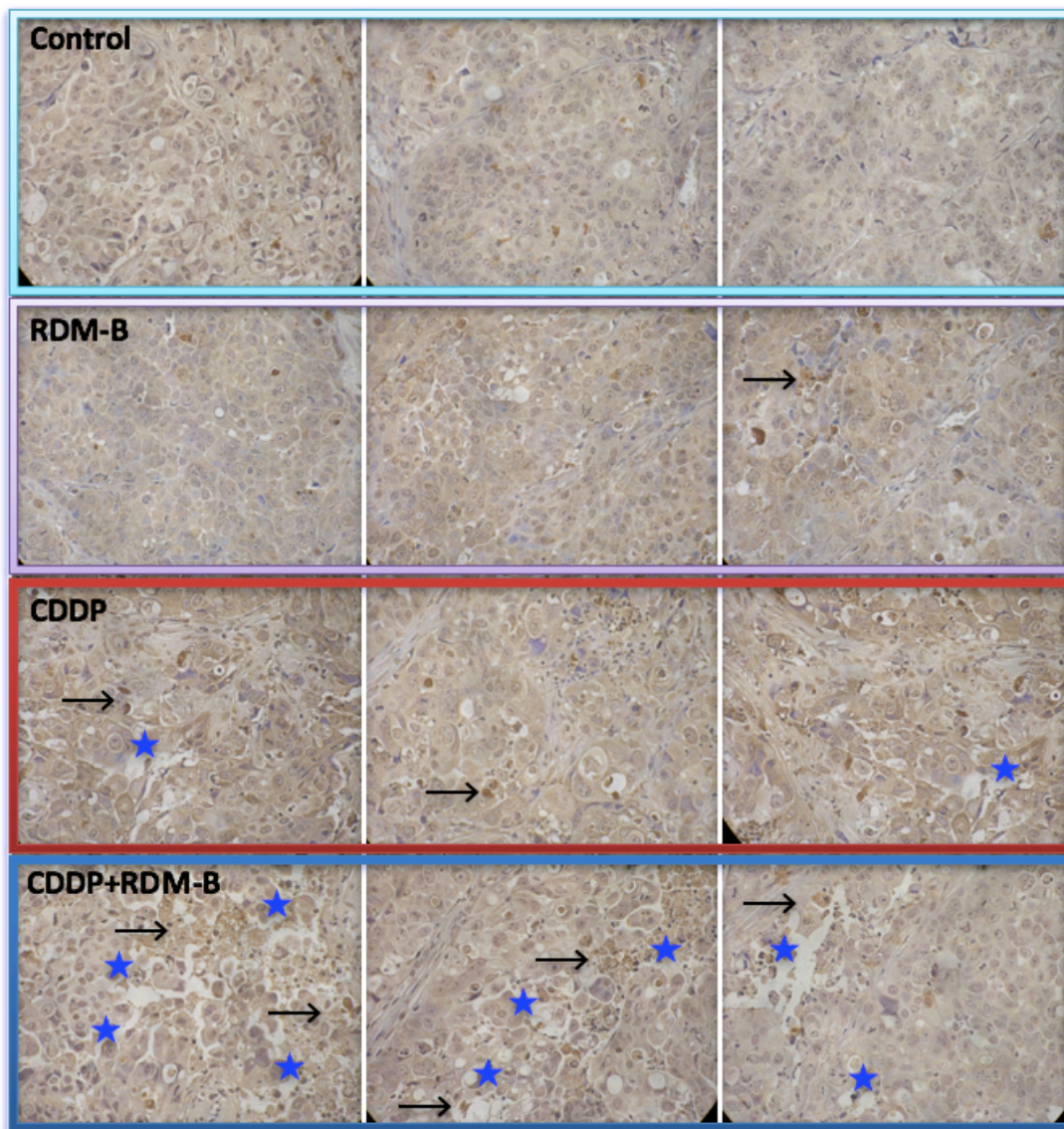
Figure 4-7: Representative TUNEL pictures of tumor sections from NIH:OVCAR-3 tumor-bearing mice receiving different treatments. Black arrows and blue stars are used to indicate positively stained (apoptotic) cells and tumor structure changes, respectively.

As can be seen from the pictures, tumor tissues in the control and Rhodamine-B groups were similar: cells were uniformly distributed, connection tissues were well shaped, with few cells stained dark brown (apoptotic).

Tumor tissues from the Cisplatin group had cells stained with dark brown, indicating Cisplatin treatment induced *in vivo* apoptosis in the NIH:OVCAR-3 tumors. Besides, the tumor structure was altered by the treatment: cells were no longer uniformly distributed, cell shape changed, and we could even observe some "blank" spaces. In the combination group, tumor change was much more significant. More cells were stained dark brown, with a lot of cells isolated and condensed. More hollows were observed in the tumor tissue; tumor destruction was more severe.

These pictures were consistent with our tumor volume measurement. The combination of Cisplatin and Rhodamine-B more effectively treated NIH:OVCAR-3 tumors through inducing more apoptosis.

4.3.3 In Vivo Apoptosis Detection in the Gut

Gut samples were processed the same as tumor samples.

Representative pictures of NIH:OVCAR-3 gut sections are shown in Figure 4-8.

These pictures showed that Rhodamine-B induced mild gut damage. Cisplatin induced significant gut toxicity; however, the addition of Rhodamine-B did not show further gut damage from the pictures.
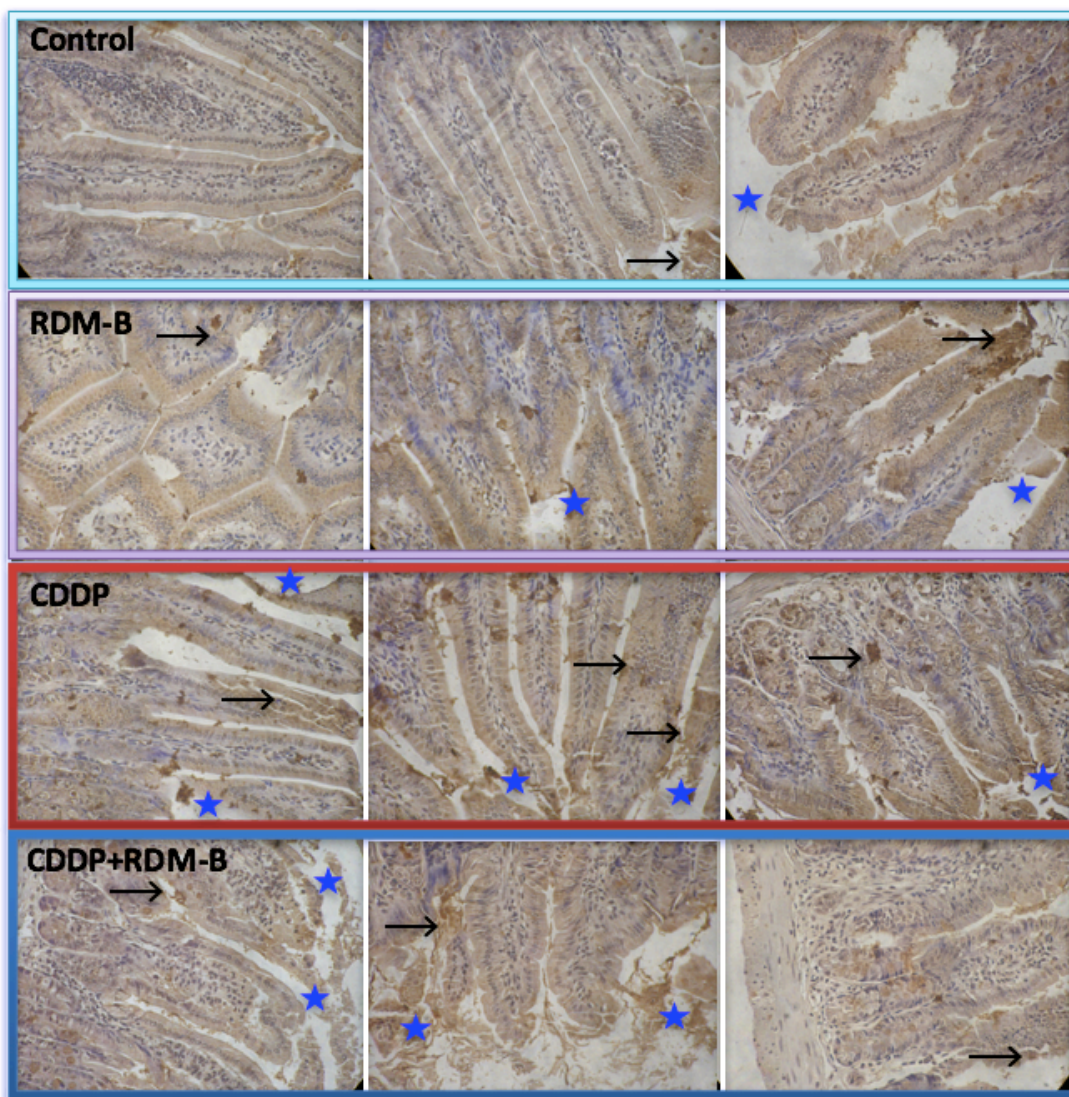
Figure 4-8: Representative TUNEL pictures of gut sections from NIH:OVCAR-3 tumor-bearing mice receiving different treatments. Black arrows and blue stars are used to indicate positively stained (apoptotic) cells and structure changes, respectively.

4.3.4 *In Vivo* Acute Toxicity Studies

Cisplatin-induced toxicity has been extensively studied and has been introduced in Chapter 1. Increase in serum creatinine and urea, imbalanced electrolytes' levels have been reported in Cisplatin-treated patients[387]. Though we have observed significant enhancement in tumor growth inhibition and even tumor shrinkage by treating mice with the combination of Cisplatin and Rhodamine-B, we need to study whether the addition of Rhodamine-B introduces additional toxicity.

As described previously, two mice from each group were euthanized for serum sample collection. Samples were sent to the University of Guelph Animal Health Laboratory for analysis.

4.3.4.1 Hepatotoxicity

In this test, serum ALT, ALP, and total bilirubin levels were measured to assess acute hepatotoxicity. Two different treatment regiments were given for the two xenograft models: A549 and NIH:OVCAR-3. For the A549 model, 2.5 mg/kg Cisplatin with/without 8 mg/kg Rhodamine-B were given on day 1, 3, and 5 (3 treatments in total); however, for the NIH:OVCAR-3 model, the same concentrations of Cisplatin and Rhodamine-B were given on days 1, 3, 5, and 7 (4 treatments in total). For each model, serum samples from two mice/group were collected and analyzed.

The serum level for any marker was represented by the average of the two, and the errors represent the standard error of the mean ($\pm$ s.e.m.).

The results for hepatotoxicity are shown below in Figure 4-9:

114
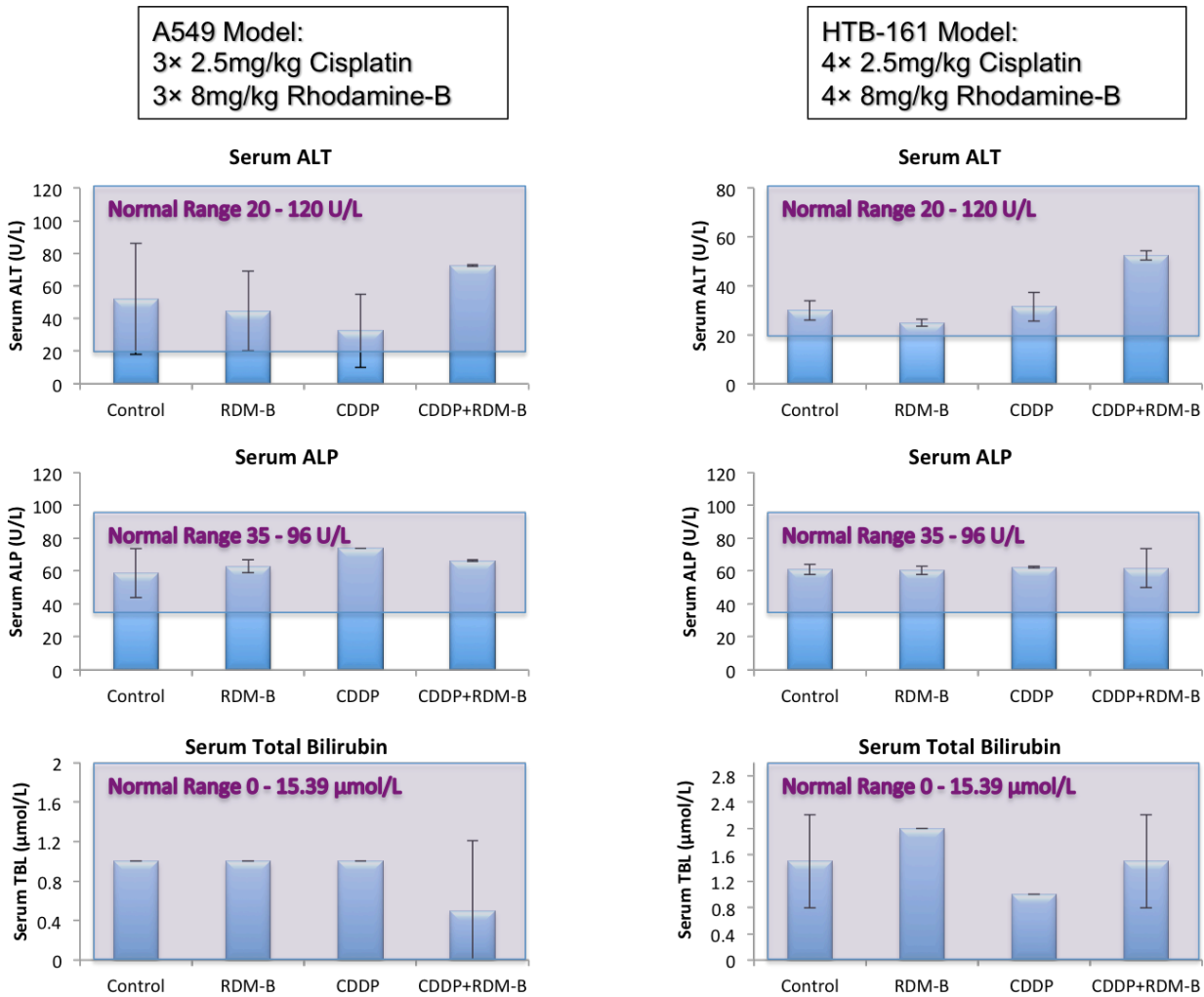
Figure 4-9: ALT, ALP, and total bilirubin serum levels in mice (bearing A549 and NIH:OVCAR-3 tumors) 24 hours after treatment. Light-purple rectangles represent normal serum levels.

Normal serum ALT, ALP, and total bilirubin levels are represented by the light-purple rectangles and the numbers are also indicated on the graphs. As can be seen, none of the given treatments induced significant increase in serum ALT, ALP, or total bilirubin levels; that is to say, no hepatotoxicity was induced. It can be confirmed that the addition of Rhodamine-B to the Cisplatin treatment does not induce additional hepatotoxicity.

115

The hepatic Common Toxicity Criteria of the National Cancer Institute (version 2.0) is outlined below in Table 4-1:

Grade	Normal Range	0	1	2	3	4
Description		None	Mild	Moderate	Severe	Life-threatening or disabling
Alanine Aminotransferase (ALT)	20-120 U/L	WNL	>ULN-2.5×ULN	>2.5-5.0×ULN	>5.0-20.0×ULN	>20.0×ULN
Alkaline Phosphatase (ALP)	35-96 U/L	WNL	>ULN-2.5×ULN	>2.5-5.0×ULN	>5.0-20.0×ULN	>20.0×ULN
Bilirubin	0-15.39 µmol/L	WNL	>1-1.5×ULN	>1.5-3.0×ULN	>3.0-10.0×ULN	>10.0×ULN
Creatinine	3.42-15.39 µmol/L	WNL	>1-1.5×ULN	>1.5-3.0×ULN	>3.0-6.0×ULN	>6.0×ULN
Urea	2.86-11.78 mmol/L					
WNL = within normal limits; ULN = upper limit of normal						

Table 4-1: Common hepatic toxicity criteria.

From the measured results, none of the values was out of the normal limits, even for mice in the combination group with increased serum urea and creatinine from the NIH:OVCAR-3 xenograft mouse model (with 4 treatments).

4.3.4.2 Nephrotoxicity

In this test, serum urea and creatinine levels were measured to assess acute nephrotoxicity.

The serum level results were represented by the average of the two mice from each group, and the errors represent the standard error of the mean ($\pm$ s.e.m.).

The results for nephrotoxicity of the two xenograft models A549 and NIH:OVCAR-3 are shown below in Figure 4-10:
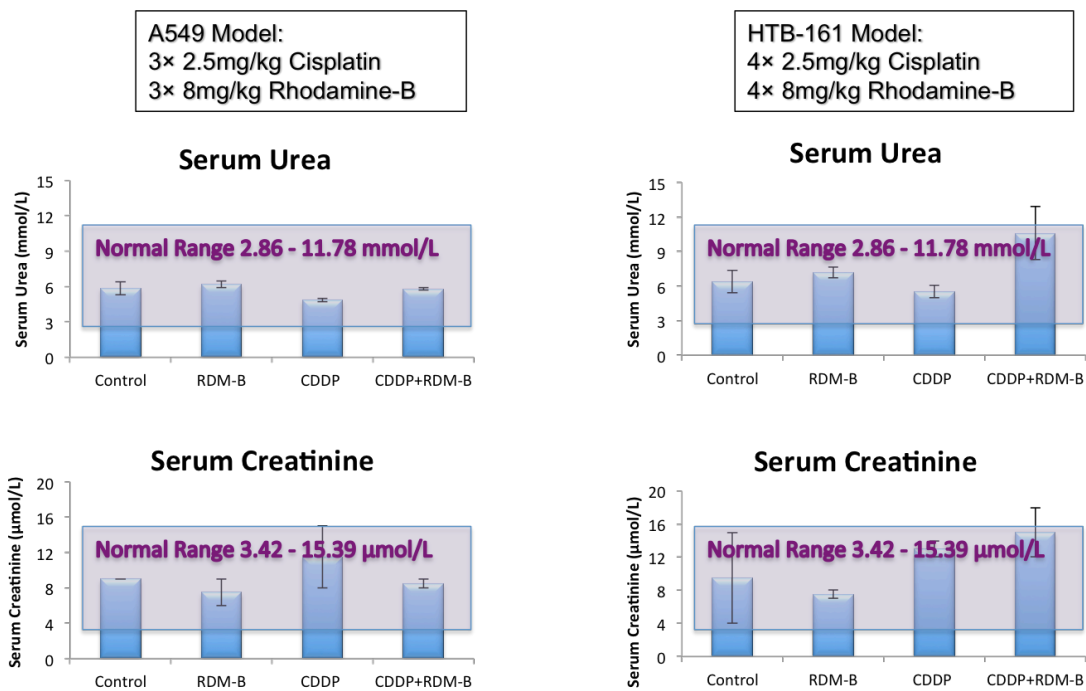
Figure 4-10: Serum urea and creatinine levels in mice (bearing A549 and NIH:OVCAR-3tumors) 24 hours after treatment. Light-purple rectangles represent normal serum ranges.

For the A549 model, all serum urea and creatinine levels fell in the normal ranges. However, for the NIH:OVCAR-3 model, an observable increase in both serum urea and creatinine were observed in the combination group, compared to the other three groups. Values were still within the normal range, while the addition of errors made them fell at the upper limit of the normal ranges. 4 treatments might introduce more severe sides effects than 3 treatments.

4.3.4.3 Electrolytes

The serum electrolytes levels of Na^+, K^+, Cl^-, and the ratio of Na^+/K^+ were measured and calculated for both the A549 and NIH:OVCAR-3 models.

Results of the A549 model are shown below in Figure 4-11:
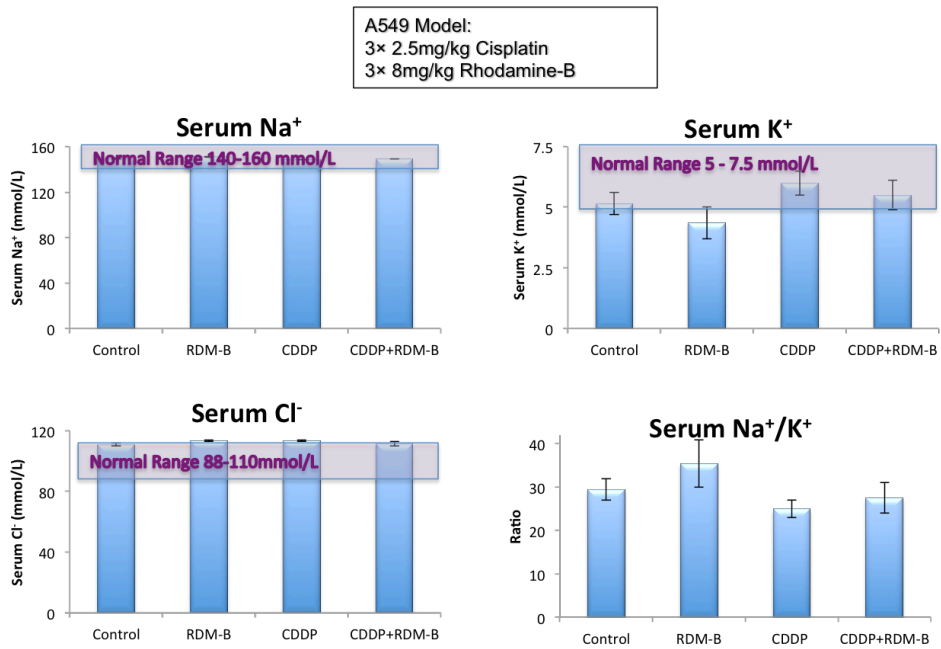
Figure 4-11: Serum Na$^+$, K$^+$, Cl$^-$ levels in mice bearing A549 tumors 24 hours after treatment.

Results of the NIH:OVCAR-3 model are shown below in Figure 4-12:
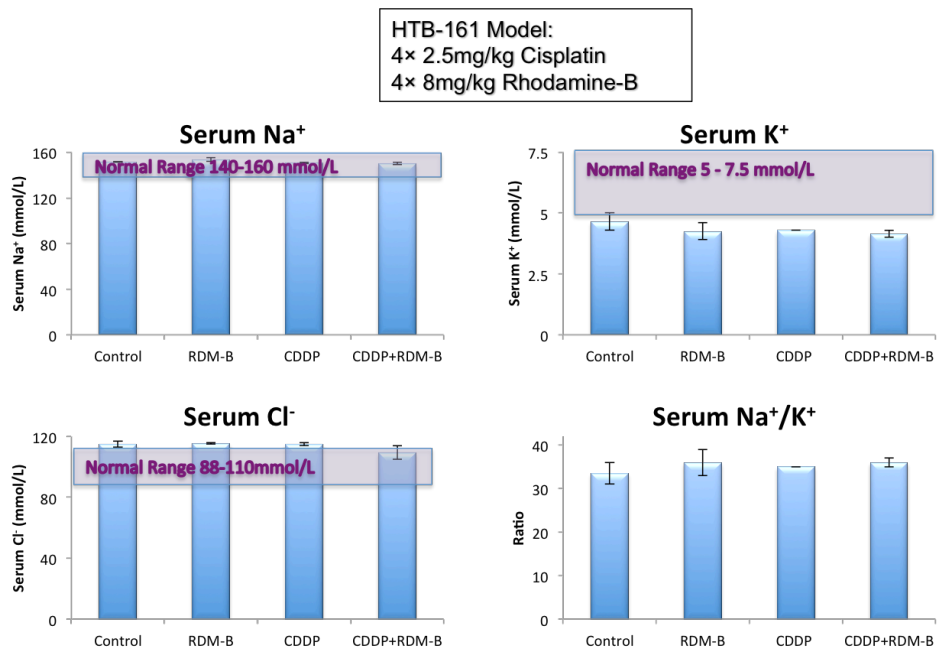
Figure 4-12: Serum Na$^+$, K$^+$, Cl$^-$ levels in mice bearing NIH:OVCAR-3 tumors 24 hours after treatment.

4.3.4.4 Physical Toxicity

Body weight was monitored along with tumor size measurement. Body weight loss is a common side effect of Cisplatin, for example in treating head and heck squamous cell cancer (HNSCC)[388]. Body loss is frequently observed in mice studies of Cisplatin[389]. Here we measure and study the body weight change by different treatments in our trials.

All measured body weights at Day 1 were normalized to 20 grams. In all three graphs, the minimum value of weight was set to 10 grams for a better visualization of the change.

Body weight measurement for the A549 model is shown in Figure 4-13:
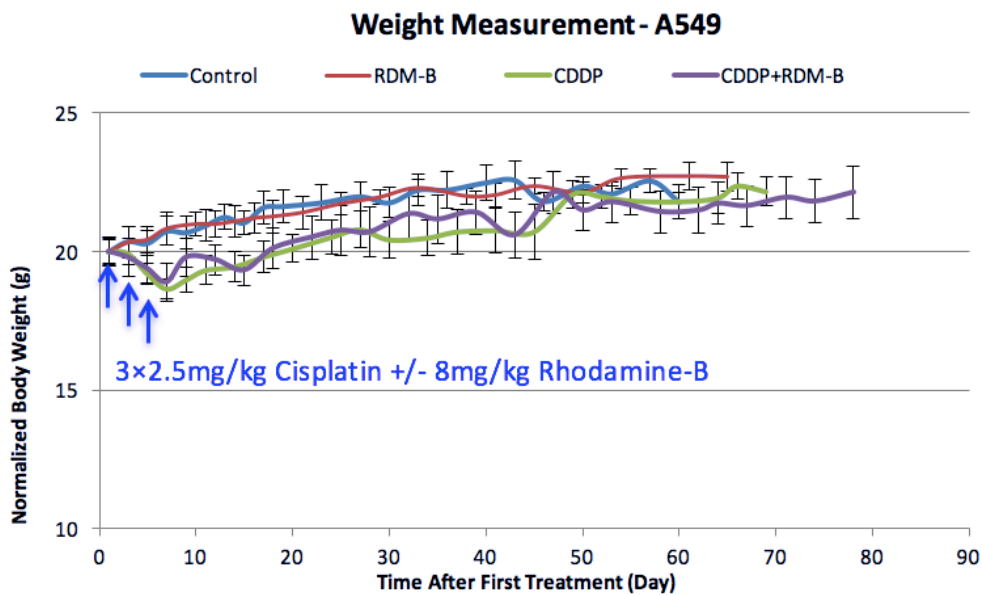
Figure 4-13: Body weight measurement of mice bearing A549 tumors. Error bars represent the standard error of the mean (s.e.m.).

As can be seen from the graph, in 60 days, mice in the control group gained body weight gradually, and this was also observed in the group of mice receiving Rhodamine-B only treatment. During the treatment days (1, 3, 5), mice receiving Cisplatin with/without Rhodamine-B lost weight; their weights started to

increase from day 7-10, a few days after the last treatment. In the A549 mouse model, it can be concluded that the body weight loss was attributed to Cisplatin, not Rhodamine-B.

Body weight measurement of the NIH:OVCAR-3 model is shown in Figure 4-14:

Weight Measurement - NIH:OVCAR-3
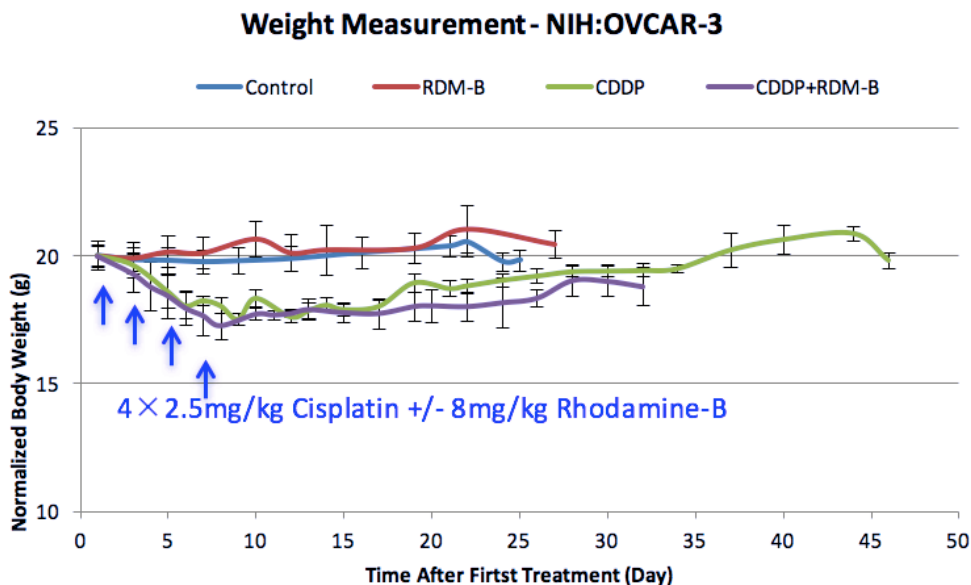
Figure 4-14: Body weight measurement of mice bearing NIH:OVCAR-3 tumors. Error bars represent the standard error of the mean (s.e.m.).

Similar trends were observed in the body weight measurement of the NIH:OVCAR-3 model. A slight body weight increase was observed in mice receiving Rhodamine-B only treatment. In this model, it is notable that the body weight loss during the treatment was more significant than that in the A549 model. 7 mice were allocated to each group initially; all mice receiving Cisplatin treatment had at least 10% of body weight loss. After sacrificing two from each group for acute toxicity analysis, one mouse from each of the Cisplatin group and the combination group was sacrificed due to severe body weight loss (endpoint reached: 20% body weight loss from day 1). Other mice gradually gained weight after the completion of treatment. Long-term results were not obtained for the combination group since one mouse reached

endpoint on Day 32, so the following measurements would be of less statistically accurate. From current results, mice in the Cisplatin group recovered slightly faster than the combination group did.

Body weight measurement of the ME-180 model is shown in Figure 4-15:
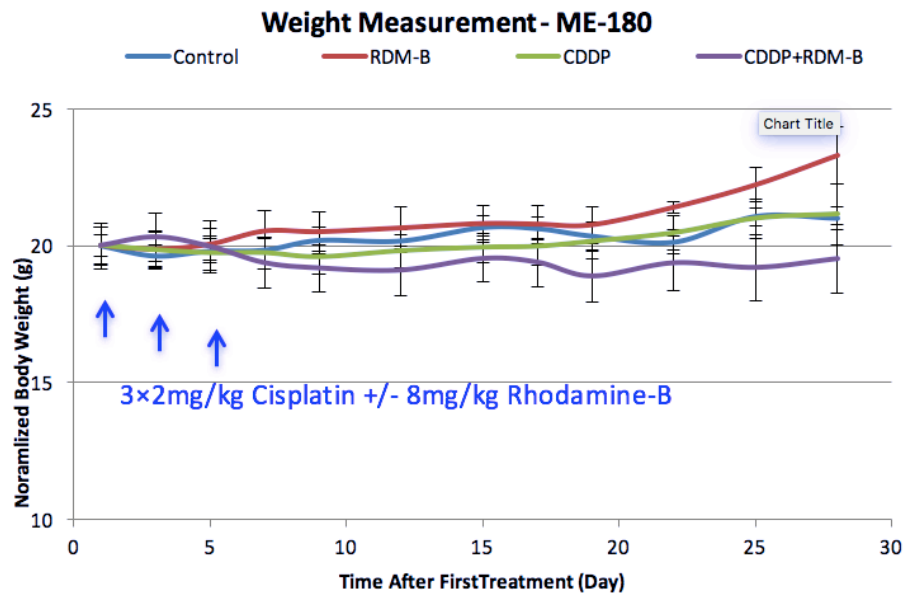
Figure 4-15: Body weight measurement of mice bearing ME-180 tumors. Error bars represent the standard error of the mean (s.e.m.).

In the ME-180 model, mice in the Rhodamine-B group gained weight faster than the control group, especially during days 18 to 27. This significant increase was not observed in the A549 model; mice in the Rhodamine-B group of the NIH:OVCAR-3 model showed a similar but much weaker trend. During the treatment, neither mice in Cisplatin group nor mice in the combination group lost weight. However, after the last treatment, the addition of Rhodamine-B caused mild body weight loss, compared to the Cisplatin-only treatment.

4.4 Conclusion and Discussion

4.4.1 Conclusion

In this Chapter, we tested the combination of Cisplatin and Rhodamine-B in three different xenograft mouse models developed by different cancer cell lines: one Cisplatin-sensitive, a cervical cancer (ME-180) cell line, and two Cisplatin-resistant cell lines, ovarian cancer (NIH:OVCAR-3) and lung cancer (A549) cell lines. In all three models, the anti-cancer effect of Cisplatin was significantly enhanced. Our combination in the two Cisplatin-resistant models showed surprisingly effective results, in both tumor volume and *shrinkage* time. In the acute toxicity analysis, results showed that the addition of Rhodamine-B did not induce additional toxicity, nor nephrotoxicity nor hepatotoxicity.

Nephrotoxicity induced by Cisplatin has been extensively studied and is the most important dose-limiting factor in Cisplatin chemotherapy[390, 391]. Results from our mouse model studies have confirmed that by using the combination of Cisplatin and Rhodamine-B, the dose of Cisplatin can be reduced to achieve the same or better chemotherapeutic effect. Figure 4-16 shows that by using our combination, the therapeutic window is broadened. Our combination has a better chemotherapeutic effect at the same maximum tolerated dose (MTD), which is only determined by Cisplatin, not Rhodamine-B.

When standard doses are administered, hepatotoxicity is rare in Cisplatin-induced toxicity[392]. It is notable that clinical standard Cisplatin doses are suggested after the therapeutic effects and toxic side effects have been balanced. However, effective tumor suppression may require higher doses or repeated low-dose treatments of Cisplatin: under both situations hepatotoxicity has been observed. High-dose Cisplatin treatment induced hepatotoxicity has drawn great attention[393, 394] due to the fact that when more aggressive Cisplatin treatment is required, hepatotoxicity becomes a dose-limiting factor.
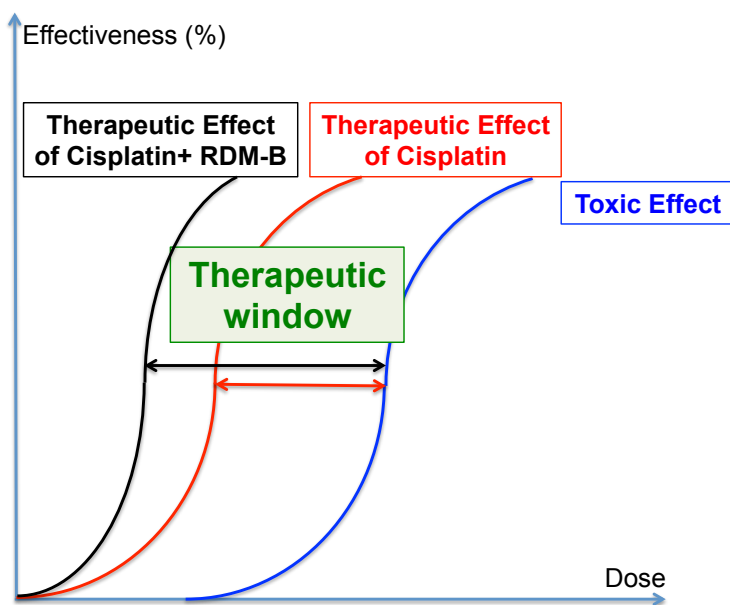
Figure 4-16: Therapeutic effect improvement by the addition of Rhodamine-B to Cisplatin-based cancer treatment.

We have confirmed that our combination enhances the anti-tumor effect of Cisplatin without inducing additional hepatotoxicity, the problem of high Cisplatin dose requirement to treat some cancers can be resolved by the combination of Rhodamine-B with Cisplatin at the MTD.

4.4.2 Discussion of the safety of Rhodamine-B as a part of Cisplatin-based combination chemotherapy

An optimal DET-based combination will be Cisplatin combined with a non-toxic electron-donating agent. Therefore, it is necessary to discuss the validity of the combination of Cisplatin and Rhodamine-B from the perspective of safety. Rhodamine-B has been extensively applied in industries like paints, papers, leather, textiles, and porcelain[395]. Due to the concern of toxicity, its applications in food and cosmetics have been prohibited. Here we give a brief discussion of the side effects induced by Rhodamine-B.

The notion of Rhodamine-B being toxic comes from a report in 2003 on the illegal use of the dye Sudan I in food. Now Rhodamine-B has been categorized "potentially both genotoxic and carcinogenic".

Reported studies of the toxicity of Rhodamine-B are summarized in the table below:

Types of Toxicity	Experiments/Administration	Result/Conclusion
Acute Toxicity	Intraperitoneal LD_{50} in the mouse	144mg/kg[396,397]
	Human exposure for 26 minutes, acute, aerosolized Rhodamine-B	Irritant effect, all 17 patients resolved within 24 hours, no sequellae evidenced[398]
	6-hour incubation of human lip fibroblasts in Rhodamine-B	Collagen synthesis inhibition[399]
Allergenicity	Not reported	
Chronic/Sub-chronic Toxicity	18 months' diet administration to rats	Retarded growth in treated rats at higher doses; rats in the highest dose group died with liver damage in 6 weeks[400]
Genotoxicity	Rhodamine-B in the Ames test in *salmonella typhimurium*	Positive, probably attributed to impurity[401]
	Rhodamine-B in the Ames test in *salmonella* and Chinese hamster ovary (CHO) cells	Increased DNA damage; however being confirmed mostly from impurities from commercial Rhodamine-B[402]
	Rhodamine-B treatment in *muntiacus muntjac* fibroblast cells	Increased chromosome aberrations[403]
	Rhodamine-B in the *in vivo* Ames test (rat liver after treatment)	Negative: no significant DNA fragmentation and no mutagenic activity observed, compared to

		control[404]
	Rhodamine-B in the Ames test	Negative mutagenic responses[405]
	Mutagenic activity test of urinary metabolites	enotoxicity not supported[406]
	Genotoxicity test in *Drosophila melanogaster* somatic/germ cell lines	Genotoxicity indicated from positive wing-spot test and sex-linked recessive lethal test[407]
Carcinogenicity	Rhodamine-B diet treatment in rats[408] (Summarized but not individually reported)	Increase in thyroid follicular adenomas and carcinomas
		Slight increase in astrocytomas and brain tumors in males
		Increase in hepatocellular carcinomas in females with high dose treatment
	Sub-cutaneous injection of Rhodamine-B in rats and mice	No link between Rhodamine-B treatment and tumor development concluded
Reproductive toxicity	Gavage administration of Rhodamine-B in rats and rabbits	No abnormalities observed in the fetuses[409] (#118, Burnett et al.)
	Diet administration of Rhodamine-B in rats	No reproductive side effects observed[409] (#119, Pierce et al.)

Table 4-2: Reported studies of the toxicities of Rhodamine-B.

By summarizing these reported references regarding the toxicities of Rhodamine-B we can get a clearer picture that if Rhodamine-B is safe to be used as a part of a Cisplatin-based anti-cancer regimen. First, the reported intraperitoneal LD_{50} of Rhodamine-B is 144 mg/kg in mice: in contrast, the results of our trials have indicated that a dose of as low as 8 mg/kg is sufficient to cause a significant enhancement in the

therapeutic efficacy of Cisplatin, remarkably in tumor shrinkage. It is worthwhile to note that in our *in vivo* studies, the used dose of Cisplatin 2.5 mg/kg is 38% of its reported intraperitoneal LD_{50} dose (6.6 mg/kg[410]) and that of Rhodamine-B is only 5.5% of its IP LD_{50} value. In other words, the effective dose of Rhodamine-B in this combination is far lower than that which could induce significant acute toxicity. Second, in the seven studies listed of the genotoxicity of Rhodamine-B, the only certain result was obtained in *Drosophila*, with others either negative or false positive due to impurities in commercial Rhodamine-B. Moreover, the effect of impurities could not be excluded in the *Drosophila* study (with reported 90% purity[407]). Third, some of the studies of carcinogenicity have demonstrated the potential tumor-inducing effect of Rhodamine-B but some have not. It is notable that in these studies, Rhodamine-B was administered with diet for 22-29 months[408]. The observed possible carcinogenicity should be a long-term accumulated effect from persistent exposure to the compound. While in our studies, as well as in the clinic, chemotherapy is usually given in a very short time period with much longer recovery between treatments. For example, in the treatment of bladder cancer, Cisplatin is intravenously given for 6-8 hours every 4 weeks. Fourth, listed studies have not shown any evidence for reproductive toxicity or allerginicity. Finally, another important rationale for the proposed combination is that Cisplatin itself is a much stronger carcinogenic agent than Rhodamine-B, and therefore the reduction of the Cisplatin dose by the introduction of the latter should be beneficial to the patients receiving the treatment. To sum up, the above listed studies of Rhodamine-B do not provide evidence that it cannot serve as a drug because it would induce significant/intolerable additional toxicities. In fact, our acute toxicity analysis has shown that the administration of Rhodamine-B at the indicated dose does not introduce measurable nephrotoxicity and hepatotoxicity in mice. The use of Rhodamine-B combined with Cisplatin is not only effective, but also safe under the indicated schedule and dose.

Chapter 5

Spectroscopic Studies of the Reaction between Cisplatin and

Rhodamine-B

5.1 Objective of This Chapter

In this Chapter, we study the mechanism of the reaction between Cisplatin and Rhodamine-B by utilizing spectroscopic techniques.

Questions to answer in this Chapter are:

(1) Do Cisplatin and Rhodamine-B react with each other?

(2) Is the observed reaction an electron transfer reaction?

5.2 Transient Absorption Measurements

5.2.1 Light Absorption

When light passes through a clear sample, the intensity of light is reduced as a result of absorption. Electronic absorption measurement is widely applied in quantitative analysis of an aqueous sample.

A fundamental description of light absorption is Beer-Lambert-Bouguer Law; in which Pierre Bouguer and Johann Heinrich Lambert discovered the linear relationship between absorbance and sample light path length, and August Beer discovered the linear relationship between absorbance and sample concentration. This absorption process with mathematical expressions are shown in Figure 5-1:
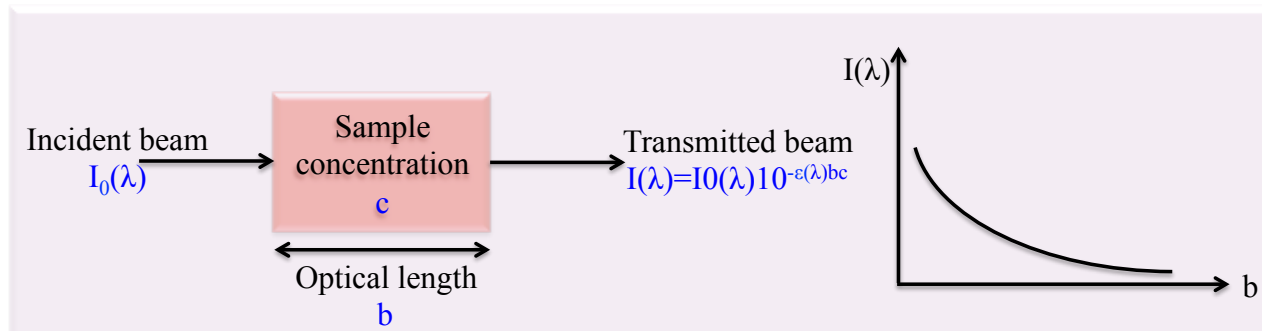
Figure 5-1: Schematic diagram showing light absorption when traveling through a sample.

Transmittance is defined as:

$$T(\lambda) = \frac{I(\lambda)}{I_o(\lambda)}$$

Absorbance is defined as:

$$A(\lambda) = log_{10}\left(\frac{I(\lambda)}{I_o(\lambda)}\right) = \varepsilon(\lambda)bc$$

In the formula, $\varepsilon(\lambda)$ is the extinction coefficient, b is the distance that light travels through a sample, and c is the sample concentration.

In the current study, we measure absorbance, a simple form that is directly proportional to sample concentration, to do analysis.

Molecularly, absorption occurs when an electron in a molecule absorbs photon(s) from the incident light and then is excited. Since molecular energies are quantized, absorption wavelength/frequency is certain in a specific environment. An absorption *spectrum*, which is often plotted as absorbance (A) versus wavelength (λ), is used to identify/quantify chromophore(s) in a sample[411]. In addition, the change of an absorption spectrum, for example, red/blue shift or absorption peak decrease, can probe interactions involving the chromophore(s) or chromophore(s)-containing assemblies[411].

5.2.2 Femtosecond time-resolved pump-probe transient absorption spectroscopy

The experimental setup for the femtosecond time-resolved pump-probe transient absorption spectroscopy is shown in Figure 5-2:
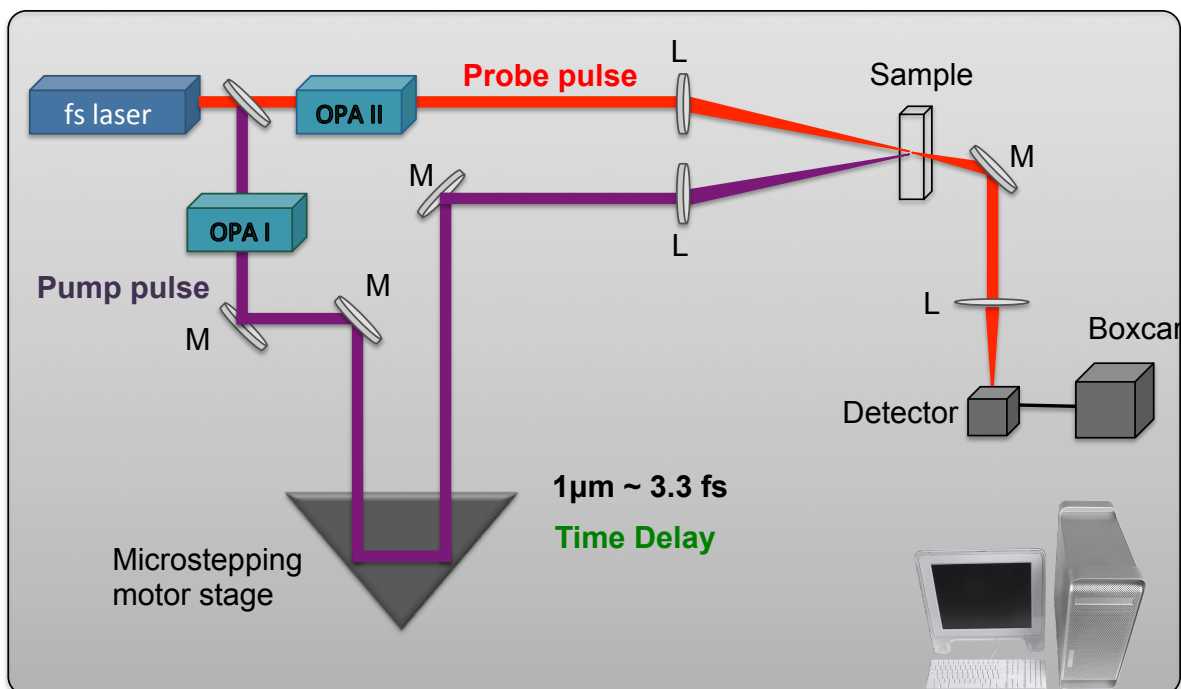
Figure 5-2: Schematic diagram of the experimental setup for femtosecond time-resolved pump-probe transient absorption spectroscopy.

In our experiment, a Ti:sappire laser system (Spectra-Physics) that produces 800 nm laser pulses is used. The pulse duration is 100-120 fs and the repletion rate is 500 Hz. As can be seen from Figure 5-2, two optical parametric amplifiers (OPA) are applied to produce two laser pulses with desired wavelengths: a "pump" pulse that initiates a reaction (to excite a molecule or to generate reacting species) and a "probe" pulse to monitor the formation and decay of a specific reaction intermediate (excited molecules or generated species). The polarization of the pump pulse with respect to the probe pulse is set to be at 54.7° (magic angle) to avoid polarization anisotropy. As Figure 5-2 shows, the time delay between

these two pulses is controlled by a Microstepping motor stage. A 1 μm optical path difference corresponds to a 3.3 fs time difference; in that way, a fs time resolution is achieved. The motion of the motor stage and the collection of data are controlled by Labview programs.

5.2.3 Results and Discussion

5.2.3.1 Transient absorption probing the formation of (pre-)hydrated electrons

Since we are studying an electron-transfer reaction, first we perform transient absorption measurement to probe the formation of (pre-)hydrated electrons.
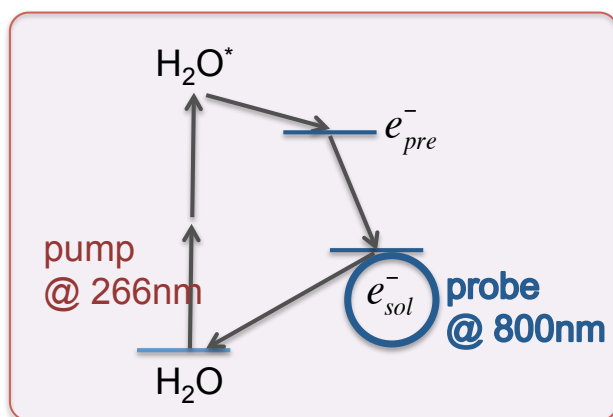
Figure 5-3: Schematic diagram showing the generation of solvated electron by UV absorption.

Two-photon absorption in the UV region by water molecules generates electrons[416]. The well-known hydrated electron has a broad absorption peaking at 720 nm[417]. It has been directly observed by time-resolved femtosecond laser spectroscopy that before a free electron becomes hydrated, it exists as a localized state absorbing in the infra-red region and is called the pre-hydrated electron[418]. The decay lifetime of the pre-hydrated electron that has absorption in the infra-red region corresponds to the rising (formation) time of the hydrated electron. Hence the reaction of the former can be directly observed by monitoring its own decay kinetics or alternatively the formation kinetics of the latter[419,420]. In this

experiment, aqueous samples were excited at 266 nm (0.2 μJ/pulse), to generate the pre-hydrated electron, and its reaction with Cisplatin in the absence/presence of Rhodamine-B was observed by monitoring the formation kinetics of the (pre-)hydrated electron that was detected at 800 nm for experimental convenience. The mechanism is shown in Figure 5-3.

The first part of this experiment aims to investigate if Rhodamine-B enhances or reduces the formation of hydrated electrons in water. Samples of pure water, 60 μM, and 120 μM aqueous Rhodamine-B solutions were measured. Results are shown in Figure 5-4:
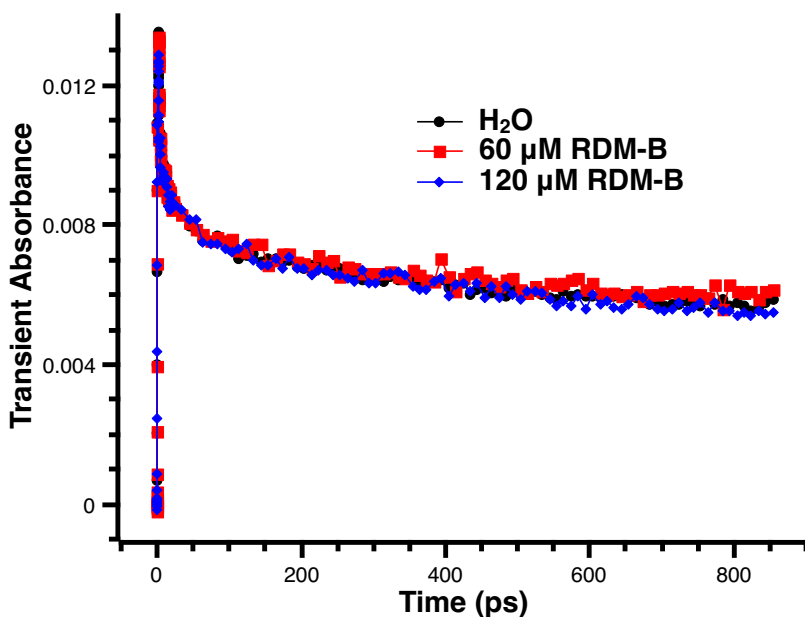
Figure 5-4: Transient absorbance of (pre-)hydrated electrons in water, 60 μM and 120 μM Rhodamine-B solutions.

As can be seen from Figure 5-4, the addition of 60 μM or 120 μM Rhodamine-B led to no change in the transient absorbance (i.e., the yield) of the (pre-)hydrated electrons. In other words, Rhodamine-B did not generate and did not capture (pre-)hydrated electrons in water.

The next part is to probe the (pre-)hydrated electrons in solutions of Cisplatin and Cisplatin combined with Rhodamine-B. Results are shown in Figure 5-5:
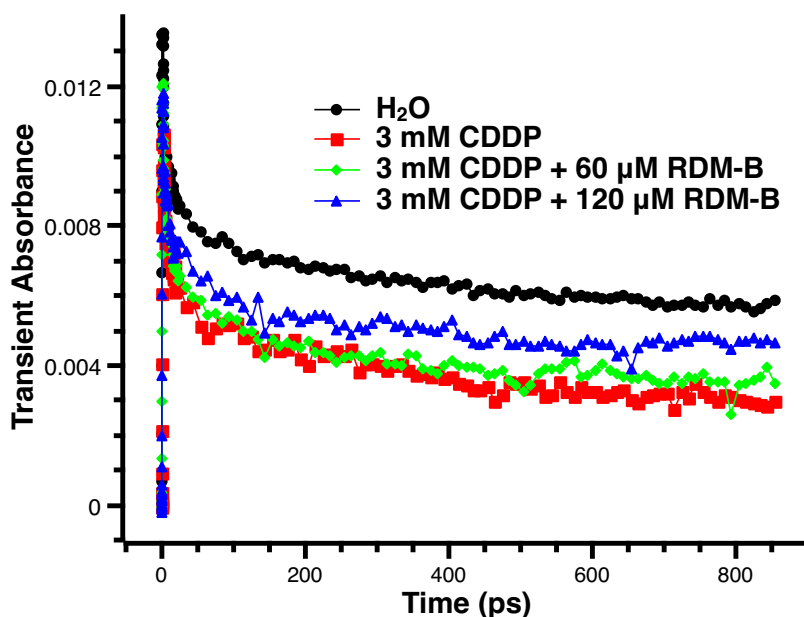
Figure 5-5: Transient absorbance of the (pre-)hydrated electron in water, 3 mM Cisplatin, and 3 mM Cisplatin with 60 μM and 120 μM Rhodamine-B.

As can be seen from Figure 5-5, it is very clear that Cisplatin decreased the initial yield of the (pre-)hydrated electrons at an ultrashort time scale. This is due to the strong reaction of Cisplatin with the ultrashort-lived pre-hydrated electron[346,420]. However, the addition of Rhodamine-B to the Cisplatin solution increased the yield of the (pre-)hydrated electrons. Since the result in Figure 5-4 has shown that Rhodamine-B neither generates nor captures electrons in water, the observed results in Figure 5-5 indicate that Rhodamine-B competed with the pre-hydrated electrons to react with Cisplatin molecules.

The above transient absorption measurements of the (pre-)hydrated electrons provide evidence that there exists a reaction between Cisplatin and Rhodamine-B and it should be an electron-transfer reaction between Cisplatin and Rhodamine-B.

132

5.2.3.2 Transient absorption probing the formation of Rhodamine-B radical cations

To further testify the nature of the observed reaction between Cisplatin and Rhodamine-B, we conducted transient absorption measurement to directly probe the formation of Rhodamine-B radical cations. The photo-degradation of Rhodamine-B has been extensively studied[350,351,412,413]. Initial steps of Rhodamine-B photo-degradation are Rhodamine-B photo-excitation and one electron oxidization of Rhodamine-B by oxygen[414]. During this process, Rhodamine-B cation radical RDM-B$^{+\bullet}$ is formed and it has been found to have absorption at 490 nm[350,415]. Therefore, by probing the species RDM-B$^{+\bullet}$ with/without Cisplatin, we could obtain information of the reaction between Cisplatin and Rhodamine-B. A standard femtosecond (fs) transient absorption measurement was carried out on Rhodamine-B water solutions with/without Cisplatin.
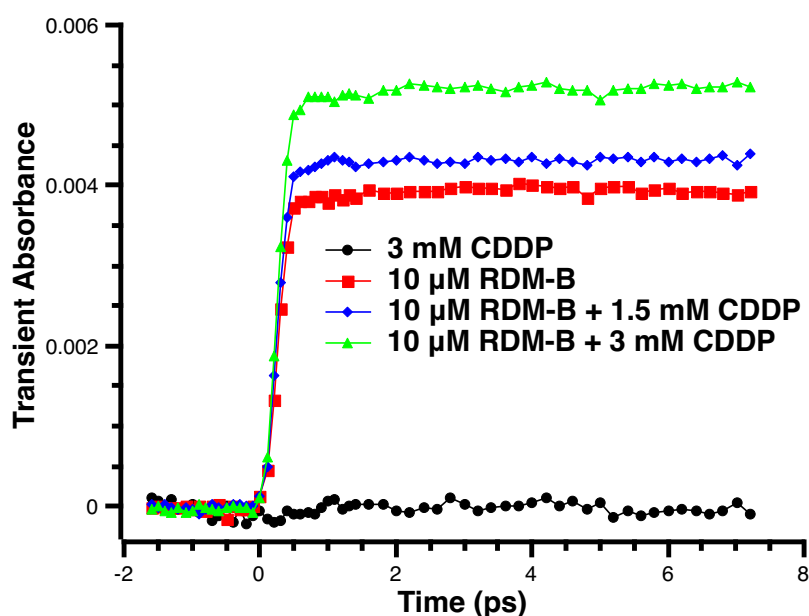
Figure 5-6: Transient absorption of Rhodamine-B radical cation RDM-B$^{+\bullet}$ in 3mM Cisplatin solution, 10 μM Rhodamine-B solution, and 10 μM Rhodamine-B with 1.5 mM and 3 mM Cisplatin solutions.

The pump pulse was chosen at 553 nm (0.2 µJ/pulse) that is the absorption peak of Rhodamine-B, and the probe pulse was chosen at 490 nm to monitor the formation of RDM-B$^{+\bullet}$. Since the reaction between Cisplatin and weakly-bound electrons is an ultra-fast process that occurs within 1 picosecond (ps)[343,346], we measured the transient absorption for only ~8 ps after the 0-point. As can be seen in Figure 5-6, in a 10 µM Rhodamine-B only water solution, the photo-excitation by 553 nm pulses gave rise to the formation of RDM-B$^{+\bullet}$; when 1.5 mM and 3 mM of Cisplatin was added to the 10 µM Rhodamine-B solution, the concentration of RDM-B$^{+\bullet}$ was significantly increased in a CDDP-concentration-dependent manner. In addition, the presence of Cisplatin accelerated the photo-degradation of Rhodamine-B, which could be seen from the increased yield of RDM-B$^{+\bullet}$. It suggests that in the solution of both Rhodamine-B and Cisplatin, Rhodamine-B donated electrons not only to oxygen, but may also to Cisplatin. The reaction between Cisplatin and Rhodamine-B is an electron-transfer reaction.

5.3 Conclusion

In this Chapter, we have investigated the reaction between Cisplatin and Rhodamine-B, through femtosecond time-resolved spectroscopic studies.

First, our femtosecond time-resolved transient absorption measurement of the formation kinetics of the (pre-)hydrated electron has shown evidence that Rhodamine-B competes with pre-hydrated electrons to react with Cisplatin. A reaction has been observed and the change in (pre-)hydrated electron formation suggests that this observed reaction is an electron-transfer reaction. Second, by measuring the transient absorption of Rhodamine-B radical cation, it has been found that the addition of Cisplatin enhances the photo-degradation of Rhodamine-B. This observation indicates that Rhodamine-B donates electrons to Cisplatin and therefore more Rhodamine-B radical cations are produced.

134

These results strongly prove that Rhodamine-B reacts with Cisplatin, and this reaction is an electron transfer reaction:

$$\text{RDM} - \text{B} \rightarrow \text{RDM} - \text{B}^* + \text{CDDP} \rightarrow \text{RDM} - \text{B}^{+\bullet} + \text{Cl}^- + \text{Pt(NH}_3)_2\text{Cl}^\bullet$$

$$\text{RDM} - \text{B} \rightarrow \text{RDM} - \text{B}^* + \text{Pt(NH}_3)_2\text{Cl}^\bullet \rightarrow \text{RDM} - \text{B}^{+\bullet} + \text{Cl}^- + \text{Pt(NH}_3)_2{}^\bullet$$
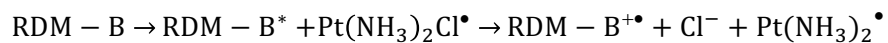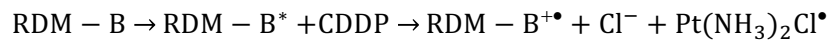
With the addition of Rhodamine-B, more radicals, $\text{Pt(NH}_3)_2\text{Cl}^\bullet$ and/or $\text{Pt(NH}_3)_2{}^\bullet$, are generated to induce DNA strand breaks and therefore to cause cell death. The observed *in vitro* and *in vivo* enhancement in Cisplatin's anti-cancer effect by its combination with Rhodamine-B is therefore a result from the dissociative electron transfer reaction between Cisplatin and Rhodamine-B.

Chapter 6

Conclusions and Future Research

Though many cancer treatments are emerging, chemotherapy remains one of the most commonly used. Cisplatin-based cancer treatment has achieved success in treating various cancers. However, severe toxicity and resistance limit its clinical application. To overcome these limitations, a precise understanding of the mechanism of Cisplatin is required. In this project, based on the newly discovered dissociative electron transfer reaction (DET) mechanism of Cisplatin, we propose the DET-based combination chemotherapy: Cisplatin and Rhodamine-B, in which Rhodamine-B is an electron donor, to achieve a better chemotherapeutic effect. In this Chapter, a summary of major results presented in this thesis is given and possible future research is discussed.

6.1 Conclusions

6.1.1 DNA lesions induced by Cisplatin

In Chapter 2, we have discussed DNA lesions induced by Cisplatin. From previous work, researchers believe that the major DNA damage induced by Cisplatin is DNA-CDDP cross-link. In both of our plasmid DNA gel electrophoresis and γH2AX labeling experiments, DNA double strand breaks (DSBs) are detected. Some studies have attributed the formation of DNA DSBs to the repair process of DNA cross-links. However, our gel electrophoresis experiment shows that DNA DSBs can be directly induced by Cisplatin without any aid of proteins. Therefore, we conclude that Cisplatin can *intrinsically* induce DNA DSBs without the participation of other cellular events.

6.1.2 Combination chemotherapy of Cisplatin and Rhodamine-B

To verify the anti-cancer effect of the proposed combination of Cisplatin and Rhodamine-B, experiments have been conducted: *in vitro* cell-based assays and *in vivo* xenograft mouse models to test the effectiveness of our combination, and spectroscopic studies to investigate the reaction between Cisplatin and Rhodamine-B.

(1) In Chapter 3, a number of *in vitro* cell-based assays are performed. First, MTT survival assay is done on different cell lines to study the toxicity and cytotoxicity of Rhodamine-B. This experiment provides a reference on its dosing in its combination with Cisplatin. We surprisingly find the tested human cancer cells are more sensitive to Rhodamine-B, than are normal cells. Second, MTT and clonogenic assays are conducted on human cervical ME-180 and HeLa, human lung A549, and human ovarian NIH:OVCAR-3 cancer cell lines to test if the combination is effective in killing these cancer cells. Drug combination is evaluated using the fractional effect method and we find Cisplatin and Rhodamine-B kill cancer cells in a synergistic manner. Moreover, this combination is not effective in killing normal cells (GM05757). Further assays are performed to investigate other cellular processes under our Cisplatin with/without Rhodamine-B treatments. Gel electrophoresis and γ H2AX labeling experiments show that by adding Rhodamine-B, the amount of DNA DSBs is greatly enhanced. Caspase 3/7 activation detection and Annexin-V-FITC labeling flow cytometry experiments show that the observed cancer-cell-killing enhancement is achieved through inducing more apoptosis.

(2) In Chapter 4, *in vivo* xenograft mouse models are developed to investigate if our combination is effective in treating mice bearing tumors, as well as to test if this combination induces additional *in vivo* toxicities in mice. Three xenograft models are built: human lung A549, human ovarian NIH:OVCAR-3, and human cervical ME-180 cancer models. In these models, tumor growth is greatly inhibited by our combination of Cisplatin and Rhodamine-B, compared to that by

Cisplatin-only treatment. Moreover, in the A549 and NIH:OVCAR-3 models, our combination induces more significant tumor *shrinkage*. These are remarkable results, which show high promise for the potential success of this combination therapy in future clinical trials. In addition, acute toxicity analysis on hepatotoxicity and nephrotoxicity is performed. The results indicate that our combination does not induce any of these toxicities.

(3) In Chapter 5, time-resolved femtosecond laser transient-absorption spectroscopic measurements are carried out to investigate the nature of the reaction between Cisplatin and Rhodamine-B. By probing (pre-)hydrated electrons upon 2-photon UV absorption of water, it is observed that the addition of Rhodamine-B increases the concentration of (pre-)hydrated electrons compared to a pure Cisplatin solution, which indicates that Rhodamine-B competed with (pre-)hydrated electrons to react with Cisplatin. By probing the radical cation RDM-B$^{+\bullet}$ formed in aqueous Rhodamine-B solution under photo-excitation, it is found that the addition of Cisplatin significantly increases the yield of RDM-B$^{+\bullet}$, which indicates that Cisplatin captures electrons from Rhodamine-B. These transient absorption results show that there exists an electron transfer reaction between Cisplatin and Rhodamine-B.

6.2 Future Work

We have completed a comprehensive *in vitro* and *in vivo* study of the proposed combination of Cisplatin and Rhodamine-B and the combination has shown high efficacy in improving the therapeutic efficacy of Cisplatin against various cancers. This is the first successful *example* of DET-based combination chemotherapy of Cisplatin shown in both *in vitro* and *in vivo* experiments. However, in order to better demonstrate the electron transfer reaction between these two agents, further time-resolved femtosecond laser spectroscopic studies should be conducted. For example, transient fluorescence up-conversion

spectroscopic studies may provide more detailed information on this reaction. In addition, it will be necessary and important to study the reaction between Cisplatin and Rhodamine-B under hypoxic conditions. Hypoxic cell-based experiments are also of interest to deeper understand this combination.

Moreover, though our results have shown that Rhodamine-B is a very promising candidate, more screenings should be continued to find other agents that might have better performance in enhancing and improving the therapy of Cisplatin in the clinic. In these investigations, both experimental studies and theoretical structural considerations should be taken into account. These considerations should include the level of synergy, toxicity, and selectivity, as well as the kinetics of the electron transfer reaction. Furthermore, the effectiveness under hypoxia is another criterion in the selection of the best combination.

In addition, the concept of DET-based combination chemotherapy can also be applied in drug delivery and targeted therapy to achieve a better chemotherapeutic outcome for cancer patients.

Bibliography

1. Statistics Canada. *Canadian Cancer Statistics - Special topic: HPV-associated cancers*. (2016).

2. Siegel, R. L., Miller, K. D. & Jemal, A. Cancer statistics. *CA Cancer J Clin* **66,** 7–30 (2016).

3. Vesely, M. D., Kershaw, M. H., Schreiber, R. D. & Smyth, M. J. Natural Innate and Adaptive Immunity to Cancer. *Annu. Rev. Immunol.* **29,** 235–271 (2011).

4. Hanahan, D. & Weinberg, R. a. The Hallmarks of Cancer. *Cell* **100,** 57–70 (2000).

5. Hanahan, D. & Weinberg, R. A. Hallmarks of Cancer: The Next Generation. *Cell* **144,** 646–674 (2011).

6. Postovit, L.-M., Seftor, E. A., Seftor, R. E. B. & Hendrix, M. J. C. A Three-Dimensional Model to Study the Epigenetic Effects Induced by the Microenvironment of Human Embryonic Stem Cells. *Stem Cells* **24,** 501–505 (2006).

7. Bissell, M. J. & Hines, W. C. Why don't we get more cancer? A proposed role of the microenvironment in restraining cancer progression. *Nat. Med.* **17,** 320–329 (2011).

8. Lobo, N. a, Shimono, Y., Qian, D. & Clarke, M. F. The Biology of Cancer Stem Cells. *Annu. Rev. Cell Dev. Biol.* **23,** 675–699 (2007).

9. Meacham, C. E. & Morrison, S. J. Tumour heterogeneity and cancer cell plasticity. *Nature* **501,** 328–337 (2013).

10. Raposo, G. & Stoorvogel, W. Extracellular vesicles: Exosomes, microvesicles, and friends. *J. Cell Biol.* **200,** 373–383 (2013).

11. Zomer, A. *et al.* In Vivo Imaging Reveals Extracellular Vesicle-Mediated Phenocopying of Metastatic Behavior. *Cell* **161,** 1046–1057 (2015).

12. Tisdale, M. J. Mechanisms of Cancer Cachexia. *Physiol. Rev.* **89,** 381–410 (2009).

13. Tsoli, M. & Robertson, G. Cancer cachexia: malignant inflammation, tumorkines, and metabolic mayhem. *Trends Endocrinol. Metab.* **24,** 174–183 (2013).

14. Kwon, Y. *et al.* Systemic Organ Wasting Induced by Localized Expression of the Secreted Insulin/IGF Antagonist ImpL2. *Dev. Cell* **33,** 36–46 (2015).

15.   Figueroa-Clarevega, A. & Bilder, D. Malignant Drosophila Tumors Interrupt Insulin Signaling to Induce Cachexia-like Wasting. *Dev. Cell* **33,** 47–55 (2015).

16.   Fagan-Dubin, L. Causes of cancer. *Cancer Nurs.* **2,** 435–441 (1979).

17.   Proctor, R. N. The history of the discovery of the cigarette-lung cancer link: evidentiary traditions, corporate denial, global toll. *Tob. Control* **21,** 87–91 (2012).

18.   Lantz, P. M., Mendez, D. & Philbert, M. a. Radon, Smoking, and Lung Cancer: The Need to Refocus Radon Control Policy. *Am. J. Public Health* **103,** 443–447 (2013).

19.   Ichihashi, M. *et al.* UV-induced skin damage. *Toxicology* **189,** 21–39 (2003).

20.   de Gruijl, F. R. Skin cancer and solar UV radiation. *Eur. J. Cancer* **35,** 2003–2009 (1999).

21.   D'Souza, G. *et al.* Case-control study of human papillomavirus and oropharyngeal cancer. *N. Engl. J. Med.* **356,** 1944–1956 (2007).

22.   Gillison, M. L. *et al.* Evidence for a causal association between human papillomavirus and a subset of head and neck cancers. *J. Natl. Cancer Inst.* **92,** 709–720 (2000).

23.   Gillison, M. L. *et al.* Distinct Risk Factor Profiles for Human Papillomavirus Type 16-Positive and Human Papillomavirus Type 16-Negative Head and Neck Cancers. *JNCI J. Natl. Cancer Inst.* **100,** 407–420 (2008).

24.   Xie, X. *et al.* Targeting HPV16 E6-p300 interaction reactivates p53 and inhibits the tumorigenicity of HPV-positive head and neck squamous cell carcinoma. *Oncogene* **33,** 1037–1046 (2014).

25.   Scudellari, M. HPV: Sex, cancer and a virus. *Nature* **503,** 330–332 (2013).

26.   Cheng, Y. W. *et al.* The association of human papillomavirus 16/18 infection with lung cancer among nonsmoking Taiwanese women. *Cancer Res.* **61,** 2799–2803 (2001).

27.   Klein, F., Amin Kotb, W. F. M. & Petersen, I. Incidence of human papilloma virus in lung cancer. *Lung Cancer* **65,** 13–18 (2009).

28.   Koshiol, J. *et al.* Assessment of human papillomavirus in lung tumor tissue. *J. Natl. Cancer Inst.* **103,** 501–507 (2011).

29.   Abbott, A. Researchers pin down risks of low-dose radiation. *Nature* **523,** 17–18 (2015).

30.   International Early Lung Cancer Action Program Investigators *et al.* Survival of patients with stage I lung cancer detected on CT screening. *N. Engl. J. Med.* **355,** 1763–1771 (2006).

31.   National Lung Screening Trial Research Team *et al.* Reduced lung-cancer mortality with low-dose computed tomographic screening. *N. Engl. J. Med.* **365,** 395–409 (2011).

32.   Rauh-Hain, J. a, Krivak, T. C., Del Carmen, M. G. & Olawaiye, A. B. Ovarian cancer screening and early detection in the general population. *Rev. Obstet. Gynecol.* **4,** 15–21 (2011).

33.   Kaur, S., Baine, M. J., Jain, M., Sasson, A. R. & Batra, S. K. Early diagnosis of pancreatic cancer: challenges and new developments. *Biomark. Med.* **6,** 597–612 (2012).

34.   Cannistra, S. A. Cancer of the Ovary. *N. Engl. J. Med.* **351,** 2519–2529 (2004).

35.   Howlader N, Noone AM, K. M. *SEER Cancer Statistics Review, 1975-2012*. (2015).

36.   Furukawa, H. *et al.* Clinicopathologic features of small pancreatic adenocarconoma: A collective study. *Cancer* **78,** 986–990 (1996).

37.   Melo, S. a. *et al.* Glypican-1 identifies cancer exosomes and detects early pancreatic cancer. *Nature* **523,** 177–182 (2015).

38.   Pan, B. T., Teng, K., Wu, C., Adam, M. & Johnstone, R. M. Electron microscopic evidence for externalization of the transferrin receptor in vesicular form in sheep reticulocytes. *J. Cell Biol.* **101,** 942–948 (1985).

39.   Demory Beckler, M. *et al.* Proteomic Analysis of Exosomes from Mutant KRAS Colon Cancer Cells Identifies Intercellular Transfer of Mutant KRAS. *Mol. Cell. Proteomics* **12,** 343–355 (2013).

40.   Litton, J. K. *et al.* Earlier age of onset of BRCA mutation-related cancers in subsequent generations. *Cancer* **118,** 321–325 (2012).

41.   Maine, D., Hurlburt, S. & Greeson, D. Cervical Cancer Prevention in the 21st Century: Cost Is Not the Only Issue. *Am. J. Public Health* **101,** 1549–1555 (2011).

42.   Chung, D. C. The genetic basis of colorectal cancer: Insights into critical pathways of tumorigenesis. *Gastroenterology* **119,** 854–865 (2000).

43.   Boland, C. R. *et al.* A National Cancer Institute Workshop on Microsatellite Instability for cancer detection and familial predisposition: development of international criteria for the determination of microsatellite instability in colorectal cancer. *Cancer Res.* **58,** 5248–5257 (1998).

44.   Ulrich, C. M., Bigler, J. & Potter, J. D. Non-steroidal anti-inflammatory drugs for cancer prevention: promise, perils and pharmacogenetics. *Nat. Rev. Cancer* **6,** 130–140 (2006).

45.   Groden, J. *et al.* Identification and characterization of the familial adenomatous polyposis coli gene. *Cell* **66,** 589–600 (1991).

46.   Srivastava, S., Verma, M. & Henson, D. E. Biomarkers for early detection of colon cancer. *Clin. Cancer Res.* **7,** 1118–1126 (2001).

47.   Bos, J. L. *et al.* Prevalence of ras gene mutations in human colorectal cancers. *Nature* **327,** 293–297 (1987).

48.   Ahlquist, D. a. Colorectal cancer screening by detection of altered human DNA in stool: Feasibility of a multitarget assay panel. *Gastroenterology* **119,** 1219–1227 (2000).

49.   Fearon, E. R. & Vogelstein, B. A genetic model for colorectal tumorigenesis. *Cell* **61,** 759–767 (1990).

50.   Hollstein, M., Sidransky, D., Vogelstein, B. & Harris, C. p53 mutations in human cancers. *Science (80-.).* **253,** 49–53 (1991).

51.   Bartel, D. P. MicroRNAs: Genomics, Biogenesis, Mechanism, and Function. *Cell* **116,** 281–297 (2004).

52.   Garzon, R., Calin, G. a. & Croce, C. M. MicroRNAs in Cancer. *Annu. Rev. Med.* **60,** 167–179 (2009).

53.   Schmitz, U. *et al. MicroRNA Cancer Regulation. Advances in Experimental Medicine and Biology* **774,** (Springer Netherlands, 2013).

54.   Lujambio, A. & Lowe, S. W. The microcosmos of cancer. *Nature* **482,** 347–355 (2012).

55.   Schultz, N. a *et al.* MicroRNA Biomarkers in Whole Blood for Detection of Pancreatic Cancer. *JAMA* **311,** 392 (2014).

56.   Organization, W. H. Cancer prevention. at <http://www.who.int/cancer/prevention/en/>

57.   Amerian Society of Clinical Oncology. What is Cancer Surgery? (2014).

58.   Cerfolio, R. J., Bryant, A. S. & Minnich, D. J. Starting a Robotic Program in General Thoracic
        Surgery: Why, How, and Lessons Learned. *Ann. Thorac. Surg.* **91,** 1729–1737 (2011).

59.   Jang, H.-J., Lee, H.-S., Park, S. Y. & Zo, J. I. Comparison of the Early Robot-Assisted
        Lobectomy Experience to Video-Assisted Thoracic Surgery Lobectomy for Lung Cancer.
        Innov. Technol. Tech. Cardiothorac. Vasc. Surg. **6,** 305–310 (2011).

60.   Veronesi, G. *et al.* Experience With Robotic Lobectomy for Lung Cancer. *Innov. Technol.
        Tech. Cardiothorac. Vasc. Surg.* **6,** 355–360 (2011).

61.   Slater, J. M. in *Ion Beam Therapy* (ed. Linz, U.) **320,** 3–16 (Springer Berlin Heidelberg,
        2012).

62.   O'Neill, P. The role of hydration and radiation quality in the induction of DNA damage-
        chemical aspects. *Adv. Sp. Res.* **14,** 221–234 (1994).

63.   Ross, G. Induction of cell death by radiotherapy. *Endocr. Relat. Cancer* **6,** 41–44 (1999).

64.   Lomax, M. E., Folkes, L. K. & O'Neill, P. Biological Consequences of Radiation-induced
        DNA Damage: Relevance to Radiotherapy. *Clin. Oncol.* **25,** 578–585 (2013).

65.   Amercican Cancer Society. *Targeted Therapy*. (2013).

66.   Yun, C.-H. *et al.* Structures of Lung Cancer-Derived EGFR Mutants and Inhibitor Complexes:
        Mechanism of Activation and Insights into Differential Inhibitor Sensitivity. *Cancer Cell* **11,**
        217–227 (2007).

67.   Maemondo, M. *et al.* Gefitinib or Chemotherapy for Non–Small-Cell Lung Cancer with
        Mutated EGFR. *N. Engl. J. Med.* **362,** 2380–2388 (2010).

68.   Kandoth, C. *et al.* Mutational landscape and significance across 12 major cancer types. *Nature*
        502, 333–339 (2013).

69.   Momand, J., Zambetti, G. P., Olson, D. C., George, D. & Levine, A. J. The mdm-2 oncogene
        product forms a complex with the p53 protein and inhibits p53-mediated transactivation. *Cell*
        69, 1237–1245 (1992).

70.   Lam, S. *et al.* Role of Mdm4 in drug sensitivity of breast cancer cells. *Oncogene* **29,** 2415–2426 (2010).

71.   Ito, M. *et al.* Comprehensive mapping of p53 pathway alterations reveals an apparent role for both SNP309 and MDM2 amplification in sarcomagenesis. *Clin. Cancer Res.* **17,** 416–426 (2011).

72.   Gembarska, A. *et al.* MDM4 is a key therapeutic target in cutaneous melanoma. *Nat. Med.* **18,** 1239–1247 (2012).

73.   Vassilev, L. T. In Vivo Activation of the p53 Pathway by Small-Molecule Antagonists of MDM2. *Science (80-.).* **303,** 844–848 (2004).

74.   Wang, B., Fang, L., Zhao, H., Xiang, T. & Wang, D. MDM2 inhibitor Nutlin-3a suppresses proliferation and promotes apoptosis in osteosarcoma cells. *Acta Biochim. Biophys. Sin. (Shanghai).* **44,** 685–691 (2012).

75.   Polański, R. *et al.* Senescence induction in renal carcinoma cells by Nutlin-3: a potential therapeutic strategy based on MDM2 antagonism. *Cancer Lett.* **353,** 211–219 (2014).

76.   Arya, A. *et al.* Nutlin-3, the small-molecule inhibitor of MDM2, promotes senescence and radiosensitises laryngeal carcinoma cells harbouring wild-type p53. *Br. J. Cancer* **103,** 186–195 (2010).

77.   Muller, F. L. *et al.* Passenger deletions generate therapeutic vulnerabilities in cancer. *Nature* **488,** 337–342 (2012).

78.   Bagchi, A. & Mills, A. a. The quest for the 1p36 tumor suppressor. *Cancer Res.* **68,** 2551–2556 (2008).

79.   Henrich, K.-O. *et al.* CAMTA1, a 1p36 Tumor Suppressor Candidate, Inhibits Growth and Activates Differentiation Programs in Neuroblastoma Cells. *Cancer Res.* **71,** 3142–3151 (2011).

80.   Bignell, G. R. *et al.* Signatures of mutation and selection in the cancer genome. *Nature* **463,** 893–898 (2010).

81.   Liu, Y. *et al.* TP53 loss creates therapeutic vulnerability in colorectal cancer. *Nature* **520,** 697–701 (2015).

82. Nijhawan, D. *et al.* Cancer Vulnerabilities Unveiled by Genomic Loss. *Cell* **150,** 842–854 (2012).

83. Newport, M. J. *et al.* A Mutation in the Interferon-γ –Receptor Gene and Susceptibility to Mycobacterial Infection. *N. Engl. J. Med.* **335,** 1941–1949 (1996).

84. Pierre-Audigier, C. *et al.* Fatal Disseminated Mycobacterium smegmatis Infection in a Child with Inherited Interferon Receptor Deficiency. *Clin. Infect. Dis.* **24,** 982–984 (1997).

85. Kaplan, D. H. *et al.* Demonstration of an interferon gamma-dependent tumor surveillance system in immunocompetent mice. *Proc. Natl. Acad. Sci.* **95,** 7556–7561 (1998).

86. Shankaran, V. *et al.* IFNgamma and lymphocytes prevent primary tumour development and shape tumour immunogenicity. *Nature* **410,** 1107–1111 (2001).

87. Corporation, D. *Cancer Immunotherapy : Fundamental Concepts and Emerging Role Cancer Immunotherapy : Fundamental Concepts and Emerging Role*. (2013).

88. Mellman, I., Coukos, G. & Dranoff, G. Cancer immunotherapy comes of age. *Nature* **480,** 480–489 (2011).

89. Kirkwood, J. M. *et al.* Immunotherapy of cancer in 2012. *CA. Cancer J. Clin.* **62,** 309–335 (2012).

90. Slamon, D. J. Proto-Oncogenes and Human Cancers. *N. Engl. J. Med.* **317,** 955–957 (1987).

91. Zhang, L. *et al.* Intratumoral T cells, recurrence, and survival in epithelial ovarian cancer. *N. Engl. J. Med.* **348,** 203–213 (2003).

92. Galon, J. *et al.* Type, density, and location of immune cells within human colorectal tumors predict clinical outcome. *Science (80-.).* **313,** 1960–1964 (2006).

93. Jochems, C. & Schlom, J. Tumor-infiltrating immune cells and prognosis: the potential link between conventional cancer therapy and immunity. *Exp. Biol. Med.* **236,** 567–579 (2011).

94. Dudley, M. E. & Rosenberg, S. a. Adoptive-cell-transfer therapy for the treatment of patients with cancer. *Nat. Rev. Cancer* **3,** 666–675 (2003).

95. Henrich, J. B. The postmenopausal estrogen/breast cancer controversy. *JAMA* **268,** 1900–1902 (1992).

96.   Fernandez, S. V. Estrogen, Alcohol Consumption, and Breast Cancer. *Alcohol. Clin. Exp. Res.* **35,** 389–391 (2011).

97.   Keen, J. C. & Davidson, N. E. The biology of breast carcinoma. *Cancer* **97,** 825–833 (2003).

98.   Harrell, J. C. *et al.* Estrogen receptor positive breast cancer metastasis: altered hormonal sensitivity and tumor aggressiveness in lymphatic vessels and lymph nodes. *Cancer Res.* **66,** 9308–9315 (2006).

99.   Zompra, A. a. *et al.* Synthesis and Biological Evaluation of New GnRH Analogues on Pituitary and Breast Cancer Cells. *Int. J. Pept. Res. Ther.* **13,** 143–149 (2007).

100.   Fabian, C. J. The what, why and how of aromatase inhibitors: hormonal agents for treatment and prevention of breast cancer. *Int. J. Clin. Pract.* **61,** 2051–2063 (2007).

101.   Bodmer, A. & Castiglione-Gertsch, M. Role of hormonal manipulations in patients with hormone-sensitive metastatic breast cancer. *Eur. J. Cancer* **47,** S28–S37 (2011).

102.   Breast, E., Trialists, C. & Group, C. Effects of chemotherapy and hormonal therapy for early breast cancer on recurrence and 15-year survival: an overview of the randomised trials. *Lancet* **365,** 1687–1717 (2005).

103.   Breast, E., Trialists, C. & Group, C. Relevance of breast cancer hormone receptors and other factors to the efficacy of adjuvant tamoxifen: patient-level meta-analysis of randomised trials. *Lancet* **378,** 771–784 (2011).

104.   Namiki, M. *et al.* Hormonal therapy. *Int. J. Clin. Oncol.* **12,** 427–432 (2007).

105.   Dow, L. E. *et al.* Apc Restoration Promotes Cellular Differentiation and Reestablishes Crypt Homeostasis in Colorectal Cancer. *Cell* **161,** 1539–1552 (2015).

106.   Brannon, a *et al.* Comparative sequencing analysis reveals high genomic concordance between matched primary and metastatic colorectal cancer lesions. *Genome Biol.* **15,** 454 (2014).

107.   DeVita, V. T. & Chu, E. A History of Cancer Chemotherapy. *Cancer Res.* **68,** 8643–8653 (2008).

108.   Gilman, A. & Philips, F. S. The biological actions and therapeutic applications of the B-chloroethyl amines and sulfides. *Science* **103,** 409–415 (1946).

109. Hall, A. G. & Tilby, M. J. Mechanisms of action of, and modes of resistance to, alkylating agents used in the treatment of haematological malignancies. *Blood Rev.* **6,** 163–173 (1992).

110. Price, C. C. *et al.* Mechanism of Action of Alkylating Agents. *Ann. N. Y. Acad. Sci.* **163,** 593–598 (1969).

111. Patrick, G. L. *An Introduction to Medicinal Chemistry*. (Oxford University Press, 2013).

112. Adams, V. R. & Burke, T. G. *Camptothecins in Cancer Therapy*. (Humana Press, 2005).

113. Wang, J. C. DNA topoisomerases. *Annu. Rev. Biochem.* **65,** 635–92 (1996).

114. Castano, I. B., Brzoska, P. M., Sadoff, B. U., Chen, H. & Christman, M. F. Mitotic chromosome condensation in the rDNA requires TRF4 and DNA topoisomerase I in Saccharomyces cerevisiae. *Genes Dev.* **10,** 2564–2576 (1996).

115. Liu, L. F. DNA topoisomerase poisons as antitumor drugs. *Annu. Rev. Biochem.* **58,** 351–75 (1989).

116. Zhang, C. X., Chen, a D., Gettel, N. J. & Hsieh, T. S. Essential functions of DNA topoisomerase I in Drosophila melanogaster. *Dev. Biol.* **222,** 27–40 (2000).

117. Pommier, Y., Leo, E., Zhang, H. & Marchand, C. DNA topoisomerases and their poisoning by anticancer and antibacterial drugs. *Chem. Biol.* **17,** 421–33 (2010).

118. Wu, C.-C. *et al.* Structural basis of type II topoisomerase inhibition by the anticancer drug etoposide. *Science (80-.).* **333,** 459–62 (2011).

119. Kaye, S. B. New antimetabolites in cancer chemotherapy and their clinical impact. *Br. J. Cancer* **78 Suppl 3,** 1–7 (1998).

120. Woolley, D. W. Antimetabolites. *Science (80-.).* **129,** 615–621 (1959).

121. Karnofsky, D. A. Mechanism of Action of Anticancer Drugs at a Cellular Level. *CA. Cancer J. Clin.* **18,** 232–234 (1968).

122. Farber, S. & Diamond, L. Temporary Remissions in Acute Leukemia in Children Produced by Folic Acid Antagonist, 4-Aminopteroyl-Glutamic Acid (Aminopterin). *N. Engl. J. Med.* **238,** 787–793 (1948).

123. Shapiro, G. I. & Harper, J. W. Anticancer drug targets: cell cycle and checkpoint control. *J.*

Clin. Invest. **104,** 1645–53 (1999).

124.   Gabrielli, B., Brooks, K. & Pavey, S. Defective cell cycle checkpoints as targets for anti-cancer therapies. *Front. Pharmacol.* **3,** 9 (2012).

125.   Stewart, Z. a, Westfall, M. D. & Pietenpol, J. a. Cell-cycle dysregulation and anticancer therapy. *Trends Pharmacol. Sci.* **24,** 139–45 (2003).

126.   Inoué, S. Microtubule dynamics in cell division: exploring living cells with polarized light microscopy. *Annu. Rev. Cell Dev. Biol.* **24,** 1–28 (2008).

127.   Peyrone, M. Ueber die Einwirkung des Ammoniaks auf Platinchlorür. *Ann. der Chemie und Pharm.* **51,** 1–29 (1844).

128.   Werner, A. Beitrag zur Konstitution anorganischer Verbindungen. *Z. Anorg. Chem* **3,** 267–330 (1893).

129.   Rosenberg, B., Camp, L. Van & Krigas, T. Inhibition of Cell Division in Escherichia coli by Electrolysis Products from a Platinum Electrode. *Nature* **205,** 698–699 (1965).

130.   Rosenberg, B., Van Camp, L., Grimley, E. B. & Thomson, A. J. The inhibition of growth or cell division in Escherichia coli by different ionic species of platinum(IV) complexes. *J. Biol. Chem.* **242,** 1347–1352 (1967).

131.   Rosenberg, B. & Vancamp, L. Platinum compounds: a new class of potent antitumour agents. *Nature* **222,** 385–386 (1969).

132.   Hanna, N. & Einhorn, L. H. Testicular Cancer: A Reflection on 50 Years of Discovery. *J. Clin. Oncol.* **32,** 3085–3092 (2014).

133.   Travis, L. B. *et al.* Testicular Cancer Survivorship: Research Strategies and Recommendations. *JNCI J. Natl. Cancer Inst.* **102,** 1114–1130 (2010).

134.   Armstrong, D. K. *et al.* Intraperitoneal Cisplatin and Paclitaxel in Ovarian Cancer. *N. Engl. J. Med.* **354,** 34–43 (2006).

135.   Rose, P. G. *et al.* Concurrent Cisplatin-Based Radiotherapy and Chemotherapy for Locally Advanced Cervical Cancer. *N. Engl. J. Med.* **340,** 1144–1153 (1999).

136.   Einhorn, L. H. First-Line Chemotherapy for Non-Small-Cell Lung Cancer: Is There a Superior

Regimen Based on Histology? *J. Clin. Oncol.* **26,** 3485–3486 (2008).

137.   Seiwert, T. Y., Salama, J. K. & Vokes, E. E. The chemoradiation paradigm in head and neck cancer. *Nat. Clin. Pract. Oncol.* **4,** 156–171 (2007).

138.   Ismaili, N., Amzerin, M. & Flechon, A. Chemotherapy in advanced bladder cancer: current status and future. *J. Hematol. Oncol.* **4,** 35 (2011).

139.   Velasquez, W. S. *et al.* Effective salvage therapy for lymphoma with cisplatin in combination with high-dose Ara-C and dexamethasone (DHAP). *Blood* **71,** 117–122 (1988).

140.   Hartmann, J. T. & Lipp, H.-P. Toxicity of platinum compounds. *Expert Opin. Pharmacother.* **4,** 889–901 (2003).

141.   Schreiner, G. E. & Maher, J. F. Toxic nephropathy. *Am. J. Med.* **38,** 409–449 (1965).

142.   Barabas, K., Milner, R., Lurie, D. & Adin, C. Cisplatin: A review of toxicities and therapeutic applications. *Vet. Comp. Oncol.* **6,** 1–18 (2008).

143.   Sastry, J. & Kellie, S. J. Severe neurotoxicity, ototoxicity and nephrotoxicity following high-dose cisplatin and amifostine. *Pediatr. Hematol. Oncol.* **22,** 441–445 (2005).

144.   Arany, I. & Safirstein, R. L. Cisplatin nephrotoxicity. *Semin. Nephrol.* **23,** 460–464 (2003).

145.   Yao, X., Panichpisal, K., Kurtzman, N. & Nugent, K. Cisplatin Nephrotoxicity: A Review. *Am. J. Med. Sci.* **334,** 115–124 (2007).

146.   Miller, R. P., Tadagavadi, R. K., Ramesh, G. & Reeves, W. B. Mechanisms of Cisplatin Nephrotoxicity. *Toxins (Basel).* **2,** 2490–2518 (2010).

147.   Berners-Price, S. J., Ronconi, L. & Sadler, P. J. Insights into the mechanism of action of platinum anticancer drugs from multinuclear NMR spectroscopy. *Prog. Nucl. Magn. Reson. Spectrosc.* **49,** 65–98 (2006).

148.   Townsend, D. M., Deng, M., Zhang, L., Lapus, M. G. & Hanigan, M. H. Metabolism of Cisplatin to a Nephrotoxin in Proximal Tubule Cells. *J. Am. Soc. Nephrol.* **14,** 1–10 (2003).

149.   Townsend, D. M. & Hanigan, M. H. Inhibition of gamma-glutamyl transpeptidase or cysteine S-conjugate beta-lyase activity blocks the nephrotoxicity of cisplatin in mice. *J. Pharmacol. Exp. Ther.* **300,** 142–8 (2002).

150. Litterst, C. L. Alterations in the toxicity of cis-Dichlorodiammineplatinum-II and in tissue localization of platinum as a function of NaCl concentration in the vehicle of administration. *Toxicol. Appl. Pharmacol.* **61,** 99–108 (1981).

151. Daugaard, G. & Abildgaard, U. Cisplatin nephrotoxicity. *Cancer Chemother. Pharmacol.* **25,** 1–9 (1989).

152. Cornelison, T. L. & Reed, E. Nephrotoxicity and Hydration Management for Cisplatin, Carboplatin, and Ormaplatin. *Gynecol. Oncol.* **50,** 147–158 (1993).

153. Santoso, J. T., Lucci, J. A., Coleman, R. L., Schafer, I. & Hannigan, E. V. Saline, mannitol, and furosemide hydration in acute cisplatin nephrotoxicity: a randomized trial. *Cancer Chemother. Pharmacol.* **52,** 13–18 (2003).

154. Hanigan, M. H. Stress response inhibits the nephrotoxicity of cisplatin. *AJP Ren. Physiol.* **288,** F125–F132 (2004).

155. Stewart, D. J. *et al.* Association of cisplatin nephrotoxicity with patient characteristics and cisplatin administration methods. *Cancer Chemother. Pharmacol.* **40,** 293–308 (1997).

156. Hartmann, J. T., Kollmannsberger, C., Kanz, L. & Bokemeyer, C. Platinum organ toxicity and possible prevention in patients with testicular cancer. *Int. J. Cancer* **83,** 866–9 (1999).

157. Hartmann, J. T. *et al.* Comparative study of the acute nephrotoxicity from standard dose cisplatin +/- ifosfamide and high-dose chemotherapy with carboplatin and ifosfamide. *Anticancer Res.* **20,** 3767–73 (2000).

158. Hrushesky, W. J. M. Circadian Timing of Cancer Chemotherapy. *Science (80-.).* **228,** 73–75 (1985).

159. Camargo, S. M. R., Francescato, H. D. C., Lavrador, M. A. S. & Bianchi, M. L. P. Oral Administration of Sodium Selenite Minimizes Cisplatin Toxicity on Proximal Tubules of Rats. *Biol. Trace Elem. Res.* **83,** 251–262 (2001).

160. Wu, Y. J., Muldoon, L. L. & Neuwelt, E. a. The chemoprotective agent N-acetylcysteine blocks cisplatin-induced apoptosis through caspase signaling pathway. *J. Pharmacol. Exp. Ther.* **312,** 424–431 (2005).

161. Hu, Y.-J. *et al.* The protective role of selenium on the toxicity of cisplatin-contained

chemotherapy regimen in cancer patients. *Biol. Trace Elem. Res.* **56,** 331–341 (1997).

162. Nazıroğlu, M., Karaoğlu, A. & Aksoy, A. O. Selenium and high dose vitamin E administration protects cisplatin-induced oxidative damage to renal, liver and lens tissues in rats. *Toxicology* **195,** 221–230 (2004).

163. Bagshaw, S. M. Theophylline for Prevention of Contrast-Induced Nephropathy. *Arch. Intern. Med.* **165,** 1087 (2005).

164. Argyriou, A. A., Bruna, J., Marmiroli, P. & Cavaletti, G. Chemotherapy-induced peripheral neurotoxicity (CIPN): An update. *Crit. Rev. Oncol. Hematol.* **82,** 51–77 (2012).

165. Glendenning, J. L. *et al.* Long-term neurologic and peripheral vascular toxicity after chemotherapy treatment of testicular cancer. *Cancer* **116,** 2322–2331 (2010).

166. Stillman, M. & Cata, J. P. Management of chemotherapy-induced peripheral neuropathy. *Curr. Pain Headache Rep.* **10,** 279–287 (2006).

167. Dunlap, B. & Paice, J. A. Chemotherapy-induced peripheral neuropathy: A need for standardization in measurement. *J. Support. Oncol.* **4,** 398–399 (2006).

168. McKeage, M. J., Hsu, T., Screnci, D., Haddad, G. & Baguley, B. C. Nucleolar damage correlates with neurotoxicity induced by different platinum drugs. *Br. J. Cancer* **85,** 1219–1225 (2001).

169. Zhang, H. *et al.* Targeting human 8-oxoguanine DNA glycosylase (hOGG1) to mitochondria enhances cisplatin cytotoxicity in hepatoma cells. *Carcinogenesis* **28,** 1629–1637 (2007).

170. McDonald, E. S. & Windebank, A. J. Cisplatin-Induced Apoptosis of DRG Neurons Involves Bax Redistribution and Cytochrome c Release But Not fas Receptor Signaling. *Neurobiol. Dis.* **9,** 220–233 (2002).

171. Scuteri, A. *et al.* Role of MAPKs in platinum-induced neuronal apoptosis. *Neurotoxicology* **30,** 312–319 (2009).

172. Extra, J. M. *et al.* Phase I study of oxaliplatin in patients with advanced cancer. *Cancer Chemother. Pharmacol.* **25,** 299–303 (1990).

173. McWhinney, S. R., Goldberg, R. M. & McLeod, H. L. Platinum neurotoxicity pharmacogenetics. *Mol. Cancer Ther.* **8,** 10–6 (2009).

174. Peters, U. *et al.* Glutathione S-transferase genetic polymorphisms and individual sensitivity to the ototoxic effect of cisplatin. *Anticancer. Drugs* **11,** 639–643 (2000).

175. Glover, D., Glick, J. H., Weiler, C., Yuhas, J. & Kligerman, M. M. Phase I trials of WR-2721 and cis-platinum. *Int. J. Radiat. Oncol.* **10,** 1781–1784 (1984).

176. Townsend, D. M. & Hanigan, M. H. Inhibition of γ-Glutamyl Transpeptidase or CysteineS-Conjugate β-Lyase Activity Blocks the Nephrotoxicity of Cisplatin in Mice. *J. Pharmacol. Exp. Ther.* **300,** 142–148 (2002).

177. Zhang, L. *et al.* Cisplatin-Induced Toxicity Is Associated with Platinum Deposition in Mouse Kidney Mitochondria in Vivo and with Selective Inactivation of the α-Ketoglutarate Dehydrogenase Complex in LLC-PK 1 Cells †. *Biochemistry* **45,** 8959–8971 (2006).

178. Reese, D. M. Anticancer drugs. *Nature* **378,** 532–532 (1995).

179. Longley, D. & Johnston, P. Molecular mechanisms of drug resistance. *J. Pathol.* **205,** 275–292 (2005).

180. Holohan, C., Van Schaeybroeck, S., Longley, D. B. & Johnston, P. G. Cancer drug resistance: an evolving paradigm. *Nat. Rev. Cancer* **13,** 714–726 (2013).

181. Bareschino, M. A. *et al.* Treatment of advanced non small cell lung cancer. *J. Thorac. Dis.* **3,** 122–133 (2011).

182. Jassem, J. Chemotherapy of advanced non-small cell lung cancer. *Ann. Oncol.* **10 Suppl 6,** 77–82 (1999).

183. Siddik, Z. H. Cisplatin: mode of cytotoxic action and molecular basis of resistance. *Oncogene* **22,** 7265–79 (2003).

184. Giaccone, G. Clinical Perspectives on Platinum Resistance. *Drugs* **59,** 9–17 (2000).

185. Galluzzi, L. *et al.* Molecular mechanisms of cisplatin resistance. *Oncogene* **31,** 1869–1883 (2012).

186. Blair, S. L. *et al.* Glutathione metabolism in patients with non-small cell lung cancers. *Cancer Res.* **57,** 152–155 (1997).

187. Shuck, S. C., Short, E. A. & Turchi, J. J. Eukaryotic nucleotide excision repair: from

understanding mechanisms to influencing biology. *Cell Res.* **18,** 64–72 (2008).

188.   Olaussen, K. A. *et al.* DNA Repair by ERCC1 in Non–Small-Cell Lung Cancer and Cisplatin-Based Adjuvant Chemotherapy. *N. Engl. J. Med.* **355,** 983–991 (2006).

189.   Shirota, Y. *et al.* ERCC1 and thymidylate synthase mRNA levels predict survival for colorectal cancer patients receiving combination oxaliplatin and fluorouracil chemotherapy. *J. Clin. Oncol.* **19,** 4298–4304 (2001).

190.   Dabholkar, M. *et al.* ERCC1 and ERCC2 expression in malignant tissues from ovarian cancer patients. *J. Natl. Cancer Inst.* **84,** 1512–1517 (1992).

191.   Vousden, K. H. & Lane, D. P. p53 in health and disease. *Nat. Rev. Mol. Cell Biol.* **8,** 275–283 (2007).

192.   Peng, H. Q. *et al.* Mutations of the p53 gene do not occur in testis cancer. *Cancer Res.* **53,** 3574–3578 (1993).

193.   Gadducci, A., Cosio, S., Muraca, S. & Genazzani, A. R. Molecular mechanisms of apoptosis and chemosensitivity to platinum and paclitaxel in ovarian cancer: biological data and clinical implications. *Eur. J. Gynaecol. Oncol.* **23,** 390–396 (2002).

194.   Scholl, S., Beuzeboc, P. & Pouillart, P. Targeting HER2 in other tumor types. *Ann. Oncol.* **12 Suppl 1,** S81-87 (2001).

195.   Calikusu, Z. *et al.* The effect of HER2 expression on cisplatin-based chemotherapy in advanced non-small cell lung cancer patients. *J. Exp. Clin. Cancer Res.* **28,** 97 (2009).

196.   Kroemer, G., Mariño, G. & Levine, B. Autophagy and the Integrated Stress Response. *Mol. Cell* **40,** 280–293 (2010).

197.   Wang, J. & Wu, G. S. Role of Autophagy in Cisplatin Resistance in Ovarian Cancer Cells. *J. Biol. Chem.* **289,** 17163–17173 (2014).

198.   Yamamoto, K., Okamoto, A., Isonishi, S., Ochiai, K. & Ohtake, Y. Heat shock protein 27 was up-regulated in cisplatin resistant human ovarian tumor cell line and associated with the cisplatin resistance. *Cancer Lett.* **168,** 173–181 (2001).

199.   Donnelly, A. & Blagg, B. Novobiocin and Additional Inhibitors of the Hsp90 C-Terminal Nucleotide- binding Pocket. *Curr. Med. Chem.* **15,** 2702–2717 (2008).

200. Hertz, R., Lewis Jr., J. & Lipsett, M. B. Five year's experience with the chemotherapy of metastatic choriocarcinoma and related trophoblastic tumors in women. *Am. J. Obstet. Gynecol.* **82,** 631–640 (1961).

201. Chabner, B. & Roberts, T. Chemotherapy and the war on cancer. *Nat. Rev. Cancer* **5,** (2005).

202. Kaiser, J. Combining targeted drugs to stop resistant tumors. *Science* **331,** 1542–5 (2011).

203. Luria, S. E. & Delbrück, M. Mutations of Bacteria from Virus Sensitivity to Virus Resistance. *Genetics* **28,** 491–511 (1943).

204. Rabik, C. a & Dolan, M. E. Molecular mechanisms of resistance and toxicity associated with platinating agents. *Cancer Treat. Rev.* **33,** 9–23 (2007).

205. Wittes, RE. Goldin, A. Unresolved Issues in Combination Chemotherapy. *Cancer Treat Rep* **70,** 105–25 (1986).

206. Pratt, William B. Taylor, P. *Principles of drug action: the basis of pharmacology.* (Chuichill Livingstone, 1990).

207. Burchenal, J. *et al.* Clinical evaluation of a new antimetabolite, 6-mercaptopurine, in the treatment of leukemia and allied diseases. *Blood* **8,** 965–999 (1953).

208. Frei, E., Elias, A., Wheeler, C., Richardson, P. & Hryniuk, W. The relationship between high-dose treatment and combination chemotherapy: the concept of summation dose intensity. *Clin. Cancer Res.* **4,** 2027–2037 (1998).

209. Chessells, J. M. *Oxford Textbook of Oncology*. (Oxford University Press, 1995).

210. Peters, G. J. *et al.* Basis for effective combination cancer chemotherapy with antimetabolites. *Pharmacol. Ther.* **87,** 227–53 (2000).

211. Gitler, M. S., Monks, A. & Sausville, E. A. Preclinical models for defining efficacy of drug combinations : mapping the road to the clinic. *Mol. Cancer Ther.* 929–932 (2003).

212. Blumenthal, R. D. *Chemosensitivity*. **1,** (Humana Press, 2005).

213. Buolamwini, J. K. & Adjei, A. A. *Novel Anticancer Drug Protocols*. (Humana Press, 2015).

214. Webb, J. L. *ENZYME AND METABOLIC INHIBITORS*. **I,** (New York and London: Academic Press., 1963).

215. Sanchez-Gonzalez, B. *et al.* Antileukemia activity of the combination of an anthracycline with a histone deacetylase inhibitor. *Blood* **108,** 1174–1182 (2006).

216. Elion, G. B., Singer, S. & Hitchings, G. H. Antagonists of nucleic acid derivatives VII. Synergism in combinations of biochemically related antimetabolites. *J. Biol. Chem.* **208,** 477–488 (1954).

217. Berenbaum, M. What is Synergy? *Pharmacol. Rev.* **1989,** 93–141 (1989).

218. Greco, William R. Bravo, Gregory. Parsons, J. C. The Search for Synergy: A Critical Review from a Response Surface Prespective. *Pharmacol. Rev.* **47,** 331–382 (1995).

219. Chou, T. C. & Talalay, P. Quantitative analysis of dose-effect relationships: the combined effects of multiple drugs or enzyme inhibitors. *Adv. Enzyme Regul.* **22,** 27–55 (1984).

220. Moulder, S. L. & Arteaga, C. L. A Phase I/II Trial of trastuzumab and gefitinib in patients with Metastatic Breast Cancer that overexpresses HER2/neu (ErbB-2). *Clin. Breast Cancer* **4,** 142–5 (2003).

221. Dancey, J. E. & Chen, H. X. Strategies for optimizing combinations of molecularly targeted anticancer agents. *Nat. Rev. Drug Discov.* **5,** 649–59 (2006).

222. Eustace, P. History and development of cisplatin in the management of malignant disease. *Cancer Nurs.* **3,** 373–378 (1980).

223. Boulikas, T., Pantos, A., Bellis, E. & Christofis, P. Designing platinum compounds in cancer: structures and mechanisms. *Cancer Ther.* **5,** 537–583 (2007).

224. Kelland, L. R. *et al.* Mini-review: discovery and development of platinum complexes designed to circumvent cisplatin resistance. *J. Inorg. Biochem.* **77,** 111–5 (1999).

225. Calvert, A., Harland, S. & Newell, D. Early Clinical Studies with cis-Diammine-1 , 1-Cyclobutane Dicarboxylate Platinum II. *Cancer Chemother. Pharmacol.* **9,** 140–147 (1982).

226. Wiltshaw, E. Ovarian trials at the Royal Marsden. *Cancer Treat. Rev.* **12,** (1985).

227. Graham, J., Mushin, M. & Kirkpatrick, P. Oxaliplatin. *Nat. Rev. Drug Discov.* **3,** 11–2 (2004).

228. Francesco, A. Di, Ruggiero, A. & Riccardi, R. Cellular and molecular aspects of drugs of the future : oxaliplatin. *Cell. Mol. Life Sci.* **59,** 1914–1927 (2002).

229. Ali, B. H. & Moundhri, M. S. Al. Agents ameliorating or augmenting the nephrotoxicity of cisplatin and other platinum compounds : A review of some recent research. **44,** 1173–1183 (2006).

230. Kilic, U. *et al.* Melatonin suppresses cisplatin-induced nephrotoxicity via activation of Nrf-2/HO-1 pathway. *Nutr. Metab. (Lond).* **10,** 7 (2013).

231. Srivastava, R. C. *et al.* Reduction of cis-platinum induced nephrotoxicity by zinc histidine complex : the possible implication of nitric oxide. *Biochem. Mol. Biol. Int.* **36,** 855–862 (1995).

232. Schuchter, L. M. Exploration of platinum-based dose-intensive chemotherapy strategies with amifostine (Ethyol). *Eur. J. Cancer* **32A Suppl,** S40-2 (1996).

233. Bianchi, R. *et al.* Protective effect of erythropoietin and its carbamylated derivative in experimental cisplatin peripheral neurotoxicity. *Clin. cancer Res.* **12,** 2607–12 (2006).

234. Ozols, R. F. Ovarian cancer: new clinical approaches. *Cancer Treat. Rev.* **18,** 77–83 (1991).

235. Hsiang, Y. H., Hertzberg, R., Hecht, S. & Liu, L. F. Camptothecin induces protein-linked DNA breaks via mammalian DNA topoisomerase I. *J. Biol. Chem.* **260,** 14873–8 (1985).

236. Hsiang, Y. & Liu, L. F. Identification of Mammalian DNA Topoisomerase I as an Intracellular Target of the Anticancer Drug Camptothecin. *Cancer Res.* **48,** 1722–1726 (1988).

237. Hertzberg, R. P., Caranfa, M. J. & Hecht, S. M. On the mechanism of topoisomerase I inhibition by camptothecin: evidence for binding to an enzyme-DNA complex. *Biochemistry* **28,** 4629–38 (1989).

238. Siddik, Z. H. Cisplatin: mode of cytotoxic action and molecular basis of resistance. *Oncogene* **22,** 7265–7279 (2003).

239. Xu, Y. Irinotecan: mechanisms of tumor resistance and novel strategies for modulating its activity. *Ann. Oncol.* **13,** 1841–1851 (2002).

240. Fukuda, M. *et al.* Synergism between cisplatin and topoisomerase I inhibitors, NB-506 and SN-38, in human small cell lung cancer cells. *Cancer Res.* **56,** 789–793 (1996).

241. Masuda, N., Kudoh, S. & Fukuoka, M. Irinotecan (CPT-11): pharmacology and clinical applications. *Crit. Rev. Oncol. Hematol.* **24,** 3–26 (1996).

242. *Global Cancer Facts & Figures. American Cancer Society* (2011).

243. Masuda, N. *et al.* CPT-11: a new derivative of camptothecin for the treatment of refractory or relapsed small-cell lung cancer. *J. Clin. Oncol.* **10,** 1225–9 (1992).

244. Kudoh, S., Takada, M. & Masuda, N. Enhanced antitumor efficacy of a combination of CPT-11, a new derivative of camptothecin, and cisplatin against human lung tumor xenografts. *Japanese J. cancer Res.* **84,** 203–207 (1993).

245. Kudoh, S. & Fujiwara, Y. Phase II study of irinotecan combined with cisplatin in patients with previously untreated small-cell lung cancer. West Japan Lung Cancer Group. *J. Clin. Oncol.* **16,** 1068–1074 (1998).

246. Evans, W. K. *et al.* VP-16 and cisplatin as first-line therapy for small-cell lung cancer. *J. Clin. Oncol.* **3,** 1471–7 (1985).

247. Roth, B. & Johnson, D. Randomized study of cyclophosphamide, doxorubicin, and vincristine versus etoposide and cisplatin versus alternation of these two regimens in extensive small-cell lung cancer: a phase III trial of the Southeastern Cancer Study Group. *J. Clin. Oncol.* **10,** 282–291 (1992).

248. Fukuoka, M. *et al.* Randomized trial of cyclophosphamide, doxorubicin, and vincristine versus cisplatin and etoposide versus alternation of these regimens in small-cell lung cancer. *J. Natl. Cancer Inst.* **83,** 855–61 (1991).

249. Noda, K. *et al.* Irinotecan plus cisplatin compared with etoposide plus cisplatin for extensive small-cell lung cancer. *N. Engl. J. Med.* **346,** 85–91 (2002).

250. Kim, H.-G. *et al.* Combination chemotherapy with irinotecan and cisplatin in elderly patients (>or= 65 years) with extensive-disease small-cell lung cancer. *Lung Cancer* **61,** 220–6 (2008).

251. Pectasides, D. *et al.* Combination chemotherapy with cisplatin, etoposide and irinotecan in patients with extensive small-cell lung cancer: A phase II study of the Hellenic Co-operative Oncology Group. *Lung cancer* **58,** 355–61 (2007).

252. Tas, F. *et al.* Addition of topotecan to standard cisplatin/etoposide combination in patients with extended stage small cell lung carcinoma. *Lung cancer* **57,** 79–83 (2007).

253. Jeong, H. C. *et al.* Phase II study of irinotecan plus cisplatin with concurrent radiotherapy for

the patients with limited-disease small-cell lung cancer. *Lung cancer* **53,** 361–6 (2006).

254. Okuma, Y. *et al.* Cisplatin and irinotecan combination chemotherapy for advanced thymic carcinoma: evaluation of efficacy and toxicity. *Lung cancer* **74,** 492–6 (2011).

255. Lim, S. *et al.* Phase II study of camtobell inj. (belotecan) in combination with cisplatin in patients with previously untreated, extensive stage small cell lung cancer. *Lung cancer* **80,** 313–8 (2013).

256. Longley, D. B., Harkin, D. P. & Johnston, P. G. 5-Fluorouracil: Mechanisms of Action and Clinical Strategies. *Nat. Rev. Cancer* **3,** 330–8 (2003).

257. Esaki, T., Nakano, S. & Tatsumoto, T. Inhibition by 5-Fluorouracil of cis-Diamminedichloroplatinum(II)-induced DNA Interstrand Cross-Link Removal in a HST-1 Human Squamous Carcinoma Cell Line. *Cancer Res.* **52,** 6501–6506 (1992).

258. Scanlon, K. J., Newman, E. M., Lu, Y. & Priest, D. G. Biochemical basis for cisplatin and 5-fluorouracil synergism in human ovarian carcinoma cells. *Proc. Natl. Acad. Sci. U. S. A.* **83,** 8923–5 (1986).

259. Etienne, M. C. *et al.* Dose reduction without loss of efficacy for 5-fluorouracil and cisplatin combined with folinic acid. In vitro study on human head and neck carcinoma cell lines. *Br. J. Cancer* **63,** 372–7 (1991).

260. Johnston, P., Geoffrey, F. & Drake, J. The Cellular Interaction of 5-Fluorouracil and Cisplatin in a Human Colon Carcinoma Cell Line. *Eur. J. CancerJournal Cancer* **32,** 2148–2154 (1996).

261. Pratesi, G., Gianni, L., Manzotti, C. & Zunino, F. Sequence dependence of the antitumor and toxic effects of 5-fluorouracil and cis-diamminedichloroplatinum combination on primary colon tumors in mice. *Cancer Chemother. Pharmacol.* **21,** 237–240 (1988).

262. Fujishima, H. *et al.* Inhibition by 5-fluorouracil of ERCC1 and gamma-glutamylcysteine synthetase messenger RNA expression in a cisplatin-resistant HST-1 human squamous carcinoma cell line. *Oncol. Res.* **9,** 167–72 (1997).

263. Nishiyama, M. *et al.* Low-dose cisplatin and 5-fluorouracil in combination can repress increased gene expression of cellular resistance determinants to themselves. *Clin. Cancer Res.*

5, 2620–2628 (1999).

264. Cancer Research UK. UK Cancer Incidence (2010) by Country Summary, April 2013. (2013).

265. Sklaroff, R. & Yagoda, A. Cis-diamminedichloride platinum II (DDP) in the treatment of penile carcinoma. *Cancer* **1,** 1563–1565 (1979).

266. Ahmed, T., Sklaroff, R. & Yagoda, A. Sequential trials of methotrexate, cisplatin and bleomycin for penile cancer. *J. Urol.* **132,** 465–8 (1984).

267. Gagliano, R. G. *et al.* cis-Diamminedichloroplatinum in the treatment of advanced epidermoid carcinoma of the penis: a Southwest Oncology Group Study. *J. Urol.* **141,** 66–7 (1989).

268. Theodore, C. *et al.* A phase II multicentre study of irinotecan (CPT 11) in combination with cisplatin (CDDP) in metastatic or locally advanced penile carcinoma (EORTC PROTOCOL 30992). *Ann. Oncol.* **19,** 1304–7 (2008).

269. Hussein, a M., Benedetto, P. & Sridhar, K. S. Chemotherapy with cisplatin and 5-fluorouracil for penile and urethral squamous cell carcinomas. *Cancer* **65,** 433–8 (1990).

270. Fisher, H. A. Neoadjuvant therapy with cisplatin and 5-fluorouracil for stage III squamous cell carcinoma of the penis. *J. Urol. Off. Organ Am. Urol. Assoc.* **143,** 352A

271. Shamma, F. V., Ous, S. & Fossa, S. D. Cisplatin and 5-Fluorouracil in advanced cancer of the penis. *J. Urol.* **147,** (1992).

272. Gibson, M. K. *et al.* Randomized phase III evaluation of cisplatin plus fluorouracil versus cisplatin plus paclitaxel in advanced head and neck cancer (E1395): an intergroup trial of the Eastern Cooperative Oncology Group. *J. Clin. Oncol.* **23,** 3562–7 (2005).

273. Lefebvre, J.-L. *et al.* Larynx Preservation in Pyriform Sinus Cancer: Preliminary Results of a European Organization for Research and Treatment of Cancer Phase III Trial. *JNCI J. Natl. Cancer Inst.* **88,** 890–899 (1996).

274. Domenge, C. *et al.* Randomized trial of neoadjuvant chemotherapy in oropharyngeal carcinoma. French Groupe d'Etude des Tumeurs de la Tête et du Cou (GETTEC). *Br. J. Cancer* **83,** 1594–8 (2000).

275. Sandler, a & Ettinger, D. S. Gemcitabine: single-agent and combination therapy in non-small

cell lung cancer. *Oncologist* **4,** 241–51 (1999).

276. Storniolo, a M. *et al.* An investigational new drug treatment program for patients with gemcitabine: results for over 3000 patients with pancreatic carcinoma. *Cancer* **85,** 1261–8 (1999).

277. Huang, Peng; Chubb, Sherri; and Plunkett, W. Termination of DNA synthesis by 9-beta-D-arabinofuranosyl-2-fluoroadenine. A mechanism for cytotoxicity. *J. Biol. Chem.* **265,** 16617–16625 (1990).

278. Huang, P., Chubb, S., Hertel, L. W., Grindey, G. B. & Plunkett, W. Action of 2′, 2′-Difluorodeoxycytidine on DNA Synthesis. *Cancer Res.* **51,** 6110–6117 (1991).

279. Mini, E., Nobili, S., Caciagli, B., Landini, I. & Mazzei, T. Cellular pharmacology of gemcitabine. *Ann. Oncol.* **17 Suppl 5,** v7-12 (2006).

280. Bergman, a M., Ruiz van Haperen, V. W., Veerman, G., Kuiper, C. M. & Peters, G. J. Synergistic interaction between cisplatin and gemcitabine in vitro. *Clin. Cancer Res.* **2,** 521–30 (1996).

281. van Moorsel, C. J. *et al.* Mechanisms of synergism between cisplatin and gemcitabine in ovarian and non-small-cell lung cancer cell lines. *Br. J. Cancer* **80,** 981–90 (1999).

282. Ducreux, M. *et al.* A randomised trial comparing 5-FU with 5-FU plus cisplatin in advanced pancreatic carcinoma. *Ann. Oncol.* **13,** 1185–1191 (2002).

283. Kornek, G. V. Mitomycin C in combination with capecitabine or biweekly high-dose gemcitabine in patients with advanced biliary tract cancer: a randomised phase II trial. *Ann. Oncol.* **15,** 478–483 (2004).

284. Glimelius, B. *et al.* Chemotherapy improves survival and quality of life in advanced pancreatic and biliary cancer. *Ann. Oncol.* **7,** 593–600 (1996).

285. Rao, S. *et al.* Phase III study of 5FU, etoposide and leucovorin (FELV) compared to epirubicin, cisplatin and 5FU (ECF) in previously untreated patients with advanced biliary cancer. *Br. J. Cancer* **92,** 1650–4 (2005).

286. Valle J, Wasan H, P. D. et al. Cisplatin plus gemcitabine versus gemcitabine for biliary tract cancer. *N. Engl. J. Med.* **362,** 1273–1281 (2010).

287. Scagliotti, G. V. *et al.* Phase III study comparing cisplatin plus gemcitabine with cisplatin plus pemetrexed in chemotherapy-naive patients with advanced-stage non-small-cell lung cancer. *J. Clin. Oncol.* **26,** 3543–51 (2008).

288. Hennessy, B. T., Coleman, R. L. & Markman, M. Ovarian cancer. *Lancet* **374,** 1371–82 (2009).

289. Lorusso, D., Malaguti, P. & Scambia, G. NGR-hTNF plus Doxorubicin in Recurrent Ovarian Cancer. *Eur. Oncol. Haematol.* **8,** 107–110 (2012).

290. McGuire, W. P. *et al.* Taxol: a unique antineoplastic agent with significant activity in advanced ovarian epithelial neoplasms. *Ann. Intern. Med.* **111,** 273–9 (1989).

291. Einzig, a I., Wiernik, P. H., Sasloff, J., Runowicz, C. D. & Goldberg, G. L. Phase II study and long-term follow-up of patients treated with taxol for advanced ovarian adenocarcinoma. *J. Clin. Oncol.* **10,** 1748–53 (1992).

292. Kohn, E. C. *et al.* Dose-intense taxol: high response rate in patients with platinum-resistant recurrent ovarian cancer. *J. Natl. Cancer Inst.* **86,** 18–24 (1994).

293. Thigpen, J. T., Blessing, J. a, Ball, H., Hummel, S. J. & Barrett, R. J. Phase II trial of paclitaxel in patients with progressive ovarian carcinoma after platinum-based chemotherapy: a Gynecologic Oncology Group study. *J. Clin. Oncol.* **12,** 1748–53 (1994).

294. McGuire, W. & Hoskins, W. Cyclophosphamide and cisplatin compared with paclitaxel and cisplatin in patients with stage III and stage IV ovarian cancer. *N. Engl. J. Med.* **334,** 1–6 (1996).

295. Comella, P. *et al.* Efficacy of the combination of cisplatin with either gemcitabine and vinorelbine or gemcitabine and paclitaxel in the treatment of locally advanced or metastatic non-small-cell lung cancer: a phase III randomised trial of the Southern Italy Cooperative On. *Ann. Oncol.* **18,** 324–30 (2007).

296. Koneri, K. *et al.* Five-year survival of alpha-fetoprotein-producing gastric cancer with synchronous liver metastasis: a case report. *J. Gastric Cancer* **13,** 58–64 (2013).

297. Frasci, G. *et al.* Cisplatin-epirubicin-paclitaxel weekly administration in advanced breast cancer: a phase I study of the Southern Italy Cooperative Oncology Group. *Breast Cancer Res.*

Treat. **56,** 239–52 (1999).

298. Huang, J. *et al.* A phase II study of biweekly paclitaxel and cisplatin chemotherapy for recurrent or metastatic esophageal squamous cell carcinoma: ERCC1 expression predicts response to chemotherapy. *Med. Oncol.* **30,** 343 (2013).

299. Vasey, P. A. *et al.* Docetaxel and cisplatin in combination as first-line chemotherapy for advanced epithelial ovarian cancer. Scottish Gynaecological Cancer Trials Group. *J. Clin. Oncol.* **17,** 2069–2080 (1999).

300. Roth, A., Maibach, R. & Martinelli, G. Docetaxel (Taxotere®)-cisplatin (TC): an effective drug combination in gastric carcinoma. *Ann. Oncol.* **11,** 301–306 (2000).

301. Haddad, R. *et al.* Docetaxel, cisplatin, and 5-fluorouracil-based induction chemotherapy in patients with locally advanced squamous cell carcinoma of the head and neck: the Dana Farber Cancer Institute experience. *Cancer* **97,** 412–8 (2003).

302. Haddad, R. Docetaxel, Cisplatin, 5-Fluorouracil (TPF)-Based Induction Chemotherapy for Head and Neck Cancer and the Case for Sequential, Combined-Modality Treatment. *Oncologist* **8,** 35–44 (2003).

303. Mendelsohn, J. The epidermal growth factor receptor as a target for cancer therapy. *Endocr. Relat. Cancer* **8,** 3–9 (2001).

304. Mendelsohn, J. Antibody-mediated EGF receptor blockade as an anticancer therapy: from the laboratory to the clinic. *Cancer Immunol. Immunother.* **52,** 342–6 (2003).

305. Walden, M. J. & Aygun, N. Head and neck cancer. *Semin. Roentgenol.* **48,** 75–86 (2013).

306. Ang, K. K., Andratschke, N. H. & Milas, L. Epidermal growth factor receptor and response of head-and-neck carcinoma to therapy. *Int. J. Radiat. Oncol. Biol. Phys.* **58,** 959–65 (2004).

307. Huang, S. M., Bock, J. M. & Harari, P. M. Epidermal growth factor receptor blockade with C225 modulates proliferation, apoptosis, and radiosensitivity in squamous cell carcinomas of the head and neck. *Cancer Res.* **59,** 1935–1940 (1999).

308. Harari, P. M. & Huang, S. M. Head and neck cancer as a clinical model for molecular targeting of therapy: combining EGFR blockade with radiation. *Int. J. Radiat. Oncol. Biol. Phys.* **49,** 427–33 (2001).

309. Fan, Z., Baselga, J., Masui, H. & Mendelsohn, J. Antitumor Effect of Anti-Epidermal Growth Factor Receptor Monoclonal Antibodies plus cis-Diamminedichloroplatinum on Well Established A431 Cell Xenografts. *Cancer Res.* **53,** 4637–4642 (1993).

310. Baselga, J. *et al.* Phase I studies of anti-epidermal growth factor receptor chimeric antibody C225 alone and in combination with cisplatin. *J. Clin. Oncol.* **18,** 904–14 (2000).

311. Shin, D. M. *et al.* Epidermal growth factor receptor-targeted therapy with C225 and cisplatin in patients with head and neck cancer. *Clin. Cancer Res.* **7,** 1204–1213 (2001).

312. Burtness, B., Goldwasser, M. a, Flood, W., Mattar, B. & Forastiere, A. a. Phase III randomized trial of cisplatin plus placebo compared with cisplatin plus cetuximab in metastatic/recurrent head and neck cancer: an Eastern Cooperative Oncology Group study. *J. Clin. Oncol.* **23,** 8646–54 (2005).

313. Baselga, J. *et al.* Phase II multicenter study of the antiepidermal growth factor receptor monoclonal antibody cetuximab in combination with platinum-based chemotherapy in patients with platinum-refractory metastatic and/or recurrent squamous cell carcinoma of the head and n. *J. Clin. Oncol.* **23,** 5568–77 (2005).

314. León, X. *et al.* A Retrospective Analysis of the Outcome of Patients with Recurrent and/or Metastatic Squamous Cell Carcinoma of the Head and Neck Refractory to a Platinum-based Chemotherapy. *Clin. Oncol.* **17,** 418–424 (2005).

315. Vermorken, J. B. *et al.* Platinum-based chemotherapy plus cetuximab in head and neck cancer. *N. Engl. J. Med.* **359,** 1116–27 (2008).

316. Vermorken, J. B. *et al.* Phase II study of pemetrexed in combination with cisplatin and cetuximab in recurrent or metastatic squamous cell carcinoma of the head and neck. *Eur. J. Cancer* **49,** 2877–83 (2013).

317. Glisson, B. & Kurie, J. Cisplatin, Etoposide, and Paclitaxel in the Treatment of Patients With Extensive Small-Cell Lung Carcinoma. *J. Clin. Oncol.* **17,** 2309–2315 (1999).

318. Hanna, N. *et al.* Randomized phase III trial comparing irinotecan/cisplatin with etoposide/cisplatin in patients with previously untreated extensive-stage disease small-cell lung cancer. *J. Clin. Oncol.* **24,** 2038–43 (2006).

319. Lara, P. N. *et al.* Phase III trial of irinotecan/cisplatin compared with etoposide/cisplatin in extensive-stage small-cell lung cancer: clinical and pharmacogenomic results from SWOG S0124. *J. Clin. Oncol.* **27,** 2530–5 (2009).

320. Zatloukal, P. *et al.* A multicenter international randomized phase III study comparing cisplatin in combination with irinotecan or etoposide in previously untreated small-cell lung cancer patients with extensive disease. *Ann. Oncol.* **21,** 1810–6 (2010).

321. Arnesano, F., Losacco, M. & Natile, G. An Updated View of Cisplatin Transport. *Eur. J. Inorg. Chem.* **2013,** 2701–2711 (2013).

322. Andrews, P. a, Velury, S., Mann, S. C. & Howell, S. B. cis-Diamminedichloroplatinum(II) accumulation in sensitive and resistant human ovarian carcinoma cells. *Cancer Res.* **48,** 68–73 (1988).

323. Hall, M. D., Okabe, M., Shen, D.-W., Liang, X.-J. & Gottesman, M. M. The Role of Cellular Accumulation in Determining Sensitivity to Platinum-Based Chemotherapy. *Annu. Rev. Pharmacol. Toxicol.* **48,** 495–535 (2008).

324. Yu, F., Megyesi, J. & Price, P. M. Cytoplasmic initiation of cisplatin cytotoxicity. *AJP Ren. Physiol.* **295,** F44–F52 (2008).

325. Gibson, D. The mechanism of action of platinum anticancer agents—what do we really know about it? *Dalt. Trans.* 10681 (2009). doi:10.1039/b918871c

326. Kasherman, Y., Sturup, S. & Gibson, D. Trans labilization of am(m)ine ligands from platinum(II) complexes by cancer cell extracts. *JBIC J. Biol. Inorg. Chem.* **14,** 387–399 (2009).

327. Cullen, K. J., Yang, Z., Schumaker, L. & Guo, Z. Mitochondria as a critical target of the chemotheraputic agent cisplatin in head and neck cancer. *J. Bioenerg. Biomembr.* **39,** 43–50 (2007).

328. Jung, Y. & Lippard, S. J. Direct Cellular Responses to Platinum-Induced DNA Damage. *Chem. Rev.* **107,** 1387–1407 (2007).

329. Wang, D. & Lippard, S. J. Cellular processing of platinum anticancer drugs. *Nat. Rev. Drug Discov.* **4,** 307–320 (2005).

330. Eastman, A. Separation and characterization of products resulting from the reaction of cis-diamminedichloroplatinum(II) with deoxyribonucleosides. *Biochemistry* **21,** 6732–6736 (1982).

331. Robins, A. B. The reaction of 14C-labelled platinum ethylenediamine dichloride with nucleic acid constituents. *Chem. Biol. Interact.* **6,** 35–45 (1973).

332. Fichtinger-Schepman, A. M. J., Van der Veer, J. L., Den Hartog, J. H. J., Lohman, P. H. M. & Reedijk, J. Adducts of the antitumor drug cis-diamminedichloroplatinum(II) with DNA: formation, identification, and quantitation. *Biochemistry* **24,** 707–713 (1985).

333. Eastman, A. Reevaluation of interaction of cis-dichloro(ethylenediamine)platinum(II) with DNA. *Biochemistry* **25,** 3912–3915 (1986).

334. Takahara, P. M. *et al.* Crystal structure of double-stranded DNA containing the major adduct of the anticancer drug cisplatin. *Nature* **377,** 649–652 (1995).

335. Gelasco, A. & Lippard, S. J. NMR Solution Structure of a DNA Dodecamer Duplex Containing a cis -Diammineplatinum(II) d(GpG) Intrastrand Cross-Link, the Major Adduct of the Anticancer Drug Cisplatin. *Biochemistry* **37,** 9230–9239 (1998).

336. Trimmer, E. E., Zamble, D. B., Lippard, S. J. & Essigmann, J. M. Human Testis-Determining Factor SRY Binds to the Major DNA Adduct of Cisplatin and a Putative Target Sequence with Comparable Affinities. *Biochemistry* **37,** 352–362 (1998).

337. Ohndorf, U.-M., Whitehead, J. P., Raju, N. L. & Lippard, S. J. Binding of tsHMG, a Mouse Testis-Specific HMG-Domain Protein, to Cisplatin−DNA Adducts. *Biochemistry* **36,** 14807–14815 (1997).

338. McA'Nulty, M. M., Whitehead, J. P. & Lippard, S. J. Binding of Ixr1, a Yeast HMG-Domain Protein, to Cisplatin−DNA Adducts in Vitro and in Vivo. *Biochemistry* **35,** 6089–6099 (1996).

339. Huang, J. C., Zamble, D. B., Reardon, J. T., Lippard, S. J. & Sancar, A. HMG-domain proteins specifically inhibit the repair of the major DNA adduct of the anticancer drug cisplatin by human excision nuclease. *Proc. Natl. Acad. Sci.* **91,** 10394–10398 (1994).

340. Kozelka, J. Molecular origin of the sequence-dependent kinetics of reactions between cisplatin derivatives and DNA. *Inorganica Chim. Acta* **362,** 651–668 (2009).

341.   Huang, H. *et al.* Solution Structure of a Cisplatin-Induced DNA lnterstrand Cross-Link. *Science (80-.).* **270,** 1842–1845 (1995).

342.   Todd, R. C., Lovejoy, K. S. & Lippard, S. J. Understanding the effect of carbonate ion on cisplatin binding to DNA. *J. Am. Chem. Soc.* **129,** 6370–6371 (2007).

343.   Lu, Q.-B., Kalantari, S. & Wang, C.-R. Electron transfer reaction mechanism of cisplatin with DNA at the molecular level. *Mol. Pharm.* **4,** 624–8 (2007).

344.   Miller, S. E. & House, D. A. The hydrolysis products of cis-dichlorodiammineplatinum(II) 3. Hydrolysis kinetics at physiological pH. *Inorganica Chim. Acta* **173,** 53–60 (1990).

345.   Berners-Price, S. J., Frenkiel, T. A., Frey, U., Ranford, J. D. & Sadler, P. J. Hydrolysis products of cisplatin: pK a determinations via[1H, 15N] NMR spectroscopy. *J. Chem. Soc. Chem. Commun.* 789 (1992). doi:10.1039/c39920000789

346.   Lu, Q.-B. Molecular reaction mechanisms of combination treatments of low-dose cisplatin with radiotherapy and photodynamic therapy. *J. Med. Chem.* **50,** 2601–4 (2007).

347.   Kopyra, J., Koenig-Lehmann, C., Bald, I. & Illenberger, E. A single slow electron triggers the loss of both chlorine atoms from the anticancer drug cisplatin: Implications for chemoradiation therapy. *Angew. Chemie - Int. Ed.* **48,** 7904–7907 (2009).

348.   Kuduk-Jaworska, J., Chojnacki, H. & Jański, J. J. Non-empirical quantum chemical studies on electron transfer reactions in trans- and cis-diamminedichloroplatinum(II) complexes. *J. Mol. Model.* **17,** 2411–21 (2011).

349.   Luo, T. *et al.* Electron transfer-based combination therapy of cisplatin with tetramethyl-p-phenylenediamine for ovarian, cervical, and lung cancers. *Proc. Natl. Acad. Sci.* **109,** 10175–10180 (2012).

350.   Huang, J., Stockwell, D., Boulesbaa, A., Guo, J. & Lian, T. Comparison of Electron Injection Dynamics from Rhodamine B to In2O3 , SnO2, and ZnO Nanocrystalline Thin Films. *J. Phys. Chem. C* **112,** 5203–5212 (2008).

351.   Ma, Y. & Yao, J. Photodegradation of Rhodamine B catalyzed by TiO2 thin films. *J. Photochem. Photobiol. A Chem.* **116,** 167–170 (1998).

352.   Du, L., Wu, J. & Hu, C. Electrochemical oxidation of Rhodamine B on RuO2–PdO–TiO2/Ti

electrode. *Electrochim. Acta* **68,** 69–73 (2012).

353.   Nishikiori, H., Teshima, K. & Fujii, T. Photoinduced electron transfer in rhodamine B-containing amorphous titania gels. *Res. Chem. Intermed.* **41,** 3803–3816 (2015).

354.   Rosenberg, B. Charles F. Kettring prize. Fundamental studies with cisplatin. *Cancer* **55,** 2303–2316 (1985).

355.   Nowosielska, A. & Marinus, M. G. Cisplatin induces DNA double-strand break formation in Escherichia coli dam mutants. *DNA Repair (Amst).* **4,** 773–781 (2005).

356.   Frankenberg-Schwager, M. *et al.* Cisplatin-mediated DNA double-strand breaks in replicating but not in quiescent cells of the yeast Saccharomyces cerevisiae. *Toxicology* **212,** 175–184 (2005).

357.   Jackson, S. P. Sensing and repairing DNA double-strand breaks. *Carcinogenesis* **23,** 687–696 (2002).

358.   Shrivastav, M., De Haro, L. P. & Nickoloff, J. A. Regulation of DNA double-strand break repair pathway choice. *Cell Res.* **18,** 134–147 (2008).

359.   Jachymczyk, W. J., von Borstel, R. C., Mowat, M. R. A. & Hastings, P. J. Repair of interstrand cross-links in DNA of Saccharomyces cerevisiae requires two systems for DNA repair: The RAD3 system and the RAD51 system. *Mol. Gen. Genet. MGG* **182,** 196–205 (1981).

360.   Magana-Schwencke, N., Henriques, J. a, Chanet, R. & Moustacchi, E. The fate of 8-methoxypsoralen photoinduced crosslinks in nuclear and mitochondrial yeast DNA: comparison of wild-type and repair-deficient strains. *Proc. Natl. Acad. Sci.* **79,** 1722–1726 (1982).

361.   Dardalhon, M., De Massy, B., Nicolas, A. & Averbeck, D. Mitotic recombination and localized DNA double-strand breaks are induced after 8-methoxypsoralen and UVA irradiation in Saccharomyces cerevisiae. *Curr. Genet.* **34,** 30–42 (1998).

362.   Pichierri, P., Averbeck, D. & Rosselli, F. DNA cross-link-dependent RAD50/MRE11/NBS1 subnuclear assembly requires the Fanconi anemia C protein. *Hum. Mol. Genet.* **11,** 2531–2546 (2002).

168

363.   Niedernhofer, L. J. *et al.* The Structure-Specific Endonuclease Ercc1-Xpf Is Required To Resolve DNA Interstrand Cross-Link-Induced Double-Strand Breaks. *Mol. Cell. Biol.* **24,** 5776–5787 (2004).

364.   McHugh, P. J., Sones, W. R. & Hartley, J. a. Repair of Intermediate Structures Produced at DNA Interstrand Cross-Links in Saccharomyces cerevisiae. *Mol. Cell. Biol.* **20,** 3425–3433 (2000).

365.   De Silva, I. U., McHugh, P. J., Clingen, P. H. & Hartley, J. A. Defining the Roles of Nucleotide Excision Repair and Recombination in the Repair of DNA Interstrand Cross-Links in Mammalian Cells. *Mol. Cell. Biol.* **20,** 7980–7990 (2000).

366.   Hughes, J., Rees, S., Kalindjian, S. & Philpott, K. Principles of early drug discovery. *Br. J. Pharmacol.* **162,** 1239–1249 (2011).

367.   Elmore, S. Apoptosis: A Review of Programmed Cell Death. *Toxicol. Pathol.* **35,** 495–516 (2007).

368.   Kuypers, F. A. *et al.* Detection of altered membrane phospholipid asymmetry in subpopulations of human red blood cells using fluorescently labeled annexin V. *Blood* **87,** 1179–87 (1996).

369.   Trotter, P. J., Orchard, M. a & Walker, J. H. Ca2+ concentration during binding determines the manner in which annexin V binds to membranes. *Biochem. J.* **308 (Pt 2,** 591–8 (1995).

370.   Pigault, C., Follenius-Wund, A., Schmutz, M., Freyssinet, J.-M. & Brisson, A. Formation of Two-dimensional Arrays of Annexin V on Phosphatidylserine-containing Liposomes. *J. Mol. Biol.* **236,** 199–208 (1994).

371.   Kerr, J. F., Wyllie, A. H. & Currie, A. R. Apoptosis: a basic biological phenomenon with wide-ranging implications in tissue kinetics. *Br. J. Cancer* **26,** 239–257 (1972).

372.   Saraste, A. & Pulkki, K. Morphologic and biochemical hallmarks of apoptosis. *Cardiovasc. Res.* **45,** 528–537 (2000).

373.   Carlsson, G., Gullberg, B. & Hafström, L. Estimation of liver tumor volume using different formulas - an experimental study in rats. *J. Cancer Res. Clin. Oncol.* **105,** 20–3 (1983).

374.   Tomayko, M. M. & Reynolds, C. P. Determination of subcutaneous tumor size in athymic (

nude) mice. *Cancer Chemother. Pharmacol.* **24,** 148–154 (1989).

375. Bortner, C. D., Oldenburg, N. B. E. & Cidlowski, J. a. The role of DNA fragmentation in apoptosis. *Trends Cell Biol.* **5,** 21–26 (1995).

376. ZHANG, J. H. & XU, M. DNA fragmentation in apoptosis. *Cell Res.* **10,** 205–211 (2000).

377. Collins, J. A., Schandl, C. A., Young, K. K., Vesely, J. & Willingham, M. C. Major DNA Fragmentation Is a Late Event in Apoptosis. *J. Histochem. Cytochem.* **45,** 923–934 (1997).

378. Singh, A., Bhat, T. K. & Sharma, O. P. Clinical Biochemistry of Hepatotoxicity. *J. Clin. Toxicol.* **4,** 1–19 (2011).

379. Navarro, V. J. & Senior, J. R. Drug-Related Hepatotoxicity. *N. Engl. J. Med.* **354,** 731–739 (2006).

380. Ozer, J., Ratner, M., Shaw, M., Bailey, W. & Schomaker, S. The current state of serum biomarkers of hepatotoxicity. *Toxicology* **245,** 194–205 (2008).

381. Vroon, D. H. & Israili, Z. *Alkaline Phosphatase and Gamma Glutamyltransferase. Clinical Methods: The History, Physical, and Laboratory Examinations* (Butterworths, 1990).

382. Ramaiah, S. K. A toxicologist guide to the diagnostic interpretation of hepatic biochemical parameters. *Food Chem. Toxicol.* **45,** 1551–1557 (2007).

383. Burtis, C., Ashwood, E. R., Bruns, D. E. & Sawyer, B. G. *Tietz Fundamentals of Clinical Chemistry*. (Elsevier Inc., 2008).

384. Gowda, S. *et al.* A review on laboratory liver function tests. *Pan Afr. Med. J.* **3,** 17 (2009).

385. Hosten, A. O. in *Clinical Methods: The History, Physical, and Laboratory Examinations* (eds. HK, W., WD, H. & JW, H.) 874–878 (Butterworths, 1990).

386. Traynor, J., Mactier, R., Geddes, C. C. & Fox, J. G. How to measure renal function in clinical practice. *BMJ* **333,** 733–737 (2006).

387. Arunkumar, P. A., Viswanatha, G. L., Radheshyam, N., Mukund, H. & Belliyappa, M. S. Science behind cisplatin-induced nephrotoxicity in humans: A clinical study. *Asian Pac. J. Trop. Biomed.* **2,** 640–644 (2012).

388. Ghadjar, P. *et al.* Impact of weight loss on survival after chemoradiation for locally advanced

head and neck Cancer: secondary results of a randomized phase III trial (SAKK 10/94). *Radiat. Oncol.* **10,** 21 (2015).

389.   Hojman, P. *et al.* Voluntary Exercise Prevents Cisplatin-Induced Muscle Wasting during Chemotherapy in Mice. *PLoS One* **9,** e109030 (2014).

390.   Madias, N. E. & Harrington, J. T. Platinum nephrotoxicity. *Am. J. Med.* **65,** 307–14 (1978).

391.   Von Hoff, D. D. *et al.* Toxic effects of cis-dichlorodiammineplatinum(II) in man. *Cancer Treat. Rep.* **63,** 1527–1531 (2014).

392.   King, P. D. & Perry, M. C. Hepatotoxicity of chemotherapy. *Oncologist* **6,** 162–176 (2001).

393.   Waseem, M., Bhardwaj, M., Tabassum, H., Raisuddin, S. & Parvez, S. Cisplatin hepatotoxicity mediated by mitochondrial stress. *Drug Chem. Toxicol.* **38,** 452–459 (2015).

394.   Naqshbandi, A., Khan, W., Rizwan, S. & Khan, F. Studies on the protective effect of flaxseed oil on cisplatin-induced hepatotoxicity. *Hum. Exp. Toxicol.* **31,** 364–375 (2012).

395.   Xiongfeng, H., Qun, X. & Rohrer, J. *Rapid and Sensitive Determination of Rhodamine B in Cosmetics*.

396.   Anachemia. *Material Safety Data Sheet of Rhodamine B*. (2009).

397.   Sigma-Aldrich. *Material Safety Data Sheet of Rhodamine B*. (2006).

398.   Dire, D. J. & Wilkinson, J. A. Acute exposure to rhodamine B. *J. Toxicol. Clin. Toxicol.* **25,** 603–7 (1987).

399.   Kaji, T., Kawashima, T., Yamamoto, C. & Sakamoto, M. Rhodamine B inhibits collagen synthesis by human lip fibroblasts in culture. *Toxicol. Lett.* **61,** 81–87 (1992).

400.   WHO. IARC monographs on the evaluation of the carcinogenic risk of chemicals to man. Some aromatic amines and related nitro compounds - hair dyes, colouring agents and miscellaneous industrial chemicals. *Int. agency Res. cancer* **16,** 227 (1978).

401.   Brown, J. P., Dietrich, P. S. & Bakner, C. M. Mutagenicity testing of some drug and cosmetic dye lakes with the Salmonella/mammalian microsome assay. *Mutat. Res.* **66,** 181–185 (1979).

402.   Nestmann, E. R., Douglas, G. R., Matula, T. I., Grant, C. E. & Kowbel, D. J. Mutagenic activity of rhodamine dyes and their impurities as detected by mutation induction in

Salmonella and DNA damage in Chinese hamster ovary cells. *Cancer Res.* **39,** 4412–4417 (1979).

403. Lewis, I. L., Patterson, R. M. & McBay, H. C. The effects of Rhodamine B on the chromosomes of Muntiacus muntjac. *Mutat. Res. Toxicol.* **88,** 211–216 (1981).

404. Parodi, S. *et al.* DNA-damaging activity in vivo and bacterial mutagenicity of sixteen aromatic amines and azo-derivatives, as related quantitatively to their carcinogenicity. *Carcinogenesis* **2,** 1317–1326 (1981).

405. Wuebbles, B. J. & Felton, J. S. Evaluation of laser dye mutagenicity using the Ames/Salmonella microsome test. *Environ. Mutagen.* **7,** 511–22 (1985).

406. Elliott, G. S., Mason, R. W. & Edwards, I. R. Studies on the pharmacokinetics and mutagenic potential of rhodamine B. *J. Toxicol. Clin. Toxicol.* **28,** 45–59 (1990).

407. Tripathy, N. K., Nabi, M. J., Sahu, G. P. & Anand Kumar, A. Genotoxicity testing of two red dyes in the somatic and germ line cells of drosophila. *Food Chem. Toxicol.* **33,** 923–927 (1995).

408. European Food Safety Authority. Opinion of the Scientific Panel on food additives, flavourings, processing aids and materials in contact with food (AFC) to review the toxicology of a number of dyes illegally present in food in the EU. *EFSA J.* **3,** 263 (2005).

409. Abstracts of papers for the Thirteenth Annual Meeting of the Society of Toxicology, Washington, D.C. March 10–14, 1974. *Toxicol. Appl. Pharmacol.* **29,** 75–155 (1974).

410. Accord Healthcare ltd. *Material Safety Data Sheet of Cisplatin.* (2011).

411. Prasad, P. N. *Introduction to Biophotonics.* (John Wiley & Sons, Inc, 2003).

412. Wang, P., Cheng, M. & Zhang, Z. On different photodecomposition behaviors of rhodamine B on laponite and montmorillonite clay under visible light irradiation. *J. Saudi Chem. Soc.* **18,** 308–316 (2014).

413. Qu, P., Zhao, J., Shen, T. & Hidaka, H. TiO2-assisted photodegradation of dyes: A study of two competitive primary processes in the degradation of RB in an aqueous TiO2 colloidal solution. *J. Mol. Catal. A Chem.* **129,** 257–268 (1998).

414. Wilhelm, P. & Stephan, D. Photodegradation of rhodamine B in aqueous solution via

SiO2@TiO2 nano-spheres. *J. Photochem. Photobiol. A Chem.* **185,** 19–25 (2007).

415. Beaumont, P. C., Johnson, D. G. & Parsons, B. J. Excited state and free radical properties of rhodamine dyes in aqueous solution: A laser flash photolysis and pulse radiolysis study. *J. Photochem. Photobiol. A Chem.* **107,** 175–183 (1997).

416. Thomsen, C. L., Madsen, D., Keiding, S. R., Thøgersen, J. & Christiansen, O. Two-photon dissociation and ionization of liquid water studied by femtosecond transient absorption spectroscopy. *J. Chem. Phys.* **110,** 3453 (1999).

417. Hart, E. J. & Boag, J. W. Absorption Spectrum of the Hydrated Electron in Water and in Aqueous Solutions. *J. Am. Chem. Soc.* **84,** 4090–4095 (1962).

418. Migus, A., Gauduel, Y., Martin, J. L. & Antonetti, A. Excess Electrons in Liquid Water: First Evidence of a Prehydrated State with Femtosecond Lifetime. *Phys. Rev. Lett.* **58,** 1559–1562 (1987).

419. Wang, C.-R., Luo, T. & Lu, Q.-B. On the lifetimes and physical nature of incompletely relaxed electrons in liquid water. *Phys. Chem. Chem. Phys.* **10,** 4463–4470 (2008).

420. Lu, Q.-B. Effects and applications of ultrashort-lived prehydrated electrons in radiation biology and radiotherapy of cancer. *Mutat. Res. Mutat. Res.* **704,** 190–199 (2010).